Performance Analysis of Flower Pollination Optimization-based PID Controller for Regulation of Frequency of Hybrid Wind-Hydro Power Plant

Emebet Embiale Wondimu

A Thesis Submitted to

The Department of Electrical Power and Control Engineering
School of Electrical and Computing Engineering

Presented in Partial Fulfillment of the Requirement for the Degree of Master's in Electrical Power and Control Engineering (Control Engineering)

Office of Graduate Studies
Adama Science and Technology University

June, 2024

Adama, Ethiopia

Performance Analysis of Flower Pollination Optimization-based PID Controller for Regulation of Frequency of Hybrid Wind-Hydro Power Plant

Emebet Embiale Wondimu

Advisor:

Dr. Endalew Ayenew (Assistant Professor)

A Thesis Submitted to

The Department of Electrical Power and Control Engineering

School of Electrical and Computing Engineering

Presented in Partial Fulfillment of the Requirement for the Degree of Master's in Electrical Power and Control Engineering (Control Engineering)

Office of Graduate Studies

Adama Science and Technology University

June, 2024.

Adama, Ethiopia

DECLARATION

I hereby declare that this Master Thesis entitled "**Performance Analysis of Flower Pollination Optimization-based PID Controller for Regulation of Frequency of Hybrid Wind-Hydro Power Plant**" is my original work. That is, it has not been submitted for the award of any academic degree, diploma, or certificate in any other university. All sources of materials that are used for this thesis have been duly acknowledged through citation.

Emebet Embiale	______________	______________
Name of the student	Signature	Date

RECOMMENDATION

I, the advisor of this thesis, hereby certify that I have read the revised version of the thesis entitled "**Performance Analysis of Flower Pollination Optimization-based PID Controller for Regulation of Frequency of Hybrid Wind-Hydro Power Plant**" prepared under my guidance by **Emebet Embiale** submitted in partial fulfillment of the requirements for the degree of Masters of Science in control system engineering. Therefore, I recommend the submission of a revised version of the thesis to the department following the applicable procedures.

Dr. Endalew Ayenew	________________	________________
Advisor	Signature	Date

APPROVAL PAGE

I, the advisor of the thesis entitled "**Performance Analysis of Flower Pollination Optimization-based PID Controller for Regulation of Frequency of Hybrid Wind-Hydro Power Plant**" and developed by **Emebet Embiale**, hereby certify that the recommendation and suggestions made by the board of examiners are appropriately incorporated into the final version of the thesis.

Dr. Endalew Ayenew	________________	________________
Name of Advisor	Signature	Date

We, the undersigned, members of the Board of Examiners of the thesis by Emebet Embiale have read and evaluated the thesis entitled "**Performance Analysis of Flower Pollination Optimization-based PID Controller for Regulation of Frequency of Hybrid Wind-Hydro Power Plant**" and examined the candidate during open defense. This is, therefore, to certify that the thesis is accepted for partial fulfillment of the requirement of the degree of Masters of Science in control system engineering.

________________	________________	________________
Chairperson	Signature	Date
Prof. G.G. Jin	________________	________________
Internal examiner	Signature	Date
Dr. Beteley Teka	________________	________________
External examiner	Signature	Date

Final approval and acceptance of the thesis are contingent upon the submission of its final copy to the office of postgraduate Studies (OPGS) through the Department graduate council (DGC) and school graduate committee (SGC).

________________	________________	________________
Department Head	Signature	Date
________________	________________	________________
School Dean	Signature	Date
________________	________________	________________
Office of postgraduate studies, Dean	Signature	Date

ACKNOWLEDGEMENT

Firstly, I would want to give thanks to God Almighty for providing me with the ability, health, and strength to begin and complete this thesis. This accomplishment would not have been feasible without his blessings. Secondly, I am grateful to ASTU for intending to offer a Master of Science Program in Control System Engineering. The financial sponsorship support provided by ASTU is highly appreciated. Thirdly, I want to thank my advisor, Dr. Endalew Ayenew, from the bottom of my heart for all of his help with this thesis. I appreciate his patience, kindness, and superb direction. I also owe him for his insightful feedback.

Lastly, I want to sincerely thank my lovely husband, Dr. Aberu Arega, from the bottom of my heart. This accomplishment would not have been possible without his endurance and perseverance.

Emebet Embiale

TABLE OF CONTENTS

CONTENTES PAGE

LIST OF TABLES

TABLE PAGE

LIST OF FIGURES

FIGURE PAGE

LIST OF ACRONYMS

AGC	Automatic Generation Control
B2B	Back-to-Back Converter
DE	Differential Evolution
DFIG	Double Fed Induction Generator
EEA	Ethiopian Electric Utility Authority
ENTS	Ethiopia National Transmission System
FPOA	Flower Pollination Optimization Algorithm
GA	Genetic Algorithm
GSC	Grid Side Converter
GVOC	Grid Voltage Oriented Control
HPP	Hydro-Power Plant
IAE	Integral Absolute Error
ISE	Integral Square Error
ITAE	Integral Time Absolute Error
MPC	Model Predictive Controller
MPPT	Maximum Power Point Tracking
LFC	Load Frequency Control
LB	Lower Bound
PA	Pitch Angle
PI	Proportional Integral
PID	Proportional Integral Derivative
PLL	Phase Locked Loop
PMSG	Permanent Magnet Synchronous Generator

PSO	Particle Swarm Optimization
RES	Renewable Energy Source
RSC	Rotor Side Converter
SFOC	Stator Flux-Oriented Control
SSA	Salp Swarm Algorithm
TLBO	Teaching Learning-Based Optimization
TSO	Transmission System Operator
UB	Upper Bound
VSC	Voltage Source Converter
VSWT	Variable Speed Wind Turbine
WECS	Wind Energy Conversion System
WS	Wind Speed
WTs	Wind Turbines

LIST OF SYMBOLS

$C_p(\lambda_{wt}, \beta)$ – Conversion coefficient of power from wind to mechanical power.

C_{pm} – Maximum conversion coefficient of power.

D_{sy} – Damping factor of system.

H_{sy} – Inertia constant of system.

λ_{wt} – Turbine blade's speed ratio.

$\lambda_{wt\,opt}$ – Optimal Turbine blade's speed ratio.

β_b – Blade rotor Pitch angle.

ρ – Air density.

J_t – Turbine inertia.

J_g – Generator inertia.

P_{mech} – Mechanical Turbine Power.

P_{wind} – Total Power in the wind.

P_H – Rated hydropower.

τ_t – Wind Turbine's Torque.

τ_{em} – Electromagnetic torque.

V_{wind} – Wind Speed.

V_{dc} – DC link voltage.

Δf – Measured frequency deviation.

Δf_{ref} – Reference frequency deviation.

ω_t – Turbine Rotational Speed.

ω_g – The Generator Mechanical Speed.

ω_{ele} – The electrical angular speed of the generator.

ω_{sy} – Synchronous/base speed.

$\Delta\omega$ – Change in angular frequency.

ABSTRACT

The world is moving towards generating electricity from renewable energy sources (RESs) to reduce harmful pollution; wind turbines (WTs) and hydropower plants (HPPs) are the most advanced and environmentally friendly forms of electrical energy. However, the interconnection of RESs, especially WTs, with the power grid brings a challenge: keeping the grid frequency constant. Wind speed determines the fluctuating nature of wind power. Due to variations in wind speed, the outputs of double-fed induction generator (DFIG) based WT also vary. In addition, the variable nature of the load leads to a power imbalance between demand and supply. This imbalance of power may cause a deviation in the frequency of the grid from its nominal. The drop or rise of the grid frequency also causes trips offline for generators, equipment damage, and system blackout. To overcome this difficulty, a frequency regulation for grid-connected WT- hydropower plants based on flower pollination optimization algorithm-based Proportional integral derivative (FPOA-PID) controller is put forth in this work. The system consists of two PI controllers for the rotor side converter (RSC), three PI controllers for the grid side converter (GSC) of DFIG, one PID for pitch angle control, and one PID for frequency regulation. The parameters of the frequency regulation controller are tuned using FPOA and particle swarm optimization (PSO) for comparison. The dynamic performance of the system is tested in MATLAB/SIMULINK. Accordingly, the FPOA-based PID for regulation of the grid frequency has a settling time of 1.0106sec, an overshot of 0.0228Hz, an undershot of 0.0289Hz, and the final output frequency of the grid is 50Hz with 0% steady-state error (SSE). In contrast, the PSO based PID controller has a settling time of 1.9406sec, an overshot of 0.02943Hz, an undershot of 0.0375Hz with 0% SSE at 11m/s and 0.05pu load. The FPOA-based PID has better convergence performance than PSO-based PID controllers. The normal operational range of frequency (grid code is between 49.5Hz to 50.5Hz in Ethiopia National Transmission system (ENTS) and the result indicates that, with the FPOA-PID technique, the overall performance of the system showed robustness regardless of the presence of load variations and the wind speed fluctuations. A performance comparison is conducted between the proposed FPOA-PID, PSO-PID, and PI controller schemes to verify the superiority of the suggested technique in the presence of a DFIG-WT and HPP.

Keywords: VSWT, FPOA, PSO, frequency control, optimization, and DFIG.

CHAPTER ONE

1 INTRODUCTION

1.1 Background

Today in the world, the energy from RES technology is a rapidly expanding sustainable energy source. Energy from the wind and hydropower plants don't yield any results, which could damage the environment because the process of power generation will never release any pollutants into the atmosphere. Currently, the world population has increased, and then the need for electricity has increased. So, wind has gained resurrection in popularity, aiding to satisfy the rising energy demand by using sustainable energy sources (T. Burton and N. Jenkins, 2001). Along with conventional power sources, energy from RESs have a great deal of potential to be significant in the energy sector market. RES, like solar, wind, and hydropower, generate electricity with minimal greenhouse gas emissions during their whole lifecycles. The percentage of global electricity generated in 2017 that came from solar and wind power was 1.3% and 4.4%, respectively. However, they are unable to generate electricity consistently and predictably because of their inherent reliance on weather conditions. Wind turbines generate power based on the wind speed; no electricity is produced at all if the wind is too strong or too weak. Therefore, the variable wind speed affects the power quality issue, which subsequently declines the grid frequency.

The wind power generators' output power fluctuation leads large frequency deviation range, which has a certain negative impact on the grid system operations. For instance, the grid frequency deviation has had an impact on modern industrial computer systems control since it can affect equipment damage to computers, erratic operation, system crashes, lamp flickering, data loss, and so on. Lamp flickering has a dangerous result of the frequency difference from its nominal value. Immediately it impacts the human being. In addition, fluctuation in frequency can also lead to lower accuracy in the timing apparatuses found in a variety of household appliances and industrial equipment. It is crucial to note that every piece of generating machinery in electric power is built to work within specific frequency ranges. Every generating plant would be capable of operating continuously at a frequency that is close to the grid's nominal frequency, mostly between the range of 49.5 and 50.5 Hz in Europe as the grid code specified (Standard EN 50160, 2004) (Inigo Martinez de Alegria). We should consider current grid codes for effective frequency control. The integration of wind energy into the grid system, states that the wind farm must be switched off immediately if it exceeds the frequency range of 47.5-51.5 HZ (Kumari S. and Shankar G., 2020). Even if it is within this given range of frequency control deviation is required to keep the frequency near the stated value (B. Singh and S.N. Singh, 2009).

As the history of wind turbines is provided, fixed-speed induction generators are initially designed and operated to prevent the need for additional power electronic converter expenses. But, to improve the efficiency of power conversion, the system with variable speed wind turbine drive is more dominant. DFIG appreciates the variable speed functionality through a smaller size converter to minimize the cost. This explains why the DFIGs are used with wind turbines in widespread. The stator of the generator is directly connected to the grid and a back-to-back (B2B) voltage source converter (VSC) connects the DFIG's rotor to the grid at its nominal frequency (L. Zhang and W. Shepherd, 2017) (Al-Haddad, 2014). Wind turbine grid integration should follow stringent regulations and requirements in many nations.

The development of the DFIG in wind turbines and the mathematical representations and control technique are given in reference (S. Domingos and F. Oliveira, 2018). At present, double-fed wind generators have become one of the main models for commercial operation because of their low cost and good controllability. However, the wind turbine converter decouples the fan of rotor speed from the system frequency (Chaine S. Tripathy M. and Satoathy S., 2015). Optimal correction of the controller's dynamic is a necessary procedure to provide effective frequency control performance.

The conventional PIDs may be inaccurate and ineffective without best optimization tool/technique while the wind turbine's large frequency variations and stochastic behavior are present in actual power (Kumari S. and Shankar G., 2020). To improve the result and to ensure reliable performance in the design and optimization of frequency regulation controllers, along with the dependable performance of load frequency control (LFC) have drawn the interest of academics and industry (Sabahi K. and Badamchizadeh M., 2016) (Srikanth V. and Yadaiah N., 2018).

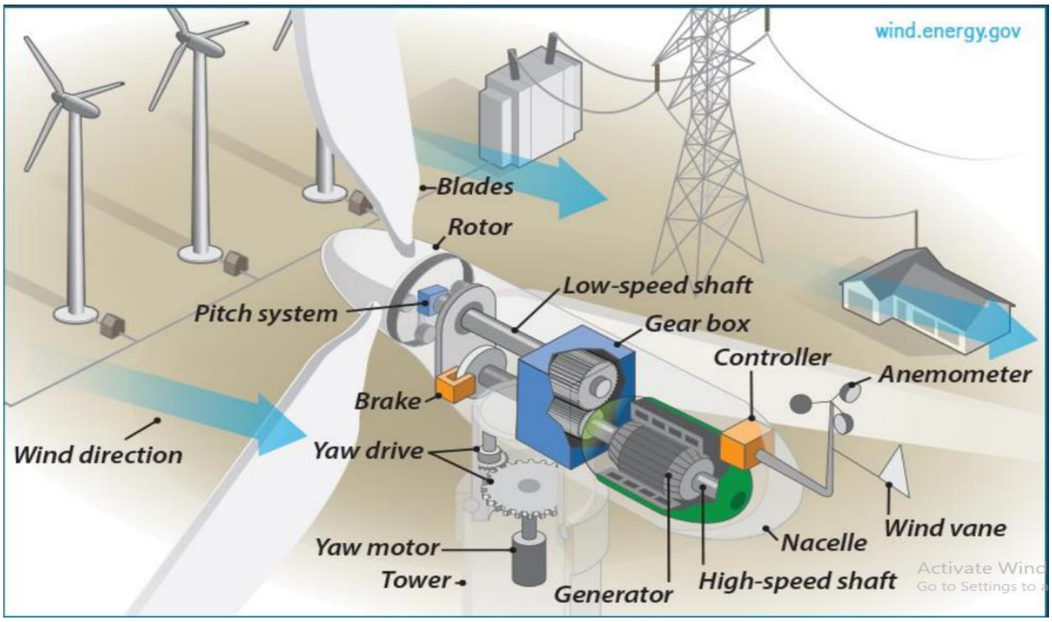

Figure 1.1: Parts of HAWT (Samaneh M., 2021)

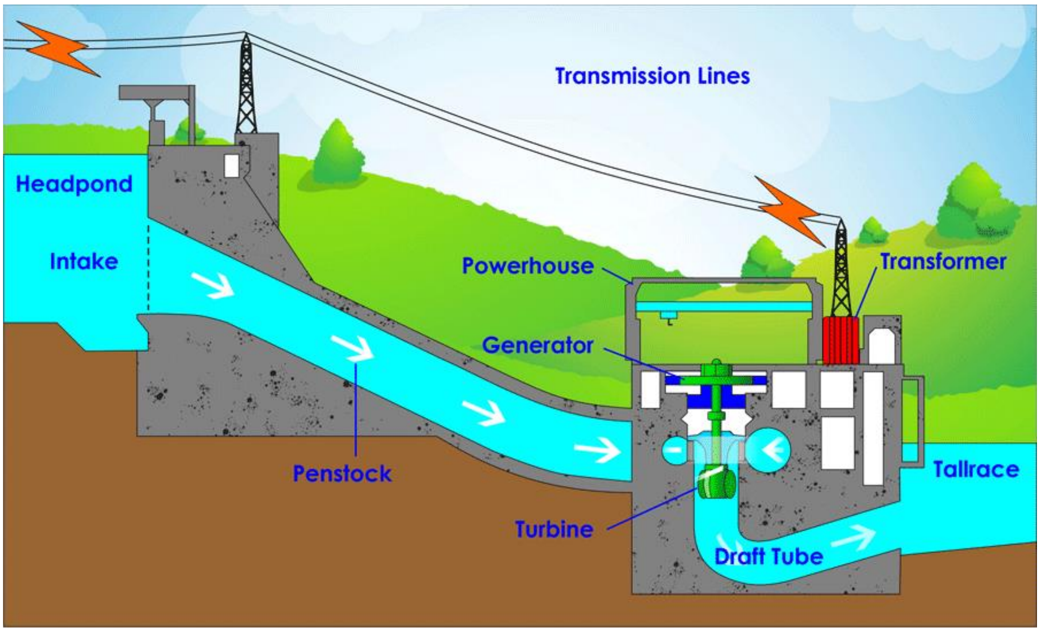

Figure 1.2: Parts of HPP and processes it follows (Khan, 2018)

1.2 Statement of the Problem

Wind energy is the greatest technology of sustainable energy to provide a sustainable supply for global development. However, it is highly unpredictable because it depends on adverse weather conditions. The irregular nature, randomness, and wind speed uncertainty tend to cause wind abandonment. This phenomenon causes a systemic mismatch between supply and demand. Also, this mismatch of energy may result in a frequency variation from its normal value. One of the difficulties of integrated wind and hydropower plants is regulating their rated frequency. The main issue for a large power plant is power generation since changes in load result in steady-state frequency changes. It is impossible to completely prevent frequency deviations that happen when generating electricity, so, keeping a steady frequency at an accepted range is difficult. This variation affects contemporary computer-controlled industrial systems negatively in many different ways like, lamp flickers, system crashes, inaccuracy of timing apparatus, erratic operation, equipment damage to the computer, data loss, and sometimes **system blackout**, etc.

To maintain the frequency during variable wind speed and load variation, factors including load change, nonlinear dynamics, and wind disturbance pose challenges to the system. Traditional control methods i.e., PI, backstepping, and PID may struggle to get the desired level of accuracy and stability under these conditions. To ensure steady, accurate, and safe operations, these challenges require advanced control technique, system modeling, and optimization tool. In this study, a FPOA-based PID controller with automatic generation control (AGC) of HPP was applied. PID controllers are widely used in industry because they effectively manage various control tasks, can handle unexpected disruptions and it is more economical. Additionally, the unknown parameters of the PID controller are optimized using a PSO algorithm.

1.3 Objectives

1.3.1 General Objective

The general objective of this study is to regulate a grid frequency for the hydropower plant-DFIG wind turbine by developing an appropriate PID control strategy using FPOA employing MATLAB/Simulink.

1.3.2 Specific Objectives

- Develop a mathematical model of the aerodynamic part of a wind turbine with a DFIG and variable speed, power electronic converter, HPP, and other components.
- Design the controllers for pitch angle, RSC, GSC, and frequency adjustment.
- Tune parameters of the designed controllers using FPOA.
- Demonstrate the merits of the proposed FPOA-based PID controller with AGC for grid frequency regulation compared with the PSO-based PID controller.
- Test and validate the result of the study with MATLAB/Simulink software.

1.4 Scope

The attention to the regulation of the frequency for grid-connected wind turbine and HPP operating in an imbalance of power generation and demand is given by this study. The mathematical modeling and design of the overall system simulations are the main topics of the study. Derive the overall mathematical models of the system by considering wind speed variation and load disturbances and design of Meta-heuristic (FPOA and PSO) based PID controller using MATLAB/SIMULINK software. The converters' electronics (both generator side and grid side converters) are included in this study.

1.5 Limitations

This study balances supply and demand by reducing the generation power when the load is low and by increasing the generation when the demand for electricity is high. There is no energy storage device to store electricity when there is low demand or excess energy in the system to balance demand and supply without reduction of generating power for grid frequency regulation. And, the systems interact with many components and controllers.

1.6 Significance

Like other sources of energy, the environment can’t be polluted by wind energy. Other sources of energy are causing human economic damage and health issues because they depend on fossil fuel combustion, such as natural gas and coal, which emit matter, carbon dioxide, nitrogen oxides, and sulfur dioxide. Renewable energies are highly demanding energies to replace carbon-based fuels. The efficiency of wind energy, frequency regulation capability, and grid system stability are improved by this shift of energy from fuel-based to renewable sources. This research will not be restricted to the mathematical design, modeling, and simulation of the proposed system it is applicable for real system application since controller is simple, stable, robust and more economical.

1.7 Motivation

Most people who live in remote areas do not have access to electricity. So that, to enhance, and simplify human life and fulfill its central principle for economic development as well as industrialization, electricity is the best solution. Wind turbines that generate electricity for remote and rural areas are the best solution. However, generating power from nuclear fission and fossil fuels has several environmental impacts, i.e. nuclear waste problem and increased concentration of CO2 (carbon dioxide) within the earth’s atmosphere, which produces the greenhouse effect. The development of RES has become a helpful component of the clean energy supply because of the continuous growth of human demand for electricity. Although wind energy and HPP are an abundant resource, they have some effect on the grid when connected to it due to wind speed variation and load fluctuation. Frequency is the measure of the ability of the electrical system to maintain the balance between power production and consumption. However, the system stability is being negatively affected by increased penetration of energy from renewable sources. To reduce risks related to frequency deviation i.e. cascading events and blackouts, the system operates at permissible level or grid code. To overcome damage to wind turbines and to stabilize the frequency of the grid using an FPOA-based PID controller.

1.8 Thesis Organization

This research work is structured as follows:

Chapter One: The thesis background, problem statement, objectives, scope, limitations, significance, and motivation of the study are explained in this chapter.

Chapter two: Theoretical background of wind turbines, DFIG, and kinds of literature related to this thesis are presented.

Chapter three: Materials used, methods to follow, mathematical modeling, and controller design of the system are described. In addition, the optimization algorithms (FPOA and PSO) are presented.

Chapter four: Deals with results and discussions on the proposed controller and optimization techniques.

Chapter Five: Summarizes the contributions of this research, concludes, and the recommendation for further works.

CHAPTER TWO

2 BASIC THEORIES AND RELATED WORKS

2.1 Basic Theories

The theoretical background of the study, and literature related to this thesis are reviewed in this section to explore the gaps in frequency regulation and possible solutions.

RES control system is a very attractive area for many researchers. Many scholars have studied this area standing with the most advanced technology. To perform a variety of tasks the proper combination of pitch actuator, drive train, generator, and controller is a mandatory technique for WT similarly for HPP, penstock, turbine, generator and control system are necessary. The two generators that energy conversion systems (WECS) utilize the most frequently are synchronous generators with permanent magnet (PMSG) and double-fed induction generators (DFIG)

Table 2.1: Comparisons between DFIG and PMSG

DFIG	PMSG
Variable speed (VS) is employed with a frequency converter of partial scale.	VS is employed with a frequency converter of full-scale
Coupled to a WT through a gearbox which increases power loss and cost for its maintenance.	A full-scale converter is integrated into the grid (gearless) so that the generated electricity passes through this converter 100%.
Requires external excitation and rotor control.	Excited by a permanent magnet and does not need rotor control. The need for large quantities of permanent magnets limits the application of PMSG.

The non-dispatchable and natural intermittent features of wind negatively impact the system's frequency regulation ability. Today different control systems are designed by applying various control algorithms to determine the best parameters of the controller that will yield the best solutions.

Table 2.2 shows the duration for which the power grid capability of operating on various frequency ranges, deviating from a reference value (50Hz) in Ethiopia and Table 2.3 is European countries' grid code.

Table 2.2: National Grid Code (Frequency ranges) in Ethiopia National Transmission System (ENTS) (Ethiopia Electricity Authority (EEA), 2018)

Frequency limit ranges (Hz)	**Duration**
49.5 – 50.5	Normal Operation.
49 – 49.5 or 50.5 – 51	Operate for 60 minutes.
48 – 49 or 51 – 51.5	Operate for 30 minutes.
47.5 – 48	Operate for 3 minutes.
47 – 47.5 or 51.5 – 52.5	Operate for 20 seconds.
< 47 for greater than 0.2 sec	The system may disconnect.
> 52.5 for greater than 4 sec	The system must disconnect.

Table 2.3: Range of frequency and period for operation (European, 2018)

Countries	**Range of frequency (Hz)**	**Duration**
Great Britain	47 – 47.5	20 sec
	47.5 – 48.5	90 min
	48.5 – 49	Determined by each TSO, not <90 min
	49 – 51	Unlimited
	51 – 51.5	90 min
	51.5 – 52	15 min
Continental Europe	47.5 – 48.5	Determined by each TSO, not < 30 min
	48.5 – 49	Determined by each TSO, not < period of 47.5 – 48.5
	49 – 51	Unlimited
	51 – 51.5	30 min
Nordic	47.5 – 48.5	30 min
	48.5 – 49	Determined by each TSO, not < 30 min
	49 – 51	Unlimited
	51 – 51.5	30 min
Northern Ireland	47.5 – 48.5	90 min
	48.5 – 49	Determined by each TSO, not < 90 min
	49 – 51	Unlimited

	51–51.5	90 min
Baltic	47.5–48.5	Determined by each TSO, not < 30 min
	48.5–49	Determined by each TSO, not < period of 47.5–48.5
	49–51	Unlimited
	51–51.5	Determined by each TSO, not < 30 min

2.2 VSWT Operation Area

WT operates under four different operation regions. Based on the specifications outlined in this proposed study, Figure 2.1 below illustrates the link between wind speed and power output. In the Figure the first region (parking mode) is the region having a speed less than cut-in (3m/s). For economic purposes, it is not recommended for a WT to operate in the cut-in WS. The second region (MPPT mode) (3m/s-11m/s) is between cut-in and rated wind speed. The cut-in WS is the lowest speed of wind that must be captured to start producing electricity.

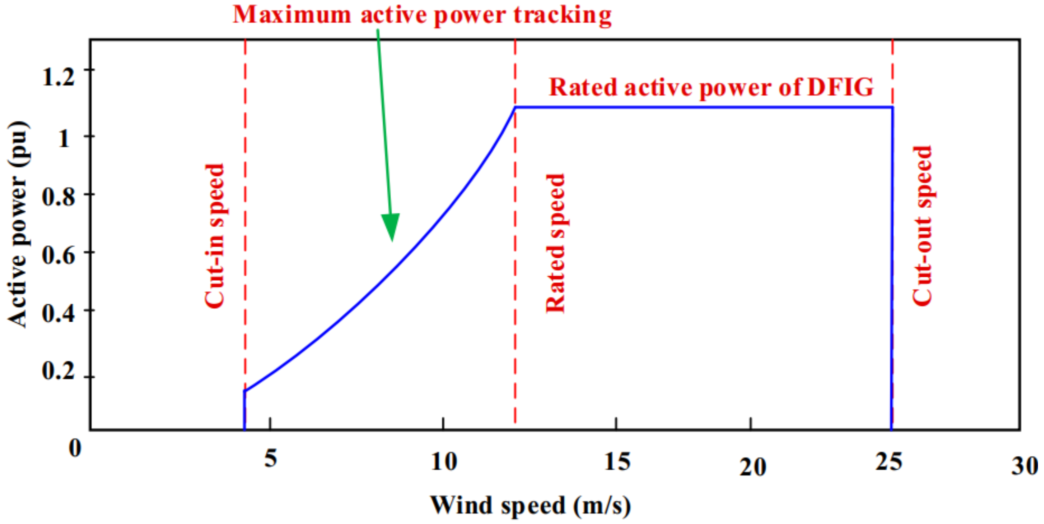

Figure 2.1: Output power VS wind speed curve (Tadesse, 2022)

The third region (constant power region) (11m/s-25m/s) is between rated and cut-out WS. Pitch angle adjustment is required in this situation to maintain the generator's torque and power consistent. To keep the generator’s output power within the accepted range, the rotor must face away from the strong wind stream. To do this, pitch angle control is used. The last region (> 25m/s) is above cut-out wind speed, which anticipates shutting down to prevent damage.

2.3 Related Works on Frequency Regulation

In this section, some earlier works related to frequency regulation were reviewed based on controller performance, cost-effectiveness, Controller complexity, transient response characteristics, and optimization method.

The design of two controllers in frequency regulation has been developed (Michael Z. Bernard, 2019**.** This work suggests a novel approach to frequency management that combines an MPC with a conventional PI controller in the face of uncertainty caused by governor and wind turbine parameters fluctuation. This paper carried out a performance comparison between the traditional PI control, MPC, and PI-MPC (proposed control) and verified the superiority of PI-MPC in the presence of DFIG WT on the one-area power system. The drawback of this study is that it doesn’t consider control challenges. MPC controller is not able to respond quickly enough to unexpected changes in the system, such as a sudden increase in load and disturbance outside prediction might not be accounted for, but the wind speed characteristics are unpredictable. In addition, it didn’t use any optimization algorithm for optimal control of grid frequency.

The dynamic model and control of grid frequency have been developed in (Zhiwei Wanga, Xiangyu Lyu, 2023). This paper evaluates and compares the performance of conventional PI, cloud PI, and fuzzy PI controllers for frequency regulation. The cloud parameters are successfully addressing the issue with bad parameters in typical PI controllers. When using the traditional PI control, the area power grid's frequency exhibits obvious variation features. The corresponding frequency deviation also exhibits significant fluctuation. Here, cloud PI is more effective than fuzzy PI. However, the simulation of the system with the proposed controller shows a large settling time. So, it verified the low-performance improvements of the suggested technique for random wind power and load.

AGC was applied to frequency control (Chao L. and Qingquan L, 2022)**.** This paper uses a multi-objective Mayfly Optimization (MMO) algorithm to tune AGC for frequency regulation of wind turbines compares it with other optimization techniques and verifies that it is the best. The drawbacks of this paper are there is no clear mathematical model of the system and the result shows a significant overshoot, the system response went above the set-point value when the load decrease, which reduces the designed system's performance. This paper recommended that to further improve system frequency response and economic benefits, a wind energy system is equipped with a PID controller.

Automatic generation control and secondary frequency adjustment of the grid system were implemented in (Xu, 2023). In this research paper, AGC was introduced and a double-fed induction generator (DFIG) was established for frequency regulation. The author concludes that the proposed AGC strategy offers a promising approach for enhancing frequency control performance. However, the proposed AGC control law results were not well displayed. Moreover, AGC without any optimization and or alone is not effective for frequency control. The author recommended that a pitch angle controller be designed for effective control of the grid frequency when the wind speed exceeds its rated value in addition to automatic generation control.

PI Controller of the LFC optimized to enhance dynamic response has been developed (D. Lakshmi, and A. Peer Fathima, 2016) using a novel FPOA technique. As a result, after comparing the performance of Ziegler-Nichols and FPOA on a PI controller, FPOA was selected to optimize the controller parameters with improved ITAE. Also, the research presented by (Stephen O. and Zenghui W, 2022) shows the effectiveness of FPOA for improving the LFC's efficiency by providing optimal parameters for FOPID by comparing it with teaching learning-based optimization (TLBO), Salp swarm algorithm (SSA), and differential evolution (DE). Therefore, FPOA is a strong option for optimizing PID controllers in frequency regulation due to its better performance.

In general, the variable load characteristics and robustness to wind speed changes make it a difficult task for maintaining constant frequency. Several robust and optimal control methods have been developed for improving frequency regulation for WECS, they all required suggested replacement of the conventional controller utilizing a new robust control system, however, rather than replacing the traditional controller using a robust control system, this study suggests a newly robust control method that combines PID controller with newly developed Metaheuristic algorithm, precisely, for grid frequency regulation. This technique is more economical, so that, PID control system will generate a more powerful control signal to govern the entire system instead of using complex and most expensive controllers. Within this work, the model of the DFIG-WT and the overall system was achieved based on metaheuristics (FPOA and PSO) algorithm-based PID controller to effectively control grid frequency.

CHAPTER THREE

3 SYSTEM MODELING AND CONTROLLER DESIGN

3.1 Introduction

Within this section, the methodology, which includes materials used and methods followed in carrying out the study, is explained. The aerodynamics, the pitching actuator, the DFIG, the power electronic converter modeling, HPP model, the controller used for frequency regulation, and other components of the system that contribute to achieving the objective are explained. Also, the controller parameters are tuned using FPOA and PSO based on fitness function (IAE).

3.2 Materials Used

MATLAB/2023a software is used for simulation to test and analyze the system model of this thesis. This software is general-purpose computing software that consists of a broad range of toolboxes. For performing numerical solutions and graphical user interfaces, it has a high-level mathematical package design. Also, MS Office 2016 is used to write the whole documentation rather than equations; and MathType is used to prepare the equations.

3.3 Methods to Follow

The techniques employed in this research to perform the required aims mainly focus on software algorithms. All the tasks that needed to be performed were developed using a flowchart.

Figure 3.1 illustrates the method followed to accomplish this thesis, which starts from the literature related to this thesis title to explore the gap and possible solutions for the problem. Following thorough studies, the mathematical modeling is determined from different sources. The wind turbine, generator, and other specifications are taken from the Adama-II wind farm, and some specifications taken from the literature are used. After the overall dynamic model is obtained for improving WT and HPPs' capacity to regulate their frequency, the controller design is carried out, and the controller's parameters are tuned using metaheuristic algorithms (FPOA and PSO). Then, the simulation is implemented using MATLAB/Simulink.

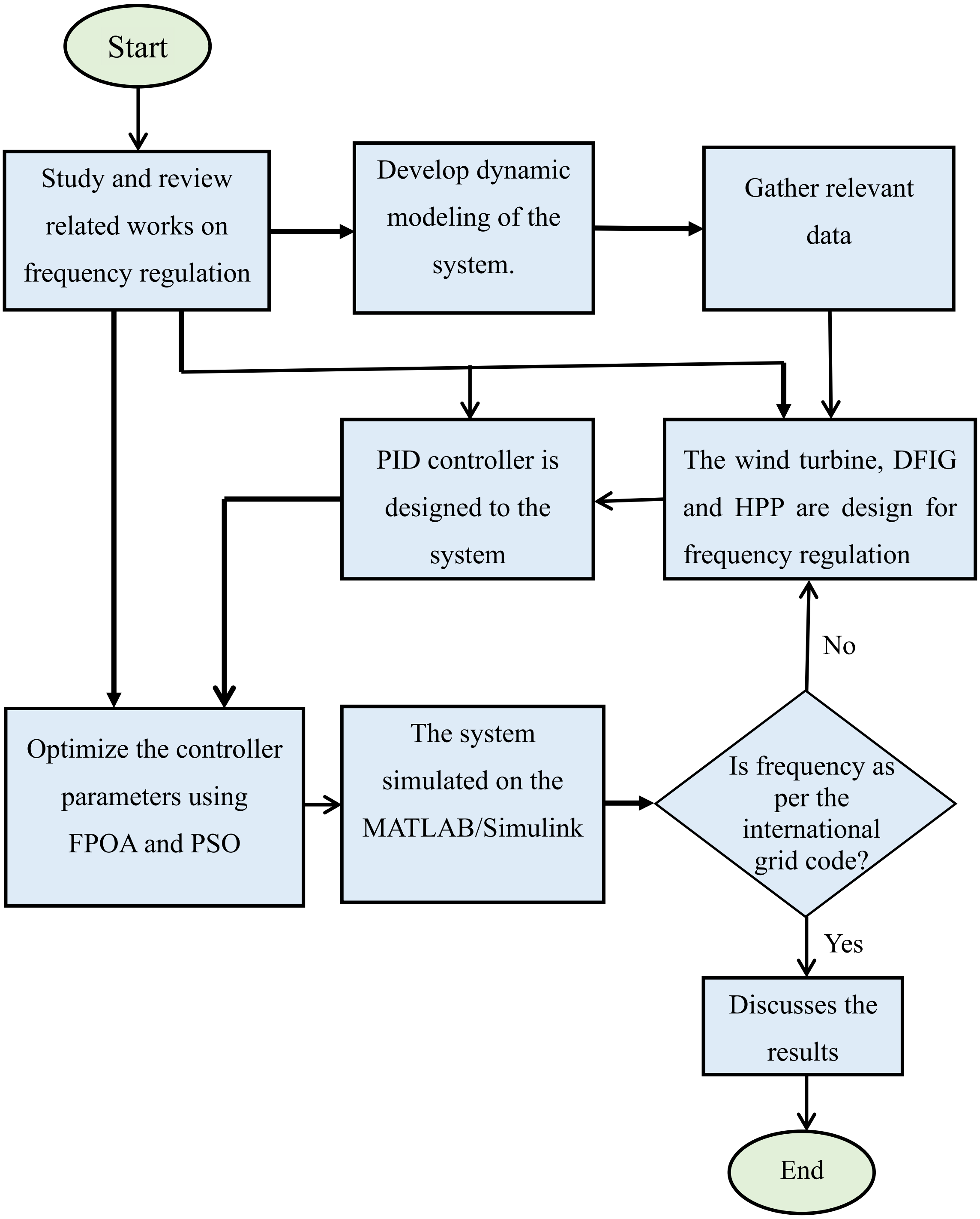

Figure 3.1: Workflow of the thesis

3.4 Block Diagram for Frequency Regulation

Figure 3.2 illustrates the suggested block diagram for the frequency regulation of HPP and WT. The system, by nature, is highly nonlinear, unstable, and complex. Thus, a controller is required to keep the system stable.

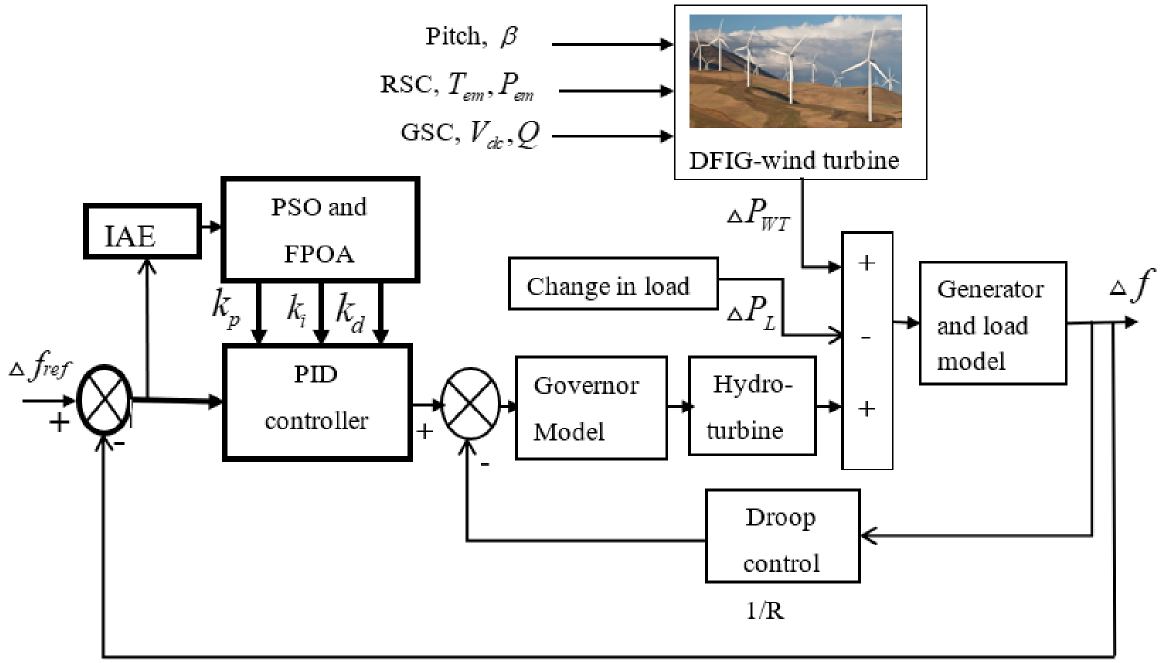

Figure 3.2: Block diagram for frequency regulation

Initial/reference frequency deviation is normally zero. The error between the reference and measured frequency deviation is minimized by using a frequency regulator. For this, a FPOA based PID controller is proposed. Direct and quadrature current of both RSC and GSC and their corresponding reference currents are controlled by using the PI controller.

3.5 Mathematical Modeling of WECS

The mathematical representations of the main WECS parts, including the DFIG, aerodynamic (WT blade), drive train, actuator system, power electronic converter, and HPP are presented in this section. Therefore, the WECS model is identified mathematically after the modeling of each component. In the modeling of WECS, the system consists of mechanical, electrical, and control systems. An aerodynamic system, pitch system, and shaft are the mechanical components of the wind turbine.

3.5.1 Aerodynamic for Wind

The science of aerodynamics is concerned with the properties of moving air, solid bodies, and air interaction. If an object with mass, M , and velocity, V undergoes a constant acceleration, its kinetic energy is equal to the work, K_e, it does to move from rest to a certain distance, S, under the influence of a force, F. And then apply Newton's second law:

$$K_e = W = F \times S \tag{3.1}$$

$$F = M\,a \tag{3.2}$$

Substituting Equation (3.2) into Equation (3.1) gives

$$K_e = Ma\,S \tag{3.3}$$

From the kinematics of solid motion:

$$V^2 = u^2 + 2a\,S \tag{3.4}$$

Since the object starts from rest, the object's initial velocity is zero and then we solve for acceleration.

$$V^2 = 0 + 2a\,S$$

$$a = \frac{V^2}{2S} \tag{3.5}$$

Substituting Equation (3.5) into Equation (3.3) yields

$$K_e = M\,\frac{V^2}{2S}\,S$$

$$K_e = \frac{1}{2} M V^2 \tag{3.6}$$

To formulate this kinetic energy, it is assumed that the solid's mass is constant. Again, assume air density doesn't change with altitude or temperature. The wind moving with a velocity, V_{wind}, has power, P_{wind}, which is the kinetic energy change rate.

$$P_{wind} = \frac{dK_e}{dt} = \frac{d(\frac{1}{2}MV^2)}{dt} = \frac{1}{2}\frac{dM}{dt}V_{wind}{}^2 \tag{3.7}$$

dM/dt is the rate of change mass.

$$\frac{dM}{dt} = \rho A V_{wind} \tag{3.8}$$

Equation (3.8) is substituted into equation (3.7):

$$P_{wind} = \frac{1}{2}\frac{dM}{dt}V_{wind}{}^2 = \frac{1}{2}\rho A V_{wind}{}^3 \tag{3.9}$$

But, $A = \pi R_b{}^2$, then the power available in the wind is:

$$P_{wind} = \frac{1}{2}\rho\pi R_b{}^2 V_{wind}{}^3 \tag{3.10}$$

Where A, R_b, V_{wind} and ρ are the swept area, blade radius, wind speed, and air density, respectively. From Equation (3.10), we can see that the wind power is proportional to the cube of wind speed and the square of the blade radius. Therefore, small variations of both wind speed and rotor radius make the extracted wind power large. However, because some kinetic energy remains in the wind after it passes through the turbine blades, it is difficult to fully extract the wind's kinetic energy. So, it captures a portion of the wind as the power coefficient, according to Albert Betz (Jayshree P. and Vijayakumar V., 2021).

3.5.2 Model of Wind Turbine

Equation (3.11) represents the mechanical power extracted by the blades of the turbine, which is the difference in power between the upstream and downstream.

$$P_{mech} = \frac{1}{2}\rho A V_{wind}(V_1^2 - V_2^2) \quad (3.11)$$

Where V_1 and V_2 are the up and downstream wind speeds at the exit and inlet of the rotor blade. The wind turbine's swept area is provided as follows:

$$A = \pi R_b^2 \quad (3.12)$$

From Equations (3.11) and (3.12), the generated power from WTs can be extracted as follows:

$$P_{mech} = \frac{1}{2}\rho \pi R_b^2 V_{wind}(V_1^2 - V_2^2) \quad (3.13)$$

A blade tip speed ratio can be produced by these down and upstream wind speeds. V_{wind} is the average of these two speeds (Y. D. S. A. H. M. M. M.Iqbal A,, 2020).

$$V_{wind} = (V_1 + V_2)/2 \quad (3.14)$$

Substituting Equation (3.14) into Equation (3.13) gives

$$P_{mech} = \frac{1}{2}\rho \pi R_b^2 (\frac{V_1 + V_2}{2})(V_1^2 - V_2^2) \quad (3.15)$$

$$P_{mech} = \frac{1}{2}\rho \pi R_b^2 (\frac{V_1}{2}(V_1^2 - V_2^2) + \frac{V_2}{2}(V_1^2 - V_2^2)) \quad (3.16)$$

$$P_{mech} = \frac{1}{2}\rho \pi R_b^2 V_1^3 \left(1 + \left(\frac{V_2}{V_1}\right) - \left(\frac{V_2}{V_1}\right)^2 - \left(\frac{V_2}{V_1}\right)^3\right) \Big/ 2 \quad (3.17)$$

The power conversion coefficient, C_p, can be obtained from Equation (3.17):

$$C_p = \left(1 + \left(\frac{V_2}{V_1}\right) - \left(\frac{V_2}{V_1}\right)^2 - \left(\frac{V_2}{V_1}\right)^3\right) \Big/ 2 \quad (3.18)$$

The ratio of tip speed λ_{wt} is the ratio of WT's blade tip speed to wind speed.

$$\lambda_{wt} = V_2/V_1 = \text{Blade tip speed / wind speed} \quad (3.19)$$

The power coefficient from Equation (3.18) can be rewritten as follows:

$$C_p = \frac{(1+\frac{V_2}{V_1})(1-\left(\frac{V_2}{V_1}\right)^2)}{2} \tag{3.20}$$

The tip speed ratio λ_{wt} can be used to determine the power coefficient, which is,

$$C_p = (1+\lambda_{wt})(1-\lambda_{wt}^2)/2 \tag{3.21}$$

The available wind energy is related to generated energy by WT through C_p. It is crucial to effectively measure the conversion of wind energy into mechanical energy. The power coefficient has no fixed value; depending on the turbine ratio of tip speed and turbine angle of blade pitch in a nonlinear relationship. The coefficient of power, C_p of the wind turbine depends on λ_{wt} and β, and the following can be used to express the mechanical power of Equation (3.13):

$$P_{mech} = \frac{1}{2}\rho\pi R_b^2 V_1^3 C_p(\lambda_{wt}, \beta) \tag{3.22}$$

When we differentiate C_p to λ_{wt}, we get the maximum value of C_p by equating to zero.

$$\frac{dC_p}{d\lambda_{wt}} = \frac{d}{d\lambda_{wt}}\left(\frac{(1+\lambda_{wt})(1-\lambda_{wt}^2)}{2}\right) = 0 \tag{3.23}$$

$$\frac{dC_p}{d\lambda_{wt}} = \frac{1}{2}\frac{d}{d\lambda_{wt}}(-\lambda_{wt}^3 - \lambda_{wt}^2 + \lambda_{wt} + 1) = 0 \Rightarrow -\frac{3}{2}\lambda_{wt}^2 - \lambda_{wt} + \frac{1}{2} = 0$$

$$\lambda_{wt} = -1 \text{ or } 1/3$$

Then substituting each value of λ_{wt} into Equation (3.21),

$$C_p = \begin{cases} 0, \text{ for } \lambda_{wt} = -1 \\ 0.593, \text{ for } \lambda_{wt} = 1/3 \end{cases}$$

This means that no more than 59.3% of the kinetic energy of the wind is converted into mechanical energy. The Betz limit is not reached in the real world, even though the best-designed wind turbines exist. As the rotor turns slowly and the wind flows between the rotor blades, a minimum energy gain is achieved. The optimum ratio of wind speed to tip speed must be built into the design of the wind turbine to extract as much energy as possible from it.

The WT's power coefficient can be determined according to the tip speed ratio λ_{wt} and the pitch angle β as follows in Equation (3.24) (Tadesse, 2022).

$$C_p(\lambda_{wt},\beta)=0.5176((116/\lambda_{wti})-0.4\beta-5)\exp(-21/\lambda_{wti})+0.0068\lambda_{wt} \quad (3.24)$$

$$1/\lambda_{wti}=1/(\lambda_{wt}+0.08\beta)-0.035/(1+\beta^3) \quad (3.25)$$

$$\lambda_{wt}=\omega_t.R_b/V_{wind} \quad (3.26)$$

Since the wind speed is very difficult to estimate, it is better to calculate the maximum power without taking the wind speed into account.

$$V_{wind}=\omega_t.R/\lambda_{wt}$$

$$P_{mech}=P_{wind}C_p(\lambda_{wt},\beta) \quad (3.27)$$

$$P_{mppt}=\frac{1}{2}\rho\pi R_b{}^2V_{wind}^2C_{pop}=\frac{1}{2}\rho\pi R_b{}^2(\omega_t.R/\lambda_{wtop})^3C_{pop} \quad (3.28)$$

Where λ_{wtop} and C_{pop} are the optimal values of tip speed ratio and power coefficient, respectively. The optimal power is also obtained if

$$C_p(\lambda_{wt})=C_p(\lambda_{wtop})=C_{p\max}$$

$$P_{opt}(\omega_t)=1/2(\rho\pi R_b{}^2(\omega_t.R_b/\lambda_{wtop})^3C_{pop})$$

$$P_{opt}(\omega_t)=\frac{1}{2}\frac{\rho\pi R_b{}^5C_{p\max}}{\lambda_{wtop}{}^3}\omega_{top}{}^3$$

$$P_{op}(\omega_t)=\ell_{opt}*\omega_{top}{}^3 \quad (3.29)$$

Where, P_{op} is the optimal value of mechanical power and ℓ_{op} is given by

$$\ell_{op}=\rho\pi R^5C_{p\max}/2\lambda_{wtop}{}^3 \quad (3.30)$$

From the rotational speed value, the optimal torque is calculated as follows:

$$\tau_{op}(\omega_t)=\frac{P_{op}(\omega_t)}{\omega_t}=\frac{1}{2}\frac{\rho\pi R_b{}^5C_{p\max}}{\lambda_{wtop}{}^3}\omega_{top}{}^2 \quad (3.31)$$

Hence, achieving optimal performance requires applying the load torque.

$$\tau_{op}(\omega_t)=\ell_{op}*\omega_{top}{}^2 \quad (3.32)$$

The DFIG characteristics must be considered to get maximum electrical generator power output. The turbine torque is also calculated from the rotational turbine speed.

$$\tau_t=P_{mech}/\omega_t \quad (3.33)$$

Wind turbine blade geometry is required to achieve the highest possible mechanical power. δ_b is dimensionless blade coefficient expressed by the ratio of the blade sections from local blade radius ‘r’ to the maximum blade radius, R_b , $\delta_b\in[0,1]$.

$$\delta_b = \frac{r}{R_b} \tag{3.34}$$

To improve the value of the power coefficient, we must get an optimal tip-speed ratio using the blade geometry principle.

$$\tan(\phi) = \frac{1-1/3}{\lambda_{wt}\delta_b(1+2/9\,\lambda_{wt}{}^2\delta_b{}^2)} \tag{3.35}$$

Substituting the Equations (3.33) and (3.34) into Equation (3.35) and when 'r' approaches to maximum blade radius then we can get:

$$\tan(\phi) = \frac{2R_b}{3r(\frac{\omega_t.R_b}{V_{wind}})} \Rightarrow \phi = \tan^{-1}(\frac{2V_{wind}}{3R_b\omega_t})$$

The pitch angle can be determined from the angle that is the rotor plane relative to the inflow angle and twist angle as follows.

$$\beta = \phi - \theta = \tan^{-1}(\frac{2V_{wind}}{3R_b\omega_t}) - \theta \tag{3.36}$$

Where, ϕ, θ are in flow angle and twist angle. Finally, the rotor angular speed is given by the following equation:

$$\omega_t = \frac{2V_{wind}}{3R_b\tan(\beta+\theta)} \tag{3.37}$$

For a typical optimal value $V_{\text{wind}} = 11\text{m/s}$, $R_b = 38\text{m}$, β=0^0 and $\theta = 6.0126^0$, ω_{trated} becomes

$$\omega_{\text{trated}} = \frac{2*11}{3*38\tan(0+6.0126)} = 1.8032\text{rad/sec} \tag{3.38}$$

3.5.3 Pitch actuator Modeling and its Controller Design

The pitch mechanism is necessary to rotate all the blades at similar or different angles. To do this the pitch control technique is a basic approach for adjusting rotational wind turbine's speed. Wind turbines with pitch control features have controllable blades along their longitudinal axis.

In an electrical pitch drive, each blade can be individually controlled by a servo motor. In this research, as an actuator DC servo motor is used. Since this pitch technique is more accurate, has a fast-dynamic reaction, requires less maintenance, and is simpler, they are more common nowadays. The dynamic characteristics between the measurement of a pitch angle β and a pitch demand β_{ref} from the pitch controller are described by the actuator model. Mathematically this is written as:

$$\frac{d\beta}{dt} = 1/\tau_p (\beta_{ref} - \beta) \tag{3.39}$$

Where, β_{ref} , β and τ_p are reference, measured and time constant of pitch angle, respectively. Rearranging Equation (3.39) we can get:

$$\tau_p \frac{d\beta}{dt} = \beta_{ref} - \beta \tag{3.40}$$

Applying Laplace transform both sides of Equation (3.40) we get:

$$\beta_{ref}(s) = (\tau_p s + 1)\beta(s) \tag{3.41}$$

In terms of the transfer function Equation (3.41) is expressed as follows:

$$\frac{\beta(s)}{\beta_{ref}(s)} = \frac{1}{\tau_p s + 1} \tag{3.42}$$

We simplify the inner closed loop of the pitch actuator and for this study assume $\tau_p = 0.01$ to increase the control effort and to get a direct relation between β_{ref} and β ; finally,

$$\frac{\beta(s)}{\beta_{ref}(s)} = \frac{1}{0.01s + 1} \tag{3.43}$$

The controller of the pitch actuator is PID as indicated in Figure 3.3. Its parameters are determined by using the Routh array considering the pitch actuator system stability as seen in Table 3.1.

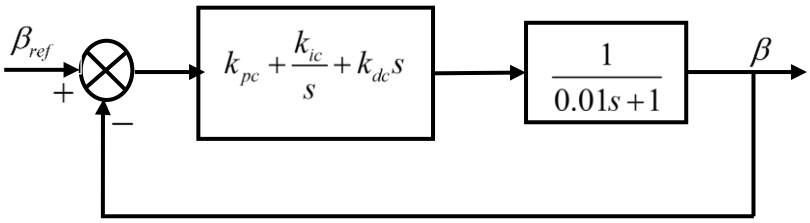

Figure 3.3: Pitch with PID controller

$$g(s) = (k_{pc} + \frac{k_{ic}}{s} + k_{dc}s) * \frac{1}{0.01s + 1}$$

$$g(s) = \frac{k_{dc}s^2 + k_{pc}s + k_{ic}}{0.01s^2 + s} \tag{3.44}$$

$$h(s) = 1 \tag{3.45}$$

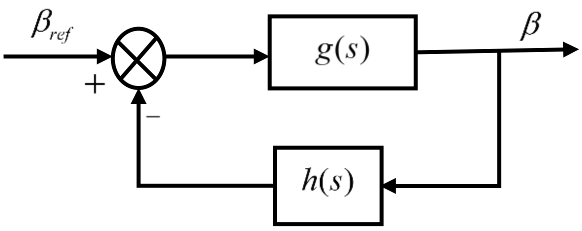

Figure 3.4: Closed-loop for pitch control

The closed-loop characteristic equation can be calculated as

$$1+g(s)h(s)=1+\frac{k_{dc}s^2+k_{pc}s+k_{ic}}{0.01s^2+s}=0 \quad (3.46)$$

$$(0.01+k_{dc})s^2+(1+k_{pc})s+k_{ic}=0 \quad (3.47)$$

Table 3.1: Routh array for stability of pitch angle

s^2	$0.01+k_{dc}$	k_{ic}
s^1	$1+k_{pc}$	0
s^0	$\frac{(1+k_{pc})*k_{ic}-0*(0.01+k_{dc})}{(1+k_{pc})}=k_{ic}$	0

From the above Table, the boundary of controller gain can be given by stability condition of the same sign:

$$\begin{cases} 0.01+k_{dc}>0 \Rightarrow k_{dc}>-0.01, \\ 1+k_{pc}>0 \Rightarrow k_{pc}>-1, \\ k_{ic}>0. \end{cases} \quad (3.48)$$

Using Equation (3.48) which putted in Table 3.6, the PID controller gain for pitch angle have optimal value in Table 3.7 after formulating fitness function and applying optimization tool.

3.5.4 Model of a Drive Train

The drive train is the mechanical components of the wind turbine that connect the rotor of the turbine to the DFIG. It consists of a gearbox, a rotor shaft, which consists of a slow and a fast-rotating shaft, and a coupling with the generator. To adjust the rotational speed of the high-speed shaft, the rotational speed is increased by the gearbox. The high-speed shaft is then connected to the DFIG, which converts mechanical energy into electrical energy.

The turbine rotor dynamic response is operated at a speed (τ_t) by the turbine torque (τ_t) as indicated in Equation (3.33). The generator's electromagnetic torque τ_{em} acts as a brake and is driven by the fast-speed shaft torque τ_{hss} .

$$J_t\frac{d\omega_t}{dt}=\tau_t-\tau_{lss}-D_t\omega_t \quad (3.49)$$

$$J_g \frac{d\omega_g}{dt} = \tau_{hss} - \tau_{em} - D_g \omega_g \tag{3.50}$$

3.5.5 Model of Double-Fed Induction Generator (DFIG)

A mathematical representation of the DFIG is the primary requirement both for analysing the steady-state and dynamic properties of WECS and for developing algorithms to control the machine. Several important assumptions need to be made before constructing the DFIG's mathematical model.

- It is symmetric in structure.
- It has a balanced three-phase system: the voltage and current waveforms have the same amplitude and are separated by 120 degrees.
- Due to eddy currents and hysteresis in the iron core of the generator, the stator and rotor's magnetic cores are linear and have negligible core losses.
- The rotor and stator mutual inductances are neglected: This is because the mutual inductance is relatively small compared to the rotor and stator windings' self-inductances.

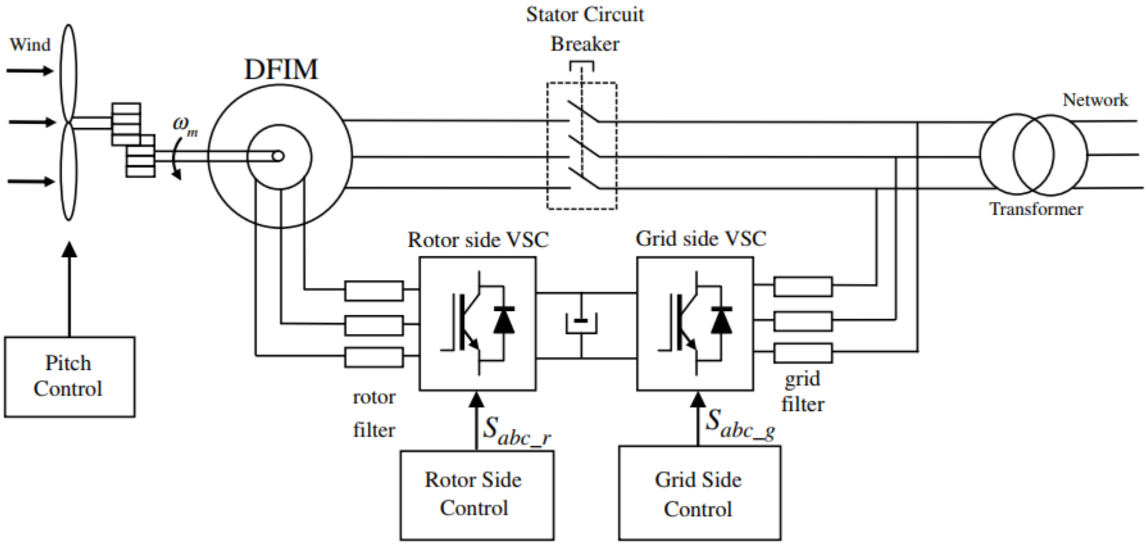

Figure 3.5: DFIG-based wind turbine system configuration (Wiley, 2011)

Under the idealized model, the magnetic linkage fluxes, voltages, and stator currents of the DFIG can be expressed by the following equations:

$$V_{3\phi s} = R_{st} i_{3\phi s} + p\lambda_{3\phi s} \tag{3.51}$$

$$V_{3\phi r} = R_r i_{3\phi r} + p\lambda_{3\phi r} \tag{3.52}$$

To make a simpler analysis of electrical generators and to enable the MATLAB simulation in WECSs, 3ϕ Stationary frame, (abc), 2ϕ synchronous frame, (dq) and stationary frame, ($\alpha\beta$) are the most common reference frames used in WECSs.

A) $\alpha\beta / abc$ and $abc / \alpha\beta$ transformation

Based on the notation for space vectors, 3ϕ magnitudes can be alternatively way to describe via the two-phase magnitudes of the same rotating space vector (Y_α & Y_β) in the complex real-imaginary plane. This fact can be represented mathematically as

$$Y = Y_\alpha + jY_\beta = \frac{2}{3}(Y_a + aY_b + a^2 Y_c) \tag{3.53}$$

Where Y maybe voltage, current, or flux and $a = e^{j(2\pi/3)}$.

The constant 2/3 in Equation (3.53) is selected to scale the space vectors following the peak amplitude of the 3ϕ magnitudes. The parameters of the space vector can be determined from the magnitudes of the abc can be used to derive the $\alpha\beta$ components of the space vector by substituting the value of a into equation (3.53) as follows:

$$\begin{aligned} Y_\alpha &= \mathrm{Re}\{Y\} = \frac{2}{3}(Y_a - \frac{1}{2}Y_b - \frac{1}{2}Y_c) \\ Y_\beta &= \mathrm{Im}\{Y\} = \frac{1}{\sqrt{3}}(Y_b - Y_c) \end{aligned} \tag{3.54}$$

We can express Equation (3.54) in matrix form as follows:

$$\begin{bmatrix} Y_\alpha \\ Y_\beta \end{bmatrix} = \frac{2}{3}\begin{bmatrix} 1 & -1/2 & -1/2 \\ 0 & \sqrt{3}/2 & -\sqrt{3}/2 \end{bmatrix}\begin{bmatrix} Y_a \\ Y_b \\ Y_c \end{bmatrix} \tag{3.55}$$

$$\begin{bmatrix} Y_a \\ Y_b \\ Y_c \end{bmatrix} = \begin{bmatrix} 1 & 0 \\ -1/2 & \sqrt{3}/2 \\ -1/2 & -\sqrt{3}/2 \end{bmatrix}\begin{bmatrix} Y_\alpha \\ Y_\beta \end{bmatrix} \tag{3.56}$$

B) $\alpha\beta / dq$ and $dq / \alpha\beta$ transformation

The angle for transformation is calculated by using the phase-locked loop method.

$$\begin{bmatrix} Y_d \\ Y_q \end{bmatrix} = \begin{bmatrix} \cos\theta_{ele\_sh} & \sin\theta_{ele\_sh} \\ -\sin\theta_{ele\_sh} & \cos\theta_{ele\_sh} \end{bmatrix}\begin{bmatrix} Y_\alpha \\ Y_\beta \end{bmatrix} \tag{3.57}$$

$$\begin{bmatrix} Y_\alpha \\ Y_\beta \end{bmatrix} = \begin{bmatrix} \cos\theta_{ele\_sh} & -\sin\theta_{ele\_sh} \\ \sin\theta_{ele\_sh} & \cos\theta_{ele\_sh} \end{bmatrix}\begin{bmatrix} Y_d \\ Y_q \end{bmatrix} \tag{3.58}$$

Where, θ_{ele_sh} is the shaft's electrical angular position.

DFIG is composed of three sets of equations: motion, flux linkage, and voltage equations. The voltage equations for the generator's stator and rotor in the arbitrary reference frame are given by:

$$\begin{cases} V_{st} = R_{st} i_{st} + \dfrac{d\lambda_{st}}{dt} + j\omega_{arf}\lambda_{st} \\ V_{ro} = R_{ro} i_{ro} + \dfrac{d\lambda_{ro}}{dt} + j(\omega_{arf} - \omega_{el})\lambda_{ro} \end{cases} \tag{3.59}$$

Where V_{st}, V_{ro}, i_{st}, i_{ro}, $\lambda_{st}, \lambda_{ro}$, and R_{st}, R_{ro} are stator and rotor voltages (V), currents (A), linkage fluxes (Wb), winding resistances (Ω), and $\omega_{arf}, \omega_{el}$ are arbitrary reference frame and rotor angular speed in (rad/s).

The second set of mathematics relates to the flux linkage between the rotor and stator.

$$\begin{cases} \lambda_{st} = (L_{lst} + L_{mg}) i_{st} + L_{mg} i_{ro} = L_{st} i_{st} + L_{mg} i_{ro} \\ \lambda_{ro} = (L_{lro} + L_{mg}) i_{ro} + L_{mg} i_{st} = L_{ro} i_{ro} + L_{mg} i_{st} \end{cases} \tag{3.60}$$

Where, $L_{st} = L_{lst} + L_{mg}$, $L_{ro} = L_{lro} + L_{mg}$ are self-inductance of stator and rotor (H), L_{lst}, L_{lro} are stator and rotor leakage inductances (H), and L_{mg} is magnetizing inductance (H). The rotor mechanical speed's dynamic behavior in terms of mechanical and electromagnetic torque is described by the motion equation:

$$\begin{cases} J\dfrac{d\omega_g}{dt} = T_g - T_{em} \\ T_{em} = -\dfrac{3P}{2}\mathrm{Re}(j\lambda_{ro} i_{ro}^{*}) \end{cases} \tag{3.61}$$

Where J, p, T_g, T_{em} and ω_g are a moment of inertia ($kg\,m^2$), pole pairs, generator shaft mechanical, electromagnetic torque, mechanical rotor speed and $\omega_g = \omega_{el}/p$ (rad/sec), respectively.

$$\begin{cases} \omega_s = 2\pi f_s \\ \omega_{slip} = \omega_s - \omega_{el} \end{cases} \tag{3.62}$$

Where ω_{slip} is the generator slip frequency.

$$\begin{cases} V_{st} = V_{dst} + jV_{qst}; \\ V_{ro} = V_{dro} + jV_{qro}; \end{cases} \begin{cases} i_{st} = i_{dst} + ji_{qst}; \\ i_{ro} = i_{dro} + ji_{qro}; \end{cases} \begin{cases} \lambda_{st} = \lambda_{dst} + j\lambda_{qst}; \\ \lambda_{ro} = \lambda_{dro} + j\lambda_{qro}. \end{cases} \tag{3.63}$$

Put Equations (3.63) into (3.59) and collect imaginary and real parts on both the right and left sides of the equality sign, we get the dq-axis voltages.

$$V_{dst} + jV_{qst} = R_{st}(i_{dst} + ji_{qst}) + p(\lambda_{dst} + j\lambda_{qst}) + j\omega_{arf}(\lambda_{dst} + j\lambda_{qst})$$
$$V_{dro} + jV_{qro} = R_{ro}(i_{dro} + ji_{qro}) + p(\lambda_{dro} + j\lambda_{qro}) + j(\omega_{arf} - \omega_{el})(\lambda_{dro} + j\lambda_{qro})$$

Therefore, obtained DFIG dq axis voltage equations at arbitrary reference frames are

$$\begin{cases} V_{dst} = R_{st}i_{dst} + p\lambda_{dst} - \omega_{arf}\lambda_{qst} \\ V_{qst} = R_{st}i_{qst} + p\lambda_{qst} + \omega_{arf}\lambda_{dst} \\ V_{dro} = R_{ro}i_{dro} + p\lambda_{dro} - (\omega_{arf} - \omega_{el})\lambda_{qro} \\ V_{qro} = R_{ro}i_{qro} + p\lambda_{qro} + (\omega_{arf} - \omega_{el})\lambda_{dro} \end{cases} \tag{3.64}$$

Next similarly, put Equations (3.63) into (3.60), and the linkage fluxes in the dq-axis are calculated as

$$\lambda_{st} = L_{st}\,i_{st} + L_{mg}i_{ro} = L_{st}(i_{dst} + ji_{qst}) + L_{mg}(i_{dro} + ji_{qro})$$
$$\lambda_{dst} + j\lambda_{qst} = L_{st}i_{dst} + jL_{st}i_{qst} + L_{mt}i_{dro} + jL_{mg}i_{qro}$$

Collecting imaginary and real parts on both the right and left sides of the equality sign, we get flu linkages in dq-axis. Repeat the same thing for rotor winding

$$\lambda_{ro} = L_{ro}i_{ro} + L_{mg}i_{st}$$
$$\lambda_{ro} = L_{ro}(i_{dro} + ji_{qro}) + L_{mg}(i_{dst} + ji_{qst})$$
$$\lambda_{dro} + j\lambda_{qro} = L_{ro}i_{dro} + jL_{ro}i_{qro} + L_{mg}i_{dst} + jL_{mg}i_{qst}$$

$$\begin{cases} \lambda_{dst} = L_{st}i_{dst} + L_{mg}i_{dro} \\ \lambda_{qst} = L_{st}i_{qst} + L_{mg}i_{qro} \\ \lambda_{dro} = L_{ro}i_{dro} + L_{mg}i_{dst} \\ \lambda_{qro} = L_{ro}i_{qro} + L_{mg}i_{qst} \end{cases} \tag{3.65}$$

The linkage fluxes and currents of dq axis is used to express electromagnetic torque T_{em} in Equation (3.61). For torque, several expressions can be obtained using mathematical manipulations. But the following expressions are most commonly used.

$$T_{em} = \begin{cases} (3P/2)(i_{qst}\lambda_{dst} - i_{dst}\lambda_{qst}) \\ (3PL_{mg}/2)(i_{qst}i_{dro} - i_{dst}i_{qro}) \\ (3PL_{mg}/2L_{ro})(i_{qst}\lambda_{dro} - i_{dst}\lambda_{qro}) \end{cases} \tag{3.66}$$

For the simulation model, the electrical rotational speed and the torque equations are represented as follows:

$$\begin{cases} P_{ss} = \frac{3}{2}(V_{dst}i_{dst} - V_{qst}i_{qst}) \\ Q_{ss} = \frac{3}{2}(V_{qst}i_{dst} - V_{dst}i_{qst}) \\ P_{rr} = \frac{3}{2}(V_{dro}i_{dro} - V_{qro}i_{qro}) \end{cases}, \quad \begin{cases} Q_{rr} = \frac{3}{2}(V_{qro}i_{dro} - V_{dro}i_{qro}) \\ \omega_{el} = \frac{p}{JS}(T_g - T_{em}) \\ T_{em} = \frac{3p}{2}(i_{qst}\lambda_{dst} - i_{dst}\lambda_{qst}) \end{cases} \tag{3.67}$$

3.5.6 Dynamic model of Rotor Side Converter (RSC)

The RSC is a critical component that controls the power flowing from the WTG rotor to the grid. It is used to convert the variable frequency produced by the rotor into a constant frequency that corresponds to the grid frequency. This allows the regulation of the electrical output power of the WTG. Space vector theory is used for expanding the dynamic dq model of RSC. General voltage equations for rotor and stator

$$\begin{cases} V_{st}^{s} = R_{st}i_{st}^{s} + \dfrac{d\lambda_{st}^{s}}{dt} & (a) \\ V_{ro}^{r} = R_{ro}i_{ro}^{r} + \dfrac{d\lambda_{ro}^{r}}{dt} & (b) \end{cases} \tag{3.68}$$

Multiplying the voltage equations (3.68) (a) and (b) by $e^{-j\theta_s}$, and $e^{-j\theta_{slip}}$, respectively to get the dq voltage equations which are expressed as a synchronously rotating frame.

$$V_{st}^{sy} = R_{st}i_{st}^{sy} + p\lambda_{st}^{sy} = \begin{cases} V_{dst} = R_{st}i_{dst} + p\lambda_{dst} - \omega_s\lambda_{qst} \\ V_{qst} = R_{st}i_{qst} + p\lambda_{qst} + \omega_s\lambda_{dst} \end{cases} \tag{3.69}$$

$$V_{ro}^{sy} = R_{ro}i_{ro}^{sy} + \frac{d\lambda_{ro}^{sy}}{dt} - j\omega_{el}\lambda_{ro}^{sy} = \begin{cases} V_{dro} = R_{ro}i_{dro} + p\lambda_{dro} - (\omega_s - \omega_{el})\lambda_{qro} \\ V_{qro} = R_{ro}i_{qro} + p\lambda_{qro} + (\omega_s - \omega_{el})\lambda_{dro} \end{cases} \tag{3.70}$$

In the same way, the linkage fluxes can be expressed as:

$$\lambda_{st}^{sy} = L_{st}i_{st}^{sy} + L_{mg}i_{ro}^{sy} = \begin{cases} \lambda_{dst} = L_{st}i_{dst} + L_{mg}i_{dro} \\ \lambda_{qst} = L_{st}i_{qst} + L_{mg}i_{qro} \end{cases} \tag{3.71}$$

$$\lambda_{ro}^{sy} = L_{ro}i_{ro}^{sy} + L_{mg}i_{st}^{sy} = \begin{cases} \lambda_{dro} = L_{mg}i_{dst} + L_{ro}i_{dro} \\ \lambda_{qro} = L_{mg}i_{qst} + L_{ro}i_{qro} \end{cases} \tag{3.72}$$

Control of RSC using Stator Flux Oriented Control (SFOC)

Vector control is the most common control techniques for RSC and is carried out in the frame, with the stator flux aligned with the d-axis performed in the dq frame. Depending on this alignment, it will be shown that i_{dro} is proportional to the Q_{ss} (reactive power of the stator) and i_{qro} is proportional to the real power of the stator or electromagnetic torque. We can find rotor voltages as a function of i_{dro}, i_{qro} and stator flux (λ_{st}). Note that quadrature stator flux is assumed to be zero.

$$\lambda_{qst} = 0 \tag{3.73}$$

$$\lambda_{dst} = |\lambda_{st}| \tag{3.74}$$

$$\omega_s - \omega_{el} = \omega_{slip} \tag{3.75}$$

Put Equations (3.71) and (3.72) into (3.70), we get the rotor d and q-axis voltages.

$$V_{dro} = R_{ro} i_{dro} + p\lambda_{dro} - \omega_{slip}\lambda_{qro} = R_{ro} i_{dro} + p(L_{mg} i_{dst} + L_{ro} i_{dro}) - \omega_{slip}(L_{mg} i_{qst} + L_{ro} i_{qro})$$

$$V_{dro} = R_{ro} i_{dro} + L_{mg}\frac{di_{dst}}{dt} + L_{ro}\frac{di_{dro}}{dt} - \omega_{slip} L_{ro} i_{qro} - \omega_{slip}\frac{L_{mg}}{L_{st}}(\lambda_{qst} - L_{mg} i_{qro})$$

$$V_{dro} = R_{ro} i_{dro} + \frac{L_{mg}}{L_{st}}\frac{d(\lambda_{dst} - L_{mg} i_{dro})}{dt} + L_{ro}\frac{di_{dro}}{dt} - \omega_{slip} L_{ro} i_{qro} + \frac{L_{mg}^2}{L_{st}}\omega_{slip} i_{qro} - \omega_{slip}\frac{L_{mg}}{L_{st}}\lambda_{qst}$$

$$V_{dro} = R_{ro} i_{dro} + \frac{L_{mg}}{L_{st}}\frac{d\lambda_{dst}}{dt} + (1 - \frac{L_{mg}^2}{L_{st} L_{ro}})L_{ro}\frac{di_{dro}}{dt} - \omega_{slip} L_{ro}(1 - \frac{L_{mg}^2}{L_{st} L_{ro}})i_{qro} - \omega_{slip}\frac{L_{mg}}{L_{st}}\lambda_{qst}$$

$$\Rightarrow V_{dro} = R_{ro} i_{dro} + \frac{L_{mg}}{L_{st}}\frac{d|\vec{\lambda}_{st}|}{dt} + \sigma L_{ro}\frac{di_{dro}}{dt} - \omega_{slip}\sigma L_{ro} i_{qro}$$

$$V_{qro} = R_{ro} i_{qro} + p\lambda_{qro} + \omega_{slip}\lambda_{dro} = R_{ro} i_{qro} + p(L_{mg} i_{qst} + L_{ro} i_{qro}) + \omega_{slip}(L_{mg} i_{dst} + L_{ro} i_{dro})$$

$$V_{qro} = R_{ro} i_{qro} + L_{mg} p i_{qst} + L_{ro} p i_{qro} + \omega_{slip} L_{mg} i_{dst} + \omega_{slip} L_{ro} i_{dro}$$

$$V_{qro} = R_{ro} i_{qro} + \frac{L_{mg}}{L_{st}}\frac{d(\lambda_{qst} - L_{mg} i_{qro})}{dt} + L_{ro} p i_{qro} + \omega_{slip}\frac{L_{mg}}{L_{st}}(\lambda_{dst} - L_{mg} i_{dro}) + \omega_{slip} L_{ro} i_{dro}$$

$$\Rightarrow V_{qro} = R_{ro} i_{qro} + \sigma L_{ro}\frac{di_{qro}}{dt} + \omega_{slip}\frac{L_{mg}}{L_{st}}|\vec{\lambda}_{st}| + \sigma\omega_{slip} L_{ro} i_{dro}$$

$$\begin{cases} V_{dro} = R_{ro} i_{dro} - \omega_{slip}\sigma L_{ro} i_{qro} + \dfrac{L_{mg}}{L_{st}}\dfrac{d|\lambda_{st}|}{dt} + \sigma L_{ro}\dfrac{di_{dro}}{dt} \\ V_{qro} = R_{ro} i_{qro} + \sigma\omega_{slip} L_{ro} i_{dro} + \omega_{slip}\dfrac{L_{mg}}{L_{st}}|\lambda_{st}| + \sigma L_{ro}\dfrac{di_{qro}}{dt} \end{cases} \tag{3.76}$$

Where $\sigma = 1 - L_{mg}{}^2 / L_{st} L_{ro}$

From Equation (3.76), since the stator winding of the DFIG is connected directly to the grid at constant frequency and voltage, the linkage flux of the stator is constant. Therefore, the term $d|\vec{\lambda}_{st}|/dt$ becomes zero. For $\alpha\beta / dq$ and $dq / \alpha\beta$ transformation, the angle θ_{slip} must be estimated.

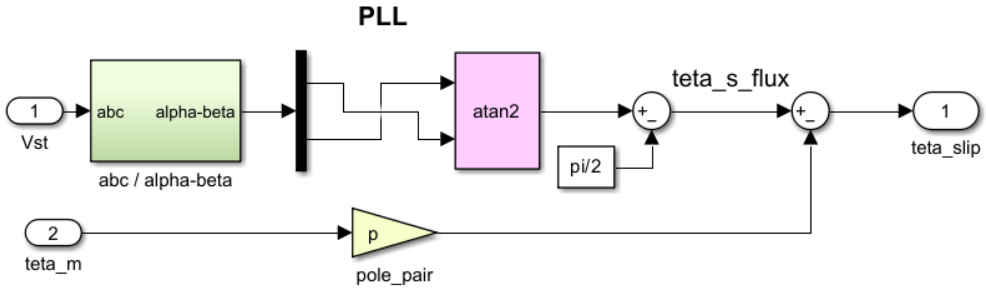

Figure 3.6: Flux angle calculation using Simulink

The angle of stator voltage is first calculated by using a phase-locked loop, and then subtracted 90° from this estimated value, we get θ_{sflux}. In addition to estimating stator voltage angle, PLL is used to reduce or reject disturbances and harmonics. After rotor voltage and calculation of flux angle have been covered, the RSC control complete system can be introduced. The torque equation in synchronously rotating reference frame can be reduced using SFOC is given below:

$$T_{em} = \frac{3}{2} p \frac{L_{mg}}{L_{st}} (\lambda_{qst} i_{dro} - \lambda_{dst} i_{qro}) = -\frac{3}{2} p \frac{L_{mg}}{L_{st}} \lambda_{dst} i_{qro} = -\frac{3}{2} p \frac{L_{mg}}{L_{st}} |\lambda_{st}| i_{qro}$$

$$T_{em} = K_{tem} i_{qro} \tag{3.77}$$

Where, $K_{tem} = -\frac{3}{2} p \frac{L_{mg}}{L_{st}} |\lambda_{st}|$

Substituting the values of p, L_{mg}, L_{st} and λ_{st} from Table A.4 in the appendix.

$$K_{tem} = -1.5 * 2 * \frac{2.5e-3}{0.0026} * 1.7933 = -5.1990$$

Like that of torque expression, the stator reactive power equation can be obtained by aligning the d-axis with the stator flux space vector as follows:

$$Q_{ss} = \frac{3}{2}(V_{qst} i_{dst} - V_{dst} i_{qst}) \Rightarrow Q_{ss} = -\frac{3}{2} \omega_s \frac{L_{mg}}{L_{st}} |\lambda_{st}| (i_{dro} - \frac{|\lambda_{st}|}{L_{mg}})$$

$$Q_{ss} = K_{Q_{ss}} (i_{dro} - \frac{|\lambda_{st}|}{L_{mg}}) \tag{3.78}$$

Where $K_{Q_{ss}} = -\frac{3}{2} \omega_s \frac{L_{mg}}{L_{st}} |\lambda_{st}|$

$$K_{Q_{ss}} = -1.5 * 314.1592 * \frac{2.5e-3}{0.0026} * 1.7933 = -816.6542$$

The control of the torque and the stator reactive power is therefore made possible by the independent control of the two rotor currents. Since the stator of the DFIG is directly connected to the grid, the stator flux is supplied by the mains voltage with constant amplitude:

$$|\lambda_{st}| \cong \frac{|V_{st}|}{\omega_s} = 1.7933 \tag{3.79}$$

Because of the direct grid connection, the DFIG stator voltage and current are both constant, and electromagnetic torque and stator reactive power are kept steady.

3.5.7 RSC Controller Design

From equation (3.76) the two PI controllers were designed for RSC as follows: The first controller is for rotor d-axis current, the second one is for q-axis current control, and the electromagnetic torque is controlled using maximum power point tracking principle (MPPT).

$$V_{dro} = R_{ro} i_{dro} - \omega_{slip} \sigma L_{ro} i_{qro} + \frac{L_{mg}}{L_{st}} \frac{d|\lambda_{st}|}{dt} + \sigma L_{ro} \frac{di_{dro}}{dt}$$

Since the λ_{st} of DFIG is constant its derivative in the above equation is zero.

$$V_{dro} = R_{ro} i_{dro} + \sigma L_{ro} \frac{di_{dro}}{dt} - \omega_{slip} \sigma L_{ro} i_{qro} = V_d - \omega_{slip} \sigma L_{ro} i_{qro}$$

$$V_d = R_{ro} i_{dro} + \sigma L_{ro} \frac{di_{dro}}{dt} \Rightarrow V_d = (R_{ro} + \sigma L_{ro} s) \Delta i_{dro}(s)$$

Rotor direct axis current is controlled by using PI. Therefore, to minimize the error between the reference and measured d-axis rotor current the controller is needed.

$\Delta i_{dro}(s) = \frac{1}{(R_{ro} + \sigma L_{ro} s)} V_d$ and $\Delta i_{dro}(s)(\mathrm{K_{p1}} + \frac{\mathrm{K_{i1}}}{s}) = V_d$ Then substituting the value of change in current in the second equation and simplifying it we get the PI controller gains in the table 3.2.

$$\mathrm{K_{p1}} = 0.5771 \text{ and } \mathrm{K}_{i1} = 491.5595 \tag{3.80}$$

$$V_{qro} = R_{ro} i_{qro} + \sigma L_{ro} \frac{di_{qro}}{dt} + \sigma \omega_{slip} L_{ro} i_{dro} + \omega_{slip} \frac{L_{mg}}{L_{st}} |\lambda_{st}|$$

$$V_{qro} = V_q + \sigma \omega_{slip} L_{ro} i_{dro} + \omega_{slip} \frac{L_{mg}}{L_{st}} |\lambda_{st}|$$

$$V_q = R_{ro} i_{qro} + \sigma L_{ro} \frac{di_{qro}}{dt} \Rightarrow V_q = (R_{ro} + \sigma L_{ro} s) \Delta i_{qro}(s)$$

Solve these equations for q-axis rotor current in similar way as the above d-axis current control, we get similar result.

$$\text{Therefore, } \begin{cases} K_{p2} = K_{p1} = 0.5771 \\ K_{i2} = K_{i1} = 491.5995 \end{cases} \tag{3.81}$$

Table 3.2: Optimal values of PI controllers for RSC

PI-1 controller for i_{dro}		PI-2 controller for i_{qro}	
K_{p1}	K_{i1}	K_{p2}	K_{i2}
0.5771	491.5995	0.5771	491.5995

3.5.8 Dynamic model of Grid Side System

GSC interfaces the DC link of the WT with the grid. It converts the DC output of the WTG into regulated AC output that is matched with the grid voltage. In this topic, the mathematical representations of the GSC system were explained to understand the dynamic behavior in a space vector form and then derive the vector control. Consequently, after the dynamic model of GSC is studied, we can go ahead and examine the control system. Using the vector control approach, the main two goals of GSC can be achieved. The first one is maintaining the DC bus voltage constant and the second one is controlling the exchange of reactive power to allow transmission of electricity through the converter.

The three-phase electrical equations of the grid side system can be derived

$$\begin{aligned} V_{aC} &= R_{gf} i_{ag} + L_{gf} \frac{di_{ag}}{dt} + V_{ag} \\ V_{bC} &= R_{gf} i_{bg} + L_{gf} \frac{di_{bg}}{dt} + V_{bg} \\ V_{cC} &= R_{gf} i_{cg} + L_{gf} \frac{di_{cg}}{dt} + V_{cg} \end{aligned} \tag{3.82}$$

The converter voltage can be expressed compactly

$$V_C^s = R_{gf} i_g^s + L_{gf} \frac{di_g^s}{dt} + V_g^s \tag{3.83}$$

Where, (V_{ag}, V_{bg}, V_{cg}), (V_{aC}, V_{bC}, V_{cC}) and (i_{ag}, i_{bg}, i_{cg}) are a, b, and c-phase grid, GSC voltages (V) and currents flow thorough the GSC's output (A). $R_{g\,f}$ is Resistance of filter (Ω) and x $L_{g\,f}$ is inductance of filter (H).

The dq Model of Grid Side Converter

In the same way, by using the transformation angle θ_{gg} multiplying Equation (3.83) by $e^{-j\theta_{gg}}$, the two-rotating frame (dq) expressions are derived as follows:

$$V_C^s.e^{-j\theta_{gg}} = R_{gf}i_g^s.e^{-j\theta_{gg}} + L_{gf}\frac{di_g^s}{dt}.e^{-j\theta_{gg}} + V_g^s.e^{-j\theta_{gg}} \tag{3.84}$$

$$V_C^r = R_{gf}i_g^r + L_{gf}\frac{di_g^r}{dt} + V_g^r + j\omega L_{gf}i_g^r \tag{3.85}$$

Where, $\theta_{gg} = \omega\, t$, the rotating reference frame angular position.

$$\begin{cases} V_C^r = V_{dC} + jV_{qC} \\ V_g^r = V_{dg} + jV_{qg} \\ i_g^r = i_{dg} + ji_{qg} \end{cases} \tag{3.86}$$

The basic vector orientation equations of dq components are obtained by decomposing techniques.

$$\begin{cases} V_{dC} = R_{gf}i_{dg} + L_{gf}\dfrac{di_{dg}}{dt} + V_{dg} - \omega L_{gf}i_{qg} \\ V_{qC} = R_{gf}i_{qg} + L_{gf}\dfrac{di_{qg}}{dt} + V_{qg} + \omega L_{gf}i_{dg} \end{cases} \tag{3.87}$$

Control of GSC using Grid Voltage Orientation

To reduce the system further, the rotational speed, ω, is assumed to be similar to synchronous speed ω_s. GVOC is done by aligning the d-axis grid voltage. Then after, the resulting grid voltage dq components yield:

$$V_{qg} = 0 \text{ and } V_{dg} = V_g \tag{3.88}$$

$$\omega = \omega_s \text{ and } \theta_{gg} = \omega t \Rightarrow \theta_{gg} = \omega_s t \tag{3.89}$$

Substituting the last two equations into the voltage Equation (3.87) is simplified as follows:

$$\begin{cases} V_{dC} = R_{gf}i_{dg} + L_{gf}\dfrac{di_{dg}}{dt} + V_{dg} - \omega_s L_{gf}i_{qg} \\ V_{qC} = R_{gf}i_{qg} + L_{gf}\dfrac{di_{qg}}{dt} + \omega_s L_{gf}i_{dg} \end{cases} \tag{3.90}$$

Depending on the above alignment, we can reduce the computations of active and reactive power.

$$\begin{cases} P_{gg} = 3/2\,\mathrm{Re}\{V_g.i_g^*\} = 3/2(V_{dg}i_{dg} + V_{qg}i_{qg}) \\ Q_{gg} = 3/2\,\mathrm{Im}\{V_g.i_g^*\} = 3/2(V_{qg}i_{dg} - V_{dg}i_{qg}) \end{cases} \tag{3.91}$$

Substituting Equation (3.88) into Equation (3.91), we get:

$$\begin{cases} P_{gg} = \frac{3}{2} V_{dg} i_{dg} = \frac{3}{2} V_g i_{dg} \\ Q_{gg} = -\frac{3}{2} V_{dg} i_{qg} = -\frac{3}{2} V_g i_{qg} \end{cases} \tag{3.92}$$

In this system, the dq components and reactive and real powers decoupled relationship has been obtained. As Equations (3.92) show the d-axis current i_{dg} is responsible for the control of real power P_{gg} value, while the current in the q-axis i_{qg} is responsible for the control of grid reactive power Q_{gg} value. The GSC output power is provided by:

$$\begin{cases} P_C = 3/2 \operatorname{Re}\{V_C . i_g^*\} = 3/2 (V_{dC} i_{dg} + V_{qC} i_{qg}) \\ Q_C = 3/2 \operatorname{Im}\{V_C . i_g^*\} = 3/2 (V_{qC} i_{dg} - V_{dC} i_{qg}) \end{cases} \tag{3.93}$$

Substituting voltage Equation (3.90) into converter power Equation (3.93) we get:

$$\begin{cases} P_C = 3/2 (R_{gf} \mid i_g \mid^2 + L_{gf} \frac{di_{dg}}{dt} i_{dg} + L_{gf} \frac{di_{qg}}{dt} i_{qg} + V_{dg} i_{dg}) \\ Q_C = 3/2 (L_{gf} \omega_s \mid i_g \mid^2 - L_{gf} \frac{di_{dg}}{dt} i_{qg} + L_{gf} \frac{di_{qg}}{dt} i_{dg} - V_{dg} i_{qg}) \end{cases} \tag{3.94}$$

By letting the dq components which include the first derivatives be zero, the power expression becomes:

$$\begin{cases} P_C = 3/2 (R_{gf} \mid i_g \mid^2 + V_{dg} i_{dg}) \\ Q_C = 3/2 (L_{gf} \omega_s \mid i_g \mid^2 - V_{dg} i_{qg}) \end{cases} \tag{3.95}$$

Vector or field-oriented control technology is the most commonly used control method for power electronic converters connected to the power grid. Since it improves the performance of converters with straightforward implementation requirements. The rotor of the DFIG delivers the wind turbine's generated power partially. Because a DC link is generated through a capacitor, the control of bus voltage V_{bus} is necessary. The real power is transmitted into the grid through the rotor crosses the DC link. To do so both RSC and GSC are necessarily available for the DC voltage needed for effective operation. From Equation (3.90)

$$V_{edc} = -\omega_s L_{gf} i_{qg} \tag{3.96}$$

$$V_{eqc} = \omega_s L_{gf} i_{dg} \tag{3.97}$$

The direct grid voltage V_{dg} is ideally constant. The reference currents (i_{dg}, i_{qg}) are decoupled from both the active and reactive power to simplify the control techniques. Hence, the current i_{qg} control implies Q_{gg} control, at the same time the current i_{dg} control implies P_{gg} control. For simulation, the constants we need from Equation (3.92) are:

$$P_{gg} = \frac{3}{2}V_{dg}i_{dg} = \frac{3}{2}V_g i_{dg} \Rightarrow i_{dg} = \frac{P_{gg}}{1.5V_{dg}} = K_{P_{gg}} P_{gg}$$

$$K_{P_{gg}} = \frac{1}{1.5V_g} = \frac{1}{1.5*230KV} = 0.002899 \quad (3.98)$$

$$Q_{gg} = -\frac{3}{2}V_{dg}i_{qg} = -\frac{3}{2}V_g i_{qg} \Rightarrow i_{qg} = \frac{Q_{gg}}{-1.5V_{dg}} = K_{Q_{gg}} Q_{gg}$$

$$K_{Q_{gg}} = \frac{1}{-1.5V_g} = \frac{1}{-1.5*230KV} = -0.002899 \quad (3.99)$$

Note that the real power P_{gg} reference value is calculated from the V_{bus} regulator and the grid voltage angle θ_{gg} is needed for Park and Clark transformations of voltage and current. θ_{gg} is obtained by using a technique called **PLL** (phase-locked loop).

$$\theta_{gg} = \tan^{-1}(\frac{V_{\beta g}}{V_{\alpha g}}) \quad (3.100)$$

3.5.9 GSC Controller Design

From Equation (3.90) the three PI controllers were designed for GSC as follows: The first controller is for rotor d-axis current and the second one is for q-axis current control.

$$V_{dC} = R_{gf}i_{dg} + L_{gf}\frac{di_{dg}}{dt} + V_{dg} - \omega_s L_{gf} i_{qg}$$

$$V_{dC} = V_{c1} + V_{dg} - \omega_s L_{gf} i_{qg}$$

$$V_{c1} = R_{gf}i_{dg} + L_{gf}\frac{di_{dg}}{dt} \Rightarrow V_{c1}(s) = (R_{gf} + L_{gf}s)\Delta i_{dg}(s) \quad (3.101)$$

The d-axis current is responsible for the control of real power. So, to minimize the error between the reference and measured d-axis rotor current, the PI controller is used.

$\Delta i_{dg}(s) = \frac{1}{(R_{gf} + L_{gf}s)}V_{c1}(s)$ and $\Delta i_{dg}(s)(\mathrm{K_{p4}} + \frac{\mathrm{K_{i4}}}{s}) = V_{c1}(s)$ Then substituting the value of change in current in the second equation and simplifying it we get the PI controller gains in Table 3.3.

$$\mathrm{K_{p4}} = 0.2513, \text{and } \mathrm{K_{i4}} = 39.4784 \quad (3.102)$$

$$V_{qC} = R_{gf}i_{qg} + L_{gf}\frac{di_{qg}}{dt} + \omega_s L_{gf} i_{dg}$$

$$V_{qC} = V_{C2} + \omega_s L_{gf} i_{dg}$$

$$V_{C2} = R_{gf} i_{qg} + L_{gf} \frac{di_{qg}}{dt} = (R_{gf} + L_{gf} s) \Delta i_{qg}(s)$$

For q-axis grid current, the procedure and values for PI controller gains are similar.

$$\begin{cases} \mathrm{K_{p5}} = \mathrm{K}_{p4} = 0.2513 \\ \mathrm{K_{i5}} = \mathrm{K_{i4}} = 39.4784 \end{cases} \quad (3.103)$$

Table 3.3: PI controllers gain values for GSC

PI-4 controller for i_{dg}		PI-5 controller for i_{qg}	
$\mathrm{K_{p4}}$	$\mathrm{K_{i4}}$	$\mathrm{K_{p5}}$	K_{i5}
0.2513	39.4784	0.2513	39.4784

3.5.10 Model of DC link

Positioning the DC connection capacitor between the machine side converter and GSC which acts as an energy storage device and is denoted as C_{bus}. The DC link active power (P_{dc}) can be obtained by the distinction between the generator rotor and grid real power. The DC link real power is expressed as shown in equation (3.105) to maintain the DC bus voltage constant. m_a is a normalizing constant (usually it has a value of 0.8).

$$V_{dc} = \sqrt{2} V_{st} / m_a \quad (3.104)$$

$$\begin{aligned} P_{gg} &= P_{dc} = V_{dc} i_{dc} = V_{dc} C_{bus} \frac{dV_{dc}}{dt} \\ i_{dc} &= P_{gg} / V_{dc} \end{aligned} \quad (3.105)$$

In this thesis, the study considered the wind turbine that is connected to the grid that contains the hydropower plant. Thus, next the model of the hydropower plant is presented.

3.6 Hydropower Plant Model

In this section, the modeling of a hydro-power plant for frequency regulation using an AGC was explained. This was aimed at minimizing the frequency fluctuations of the grid when connected with the WT. The model of the hydro-power plant was presented in (Tilahun W., Aderajew A., 2021).

3.6.1 Governor Model

The basic function of a governor is to control the speed and/or load. The speed variations of a hydroelectric power plant are sensed by a turbine speed governor, which is used to regulate the input of the turbine valve. The water flows through a pipe into the turbine, which is blocked in particular by the slide valve. The first-order expression in Equation (3.106) represents the pilot servomotor.

$$\Delta P_G = [\Delta P_{ref} - \frac{1}{R}\Delta f(s)]\frac{K_g}{1+s\tau_2} \tag{3.106}$$

Where, ΔP_G is gate position, ΔP_{ref}, is a change in reference power, Δf, is frequency deviation, R, is Droop constant, and K_g is governor constant. The above equation can be shown in the block diagram as follows:

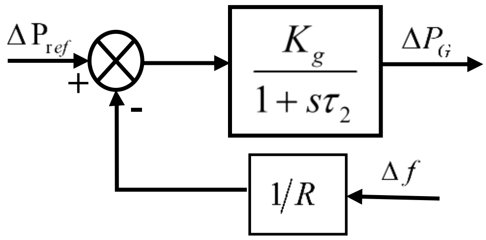

Figure 3.7: Servomotor block diagram

The transfer function of transient droop compensation is also given as:

$$\Delta P_{GH} = \frac{1+s\tau_1}{1+s\tau_3}\Delta P_G \tag{3.107}$$

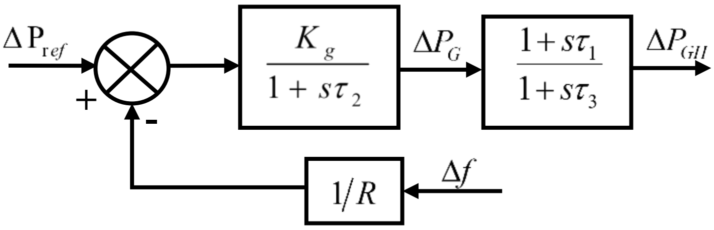

Figure 3.8: Governor Model with droop control

3.6.2 Hydro-Turbine Model

The characteristic of a water turbine is determined by the dynamics of the water flowing through the pressure pipe (penstock). The penstock and turbine properties are determined by the basic parameters i.e., water velocity, mechanical power of the turbine, and water column acceleration. Hydro-turbine full modeling is represented in (P.Kundur, 1994).

$$\frac{\Delta P_{mH}}{\Delta P_{GH}} = \frac{1-\tau_w s}{1+0.5\tau_w s} \tag{3.108}$$

Where, ΔP_{mH}, ΔP_{GH}, and τ_w are hydro-mechanical power, governor power deviation, and start time of water.

3.6.3 Generator and Load Model

The turbine DFIG rotates due to its two opposite torques i.e., mechanical, P_{mH} and electromagnetic, P_{emH} power of the generator. The equation is given as

$$2H \frac{d\Delta\omega_H}{dt} = \Delta P_{mH} - \Delta P_{emH} \tag{3.109}$$

H, determines the duration of time in (sec) that the generator can produce its rated power solely with the kinetic energy that is stored in its rotating masses. ω_H is hydro-turbine frequency. The turbines will accelerate or decelerate in response to an imbalance in the power between electrical and mechanical, which will raise or lower the frequency.

$$2H \frac{d\Delta\omega_H}{dt} = \Delta P_{mH} - \Delta P_{emH} \Rightarrow \frac{d\Delta\omega_H}{dt} = \frac{\Delta P_{mH} - \Delta P_{emH}}{2H} \tag{3.110}$$

$$\Delta\omega_H = \frac{\Delta P_{mH} - \Delta P_{emH}}{2H\,s} \tag{3.111}$$

However, certain loads can also be adjusted so that they function as a load resource deviation. By using the damping factor D_H, this phenomenon can be modeled.

$$\Delta P_{emH} = \Delta P_L + D_H \Delta\omega_H \tag{3.112}$$

$$\Delta\omega_H = \frac{1}{2Hs + D_H} (\Delta P_{mH} - \Delta P_L) \tag{3.113}$$

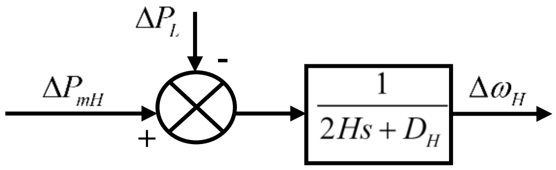

Figure 3.9: Load and generator model

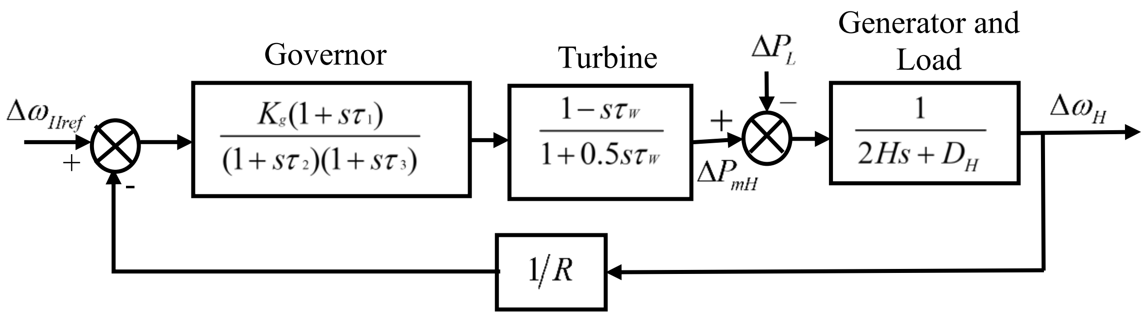

Figure 3.10: HPP model for frequency regulation

Where, ΔP_L is the load change non-frequency sensitive, and $D_H \Delta\omega_H$ the load change frequency sensitive. D_H is calculated by dividing the % change in load by the % change in frequency.

3.7 Wind-Hydropower Integration Frequency Model

The modeling of wind turbine integrated with hydropower plant for frequency regulation as shown in the block diagram

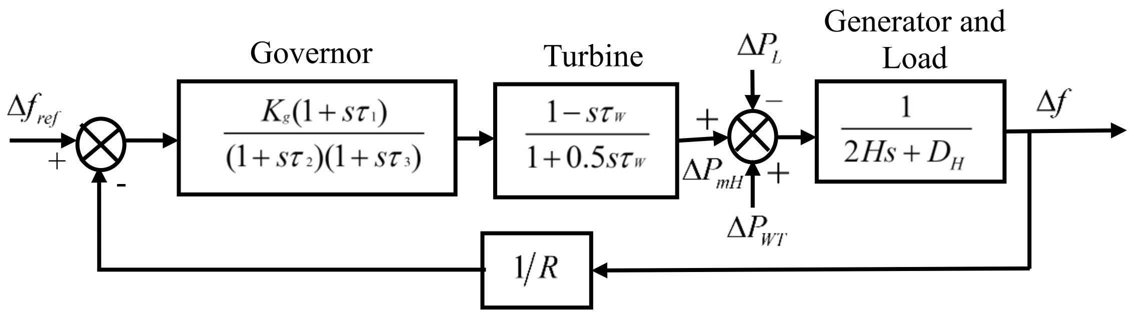

Figure 3.11: WT-HPP model for frequency regulation

3.8 Controller Design for the Frequency Regulation

Since the conversion system of wind energy is a stochastic and unstable system, the controllers must be designed as a part of the system to maintain a stable and good performance WECS. To maintain the turbine blade at the desired location, the appropriate signal of control must be needed.

3.8.1 Objectives of the Controller

In this thesis, the PID controller is intended to fulfill the following requirements and objectives:

- Maintain the voltage of the DC link for the power transfer between the grid and DFIG.
- Control real and reactive power for power balance.
- Regulate the variables to limit the rotor speed and to maintain the grid frequency stable range.
- Decrease the mechanical stress during wind speed variation.

3.8.2 PID Controller

The proportional integral derivative controller is a simple, stable, robust, and widely used control technique. It has three fundamental coefficients i.e. proportional, k_{pc}, integral, k_{ic}, and derivative, k_{dc}.

Proportional Controller: It shortens the rise time and decreases the steady-state inaccuracy, but it never totally removes the steady-state error.

Integral controller: minimizing the steps or constant input steady-state error and the effect it has on the total of the errors in the most recent (previous) period. In other words, it resets the offset that results from the proportionate action.

Derivative controller: predicts future errors based on the rate of change that is currently occurring. This has the benefit of reducing both overshoots and undershoots, improving transient responsiveness, and strengthening system stability. In general, it works to reduce the change in error.

Table 3.4: PID controller parameters effects

Gain of PID	Overshoot	Time for settling	Rise time	Steady-state error
k_{pc}	↑	Slightly change	↓	↓
k_{ic}	↑	↑	↓	Minimize
k_{dc}	↓	↓	Small change	Almost no change

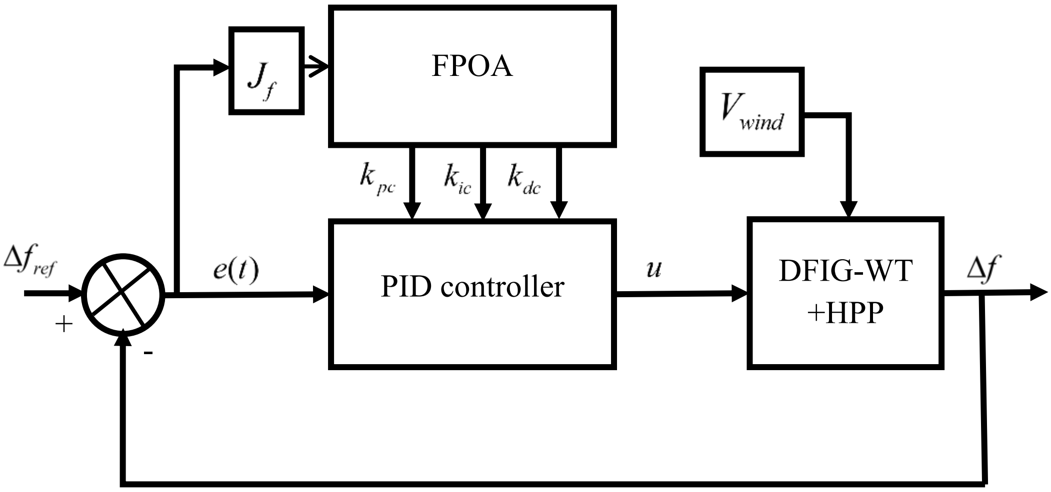

Figure 3.12: Frequency regulation with PID controller

This PID controller is used for frequency regulation of grid-connected DFIG wind turbines. The control signal u(t) is formulated in terms of PID controller coefficient and error as given below:

$$\begin{cases} u(t) = k_{pc}e(t) + k_{ic}\int e(t)dt + k_{dc}\dfrac{de(t)}{dt} \\ e(t) = \Delta f_{ref} - \Delta f \end{cases} \tag{3.114}$$

Where, Δf_{ref} and Δf are nominal and measured frequency deviation of the grid. The coefficients of the PID controller are tuned using FPOA and PSO to obtain the best possible response

3.8.3 Design of Frequency Controller

Standing from Figure 3.6 the PID controller is designed for frequency regulation as follows by assuming the frequency deviation at reference is zero.

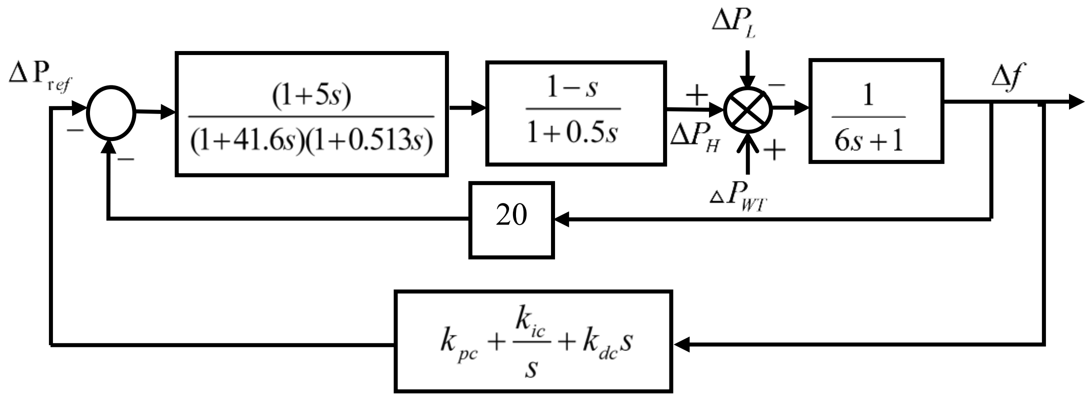

Figure 3.13: Frequency control with PID

$$h(s) = (k_{pc} + \frac{k_{ic}}{s} + k_{dc}s + 20) * \frac{(1+5s)}{(1+41.6s)(1+0.513s)} * \frac{1-s}{1+0.5s}$$

$$h(s) = \frac{(1+5s)(1-s)(k_{dc}s^2 + (20+k_{pc})s + k_{ic})}{s(1+41.6s)(1+0.513s)(1+0.5s)} \tag{3.115}$$

$$g(s) = \frac{1}{6s+1} \tag{3.116}$$

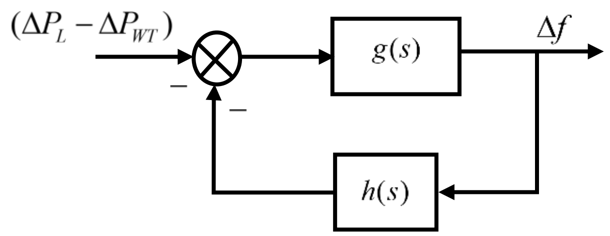

Figure 3.14: Closed loop for frequency

After simplifying the equation $1 + g(s)*h(s) = 0$, thus,

$$\begin{aligned} &64.02s^5 + (265.049 - 5k_{dc})s^4 + (298.074 + 4k_{dc} - 5k_{pc} - 100)s^3 \\ &+ (48.613 + k_{dc} - 5k_{ic} + 4k_{pc} + 80)s^2 + (4k_{ic} + k_{pc} + 21)s + k_{ic} = 0 \end{aligned} \tag{3.117}$$

To stabilize the system the controller gain can be found by applying the Routh-Hurwitz principle.

Table 3.5: Routh array for stability of frequency regulation

s^5	64.02	$198.074 + 4k_{dc} - 5k_{pc}$	$4k_{ic} + k_{pc} + 21$
s^4	$265.049 - 5k_{dc}$	$128.613 + k_{dc} - 5k_{ic}$	k_{ic}
s^3	$((265.049 - 5k_{dc})*(198.074 + 4k_{dc} - 5k_{pc}) - 64.02*(128.613 + k_{dc} - 5k_{ic}))/(265.049 - 5k_{dc}) = a$	$((265.049 - 5k_{dc})*(4k_{ic}\ k_{pc} + 21) - 64.02k_{ic})/(265.049 - 5k_{dc}) = b$	0
s^2	$a(128.613 + k_{dc} - 5k_{ic}) - b*(265.049 - 5k_{dc})/a = c$	k_{ic}	0
s^1	$(bc - ak_{ic})/c$	0	0
s^0	k_{ic}	0	0

For a stable system, the first column of the Routh array based on the characteristic equation coefficients must have the same sign. So, following this criterion

$$64.02 > 0 \tag{3.118}$$

$$265.049 - 5k_{dc} > 0 \Rightarrow k_{dc} < 53.0098 \tag{3.119}$$

$$\frac{((265.049 - 5k_{dc})*(198.074 + 4k_{dc} - 5k_{pc})\text{-}64.02*(128.613 + k_{dc} - 5k_{ic}))}{(265.049 - 5k_{dc})} = a > 0 \tag{3.120}$$

$$\frac{a(128.613 + k_{dc} - 5k_{ic}) - b(265.049 - 5k_{dc})}{a} = c > 0 \tag{3.121}$$

$$(bc - ak_{ic})/c > 0 \tag{3.122}$$

$$k_{ic} > 0 \tag{3.123}$$

After simplifying the above equations, the boundary of the controller parameters is

$$k_{pc} > -21.0000, k_{ic} > 0.0000, \text{and}\ k_{dc} < 53.0098$$

3.9 Fitness Function

To formulate a fitness function that incorporates hydro and wind turbine power plants optimal frequency regulation, the following variables, constraints, and fitness function:

Variables:

- Variation of generating hydro power: $P_H(t)$ represent the power generation from hydro power plants at time t.

$$\Delta P_H(t) = P_H(t) - P_H(t-1) \quad (3.124)$$

- Variation of generating wind Power: $P_W(t)$ represent the power generation from wind turbine power plants at time t.

$$\Delta P_W(t) = P_W(t) - P_W(t-1) \quad (3.125)$$

Constraints:

- Power Balance Constraint: The total power generation deviation from hydro $\Delta P_H(t)$ and wind sources $\Delta P_W(t)$, should meet the total load power deviation, $\Delta P_L(t)$,

$$\Delta P_H(t) + \Delta P_W(t) = \Delta P_L(t) \quad (3.126)$$

- Frequency Regulation Constraint: The power injection or withdrawal from the grid should be within the specified limits for frequency regulation, ensuring system stability:

$$f_{\min} \leq f(t) \leq f_{\max} \quad (3.127)$$

where $f(t)$, $f_{\min}$, $f_{\max}$ and f_{ref} are the system frequency at time t, the minimum system frequency for normal operation ($49.50HZ$), the maximum system frequency for normal operation ($50.50HZ$) and the desired frequency set point ($50.00HZ$), respectively.

Choosing appropriate objective functions that will be used to evaluate the fitness of each population is the most crucial stage in using any optimization techniques. Some of the fitness functions are shown below:

$$ISE = \int_0^t e(\tau)^2 d\tau \quad (3.128)$$

$$IAE = \int_0^t |e(\tau)| d\tau \quad (3.129)$$

$$ITAE = \int_0^t \tau \bullet |e(\tau)| d\tau \quad (3.130)$$

This system uses a cost function of Equation (3.129) to reduce frequency deviation. So, it is written in the form of:

$$J_f = IAE = \min \int_0^t |e(\tau)| d\tau = \min \int_0^t |\Delta f_{ref}(\tau) - \Delta f(\tau)| d\tau \quad (3.131)$$

The solution to the optimization problem provides the optimal power generation, and consumption that minimize frequency deviations.

3.10 Optimization Techniques

In this topic, FPOA and PSO are introduced briefly. For balancing demand and generation for frequency regulation, the given algorithms are used to modify PID controllers.

3.10.1 Flower Pollination Optimization Algorithm (FPOA)

The FPOA, proposed by Xin-She Yang, is a swarm-based technique of optimization inspired by nature. The main objective of flower pollination is to ensure that the fittest flowers on flowering plants survive and reproduce optimally or as many times as possible. FPOA has drawn interest from many academics in various optimization fields, because of its impressive characteristics. When FPOA is applied in a variety of optimization tasks, it performs well and requires a very small number of parameters. Furthermore, FPOA is a simple, scalable, adaptive, and flexible optimization technique. For this reason, FPOA performs well when compared to other metaheuristic algorithms when it comes to resolving a wide range of real-world or practical optimization issues from numerous domains, such as computer gaming, structural and mechanical engineering optimization, global function optimization, electrical and power systems, and many more. The process of pollinating flowers involves transferring pollen from the male to the female through the use of pollinators like insects, birds, bats, wind, etc. Transferring the pollen involves two main processes.

(A) Global pollination

Pollen is carried from one flower to another by insects, birds, bats, and others. Cross-pollination can take place across a long distance and is regarded as a global pollination process when pollinators perform Levy flights.

(B) Self-pollination

It is the process by which one flower is fertilized by pollen on the same plant from the same or different flower. Such flowering plants are pollinated in this kind of pollination through water and wind diffusion. It is known as local pollination.

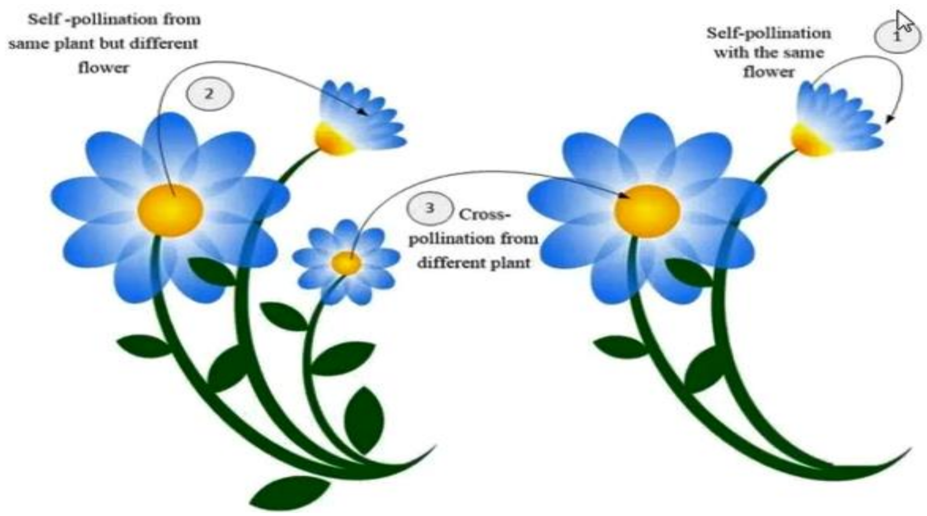

Figure 3.15: Flower pollination (D. Lakshmi, and A. Peer Fathima, 2016)

There is a switching probability $p \in [0,1]$ that controls both global and local pollination. Due to spatial proximity and additional variables such as wind and local pollination, a significant proportion p of the total pollination effort can arise. Both local and global pollination processes are the two basic phases of the method for flower pollination optimization (FPOA). The mathematical expression for global pollination is as follows:

$$y_i(r+1) = y_i(r) + \sigma(y_i(r) - y_g) \quad (3.132)$$

Where $y_i(r)$ corresponds the parameters to be tuned for optimal frequency regulation in the vector form to the solution $y_i = [k_{pc}, k_{ic}, k_{dc}]$ of pollen i at iteration r, $y_g = [k_{pg}, k_{ig}, k_{dg}]$ is the global best solutions at the present iteration, and is the step size represents the length of the pollination process.

The local pollination mathematical representation is given as

$$y_i(r+1) = y_i(r) + \partial(y_m(r) - y_n(r)) \quad (3.133)$$

Where $y_m(r)$ and $y_n(r)$ are solution vectors for pollen m and pollen n at iteration r, from various flowers of the same kind or species of plant, ∂ is a random number in the interval [0,1].

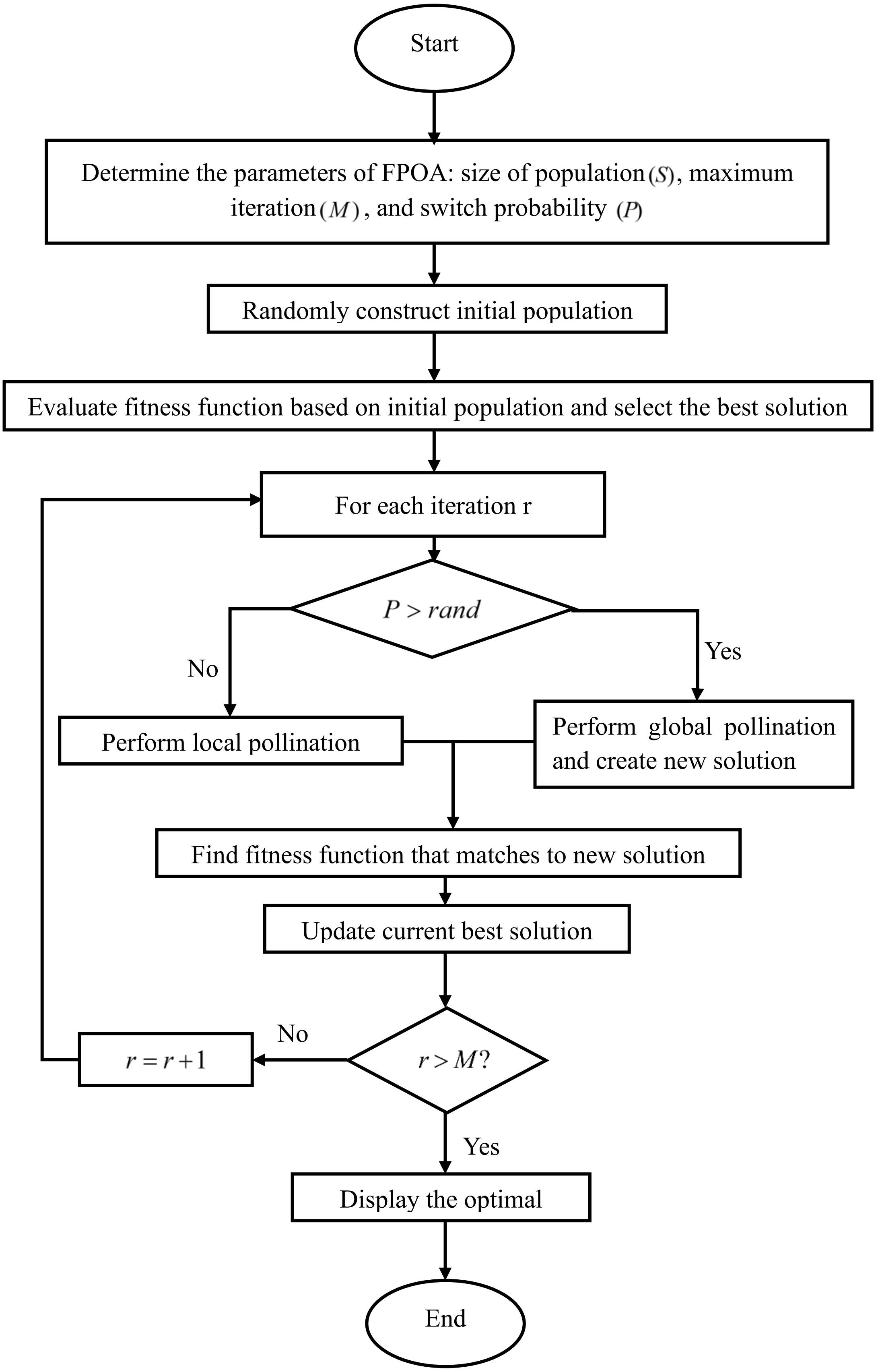

Figure 3.16: Flow chart for the FPOA

The flower pollination optimization algorithm pseudo-code is given below:

Switch probability (p), maximum iteration (M), and Fitness function (J_f) are the inputs of FPOA.

Determine the flower population S using a random solution;
Evaluate objective function and assign y_g in the initial random population;
Choose $p \in [0,1]$
While ($r < M$) **do**
    for $i = 1 : S$ **do**
        if $R < p$ **then** (for random number R)
            Generate step size (σ);
            Global pollination using $y_i(r+1) = y_i(r) + \sigma(y_i(r) - y_g)$;
        else
            Identify ∂ in the interval [0,1];
            Local pollination using $y_i(r+1) = y_i(r) + \partial(y_m(r) - y_n(r))$;
        end
        determine new solutions;
        Update them for the population if new solutions prove to be better.
    End
    Find the finest option currently available y_g;
End

Figure 3.17: Pseudo-code of the FPOA

3.10.2 Particle Swarm Optimization

It is based on the characteristics of a school of fish, a flock of birds, or a swarm or colony of insects like termites, bees, ants, and wasps. It imitates the behavior of these social organisms. In 1997, Kennedy and Eberhart initially introduced the PSO technique (Vincent N. Sajjad Hussain, 2023). Let's use vectors to express the individual's position and velocity in Equation (3.134).

$$y_i = [k_{pi}, k_{ii}, k_{di}] \text{ and } V_i = [v_{i1}, v_{i2}, v_{i3}] \tag{3.134}$$

$$\begin{cases} p_{best\,i} = (k_{pi}^{Pbest},\ k_{ii}^{Pbest},\ k_{di}^{Pbest}) \\ g_{best\,i} = (k_{pi}^{gbest},\ k_{ii}^{gbest},\ k_{di}^{gbest}) \end{cases} \tag{3.135}$$

Equation (3.135) is individual positions and their neighbors' global best position, respectively. With this data, the PSO algorithm adjusts the updated velocity of each individual represented in Equation (3.136).

$$V_i(r+1) = WV_i(r) + C_1R_1(p_{best\,i}(r) - y_i(r)) + C_2R_2(g_{besti}(r) - y_i(r)) \quad (3.136)$$

Where, $V_i(r)$ is the individual velocity at iteration r, W is the weight of inertia parameter, C_1, C_2 are the acceleration coefficient, R_1, R_2 are the random number within [0,1], $y_i(r)$ is individual position i at iteration r , and $p_{best\,i}(r), g_{best\,i}(r)$ are best individual position and global best position at iteration r. Particles can update their position by using the following expression

$$y_i(r+1) = y_i(r) + V_i(r+1) \quad (3.137)$$

Pseudo-code of PSO is shown in figure 3.18 below:

Determine all PSO parameters;
Initialize position and velocity randomly;
Assign p_{best} and g_{best} in the particles;
While ($r < M$) (M is maximum iteration)
    Find fitness value (J_f) from new particle y_i;
    If y_i is better than p_{best}
        Substitute p_{best} by y_i;
    End
    If y_i is better than g_{best}
        Replace g_{best} by y_i;
    End
    For $i:S$ (S is number of particles)
        Update y_i and V_i of particle using equation;
        $V_i(r+1) = wV_i(r) + C_1R_1(p_{best\,i}(r) - y_i(r)) + C_2R_2(g_{besti}(r) - y_i(r))$;
        $y_i(r+1) = y_i(r) + V_i(r+1)$;
    End
    $r = r + 1$;
End

Figure 3.18: Pseudo-code of the PSO algorithm

The parameters of the suggested algorithm (FPOA and PSO) are listed in Table 3.6. whereas Table 3.7 and Table 3.9 indicate the parameter tuning ranges of PID controllers gains for WT pitch actuator and frequency of the system, respectively. The tuned parameters of these controllers are in Tables 3.8 and 3.10.

Table 3.6: Proposed algorithm parameters

Optimization Algorithms	Parameters of Optimization		
FPOA	Flowers in the population (N)		30
	Maximum iteration (T)		100
	Step size (σ)		0.5
	Switching probability (p)		0.65
PSO	Swarm size (No. particles)		30
	Maximum iteration		100
	P_{best} coefficient (C_1)		2
	Neighborhood best coefficient (C_2)		2
	Inertia weight	$W_{\min}$	0.4
		$W_{\max}$	0.9

Table 3.7: Boundary of pitch angle controller gains

Boundary	k_{pc}	k_{ic}	k_{dc}
Lower bound (LB)	-1.0000	0.0000	-0.0100
Upper bound (UB)	500.0000	500.0000	500.0000

Table 3.8: Optimal value of pitch controller gains

Algorithm	PID controller coefficient			Optimal Value
	k_{pc}	k_{ic}	k_{dc}	
FPOA	2.69923	403.40916	0.0018445	0.001324

Table 3.9: Boundary of tuned parameters for frequency controller

Boundary	PID Controller parameters		
	k_{pc}	k_{ic}	k_{dc}
LB	-21.0000	0.0000	0.0000
UB	600.0000	600.0000	53.0098

The FPOA and PSO are used to modify the control settings following the suggested fitness function (IAE).

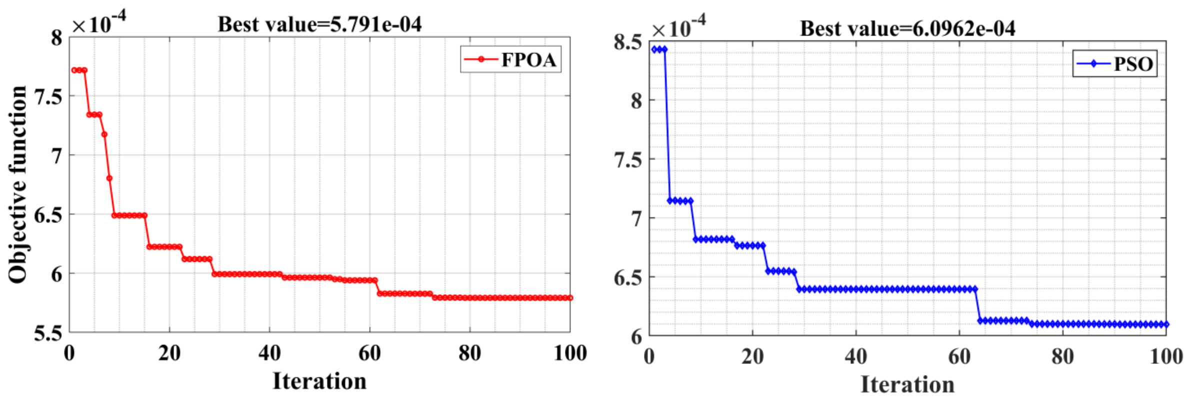

(a) FPOA (b) PSO

Figure 3.19: Convergence graph of FPOA and PSO

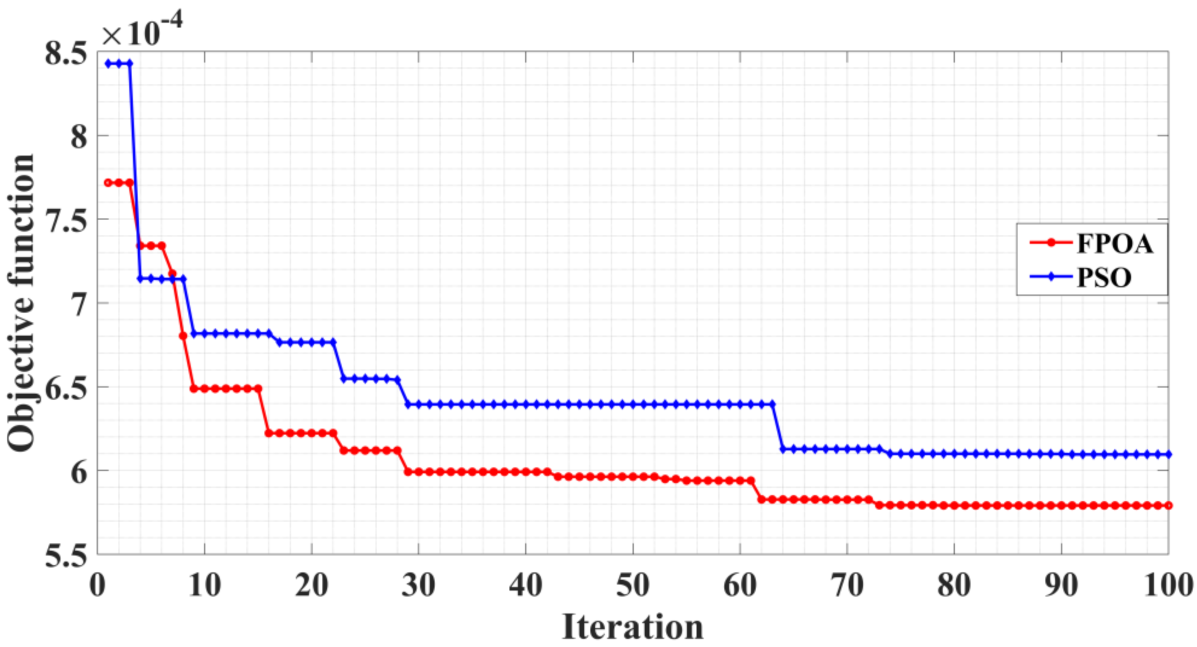

Figure 3.20: The performance of FPOA and PSO

Figure 3.19 shows the convergence capability of FPOA and PSO. FPOA is superior at the beginning and the end as this graph demonstrates. PSO converges more slowly than FPOA. Consequently, the FPOA outperforms the PSO in response by minimizing the IAE more.

Table 3.10: PID controller gains optimal value for frequency regulation.

PID controller coefficient		FPOA	PSO
PID	k_{pc}	485.3759	347.9176
	k_{ic}	439.5983	586.0329
	k_{dc}	50.9393	45.6895
Optimal value (IAE)		5.791e-04	6.0962e-04
Elapsed time		841.274389	859.267834

The FPOA is superior to PSO in response to best value (minimum IAE value) and elapsed time, or the duration of time needed to execute the code.

To test and validate the proposed method, a single area power plant that consists of WT and hydropower plant with the following features is considered.

Plant	Rating	Total generating rating power
Wind turbine	1.5MW	$1.5MW + 43MW = 44.5MW$
Hydro	43MW	

The plants are integrated with grid, sharing 0.3pu load at normal frequency (50HZ) with base power of 80MW. i.e.,

$$P_L(MW) = 0.3pu * 80MW = 24MW$$

$$\frac{24MW}{44.5MW} * 100\% = 53.93\%$$

The two generating plants can supply power of 24MW, which is 53.93% of total generating rating power.

CHAPTER FOUR

4 RESULTS AND DISCUSSIONS

4.1 Introduction

In the third chapter, RSC, GSC, pitch angle, and frequency regulation controllers were designed. To validate the performance of the proposed method, here, the results, such as controlled and uncontrolled system response have been compared and discussed in detail. The Simulink has been performed on the parameters of the system in Appendix A. The PID controller coefficients are tuned to produce a better performance of it using FPOA and PSO. To regulate the frequency of the HPP and WTG, the overall system is modeled in MATLAB/Simulink as shown in Figure 4.1.

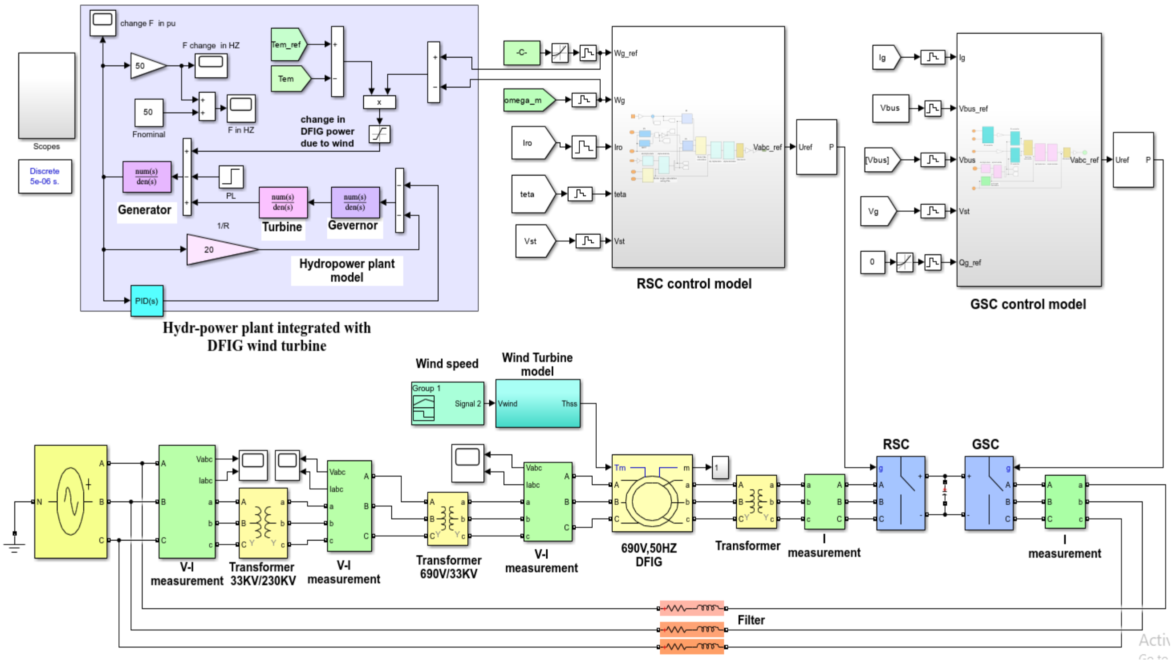

Figure 4.1: Frequency regulation MATLAB/Simulink

The above figure includes the 1.5MW wind turbine model, DFIG input and output, the two power electronic converters (RSC and GSC), and integration of the wind turbine and hydro-power plant for frequency regulation.

4.2 Simulation Results of Pitch-Controlled Wind Turbine

Wind turbine MATLAB/Simulink is designed in Figure B.1 using equations (3.22), (3.24), (3.25) and (3.26) from dynamic modeling. The turbine rotor speed is given by equation (3.37), and using variable wind speed, the system response without a pitch control system can be simulated in Figure 4.2 below. The wind turbine mechanical power is highly dependent on blade length, wind speed, pitch angle, and rotor speed. Similarly, the rotor speed also depends on wind speed and pitch angle as shown in the figure. In this study, a real wind speed is considered for simulation as shown in Figure 4.3(a), which varies between 4.885 m/s and 17.86 m/s within 150 seconds.

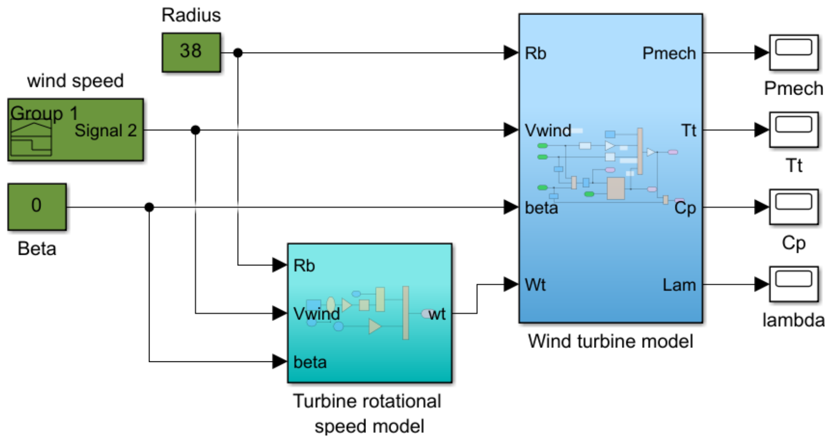

Figure 4.2: Wind turbine model without pitch control

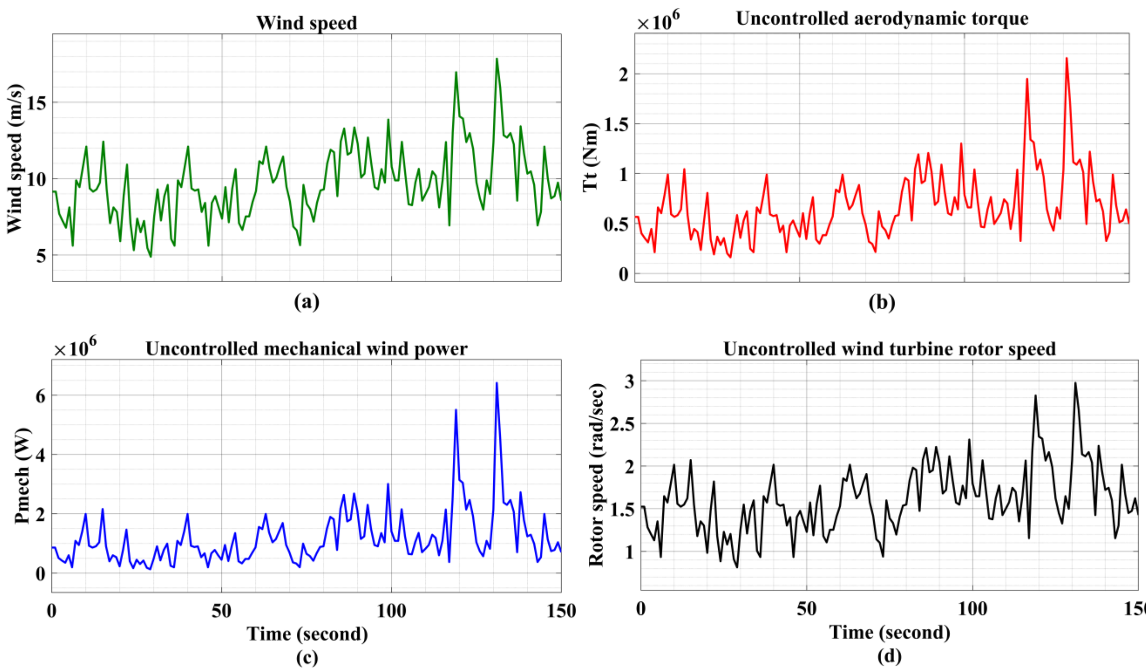

Figure 4.3: Wind Turbine input and output (a) variable wind speed, (b) uncontrolled turbine torque, (c) uncontrolled turbine mechanical power, and (d) uncontrolled turbine rotor speed

Figure 4.3(c) shows that, the uncontrolled mechanical power at variable wind speed results in very high power more than 6MW for a 1.5MW wind turbine. Also, the incoming wind speed affects the aerodynamic torque and rotor speed directly. The rated rotor speed at the rated wind speed (11m/s) is 1.8 rad/sec but the uncontrolled simulation result from Figure

4.3(d) shows at 17.86 m/s it becomes 3 rad/sec. This rotor speed is above the rated value. So, this can lead to several effects such as overvoltage, frequency deviation, the turbine generator trips or shutdown, and burning of equipment.

The pitch control system can be simulated in Figure 4.4 given below using the pitch actuator in Equation (3.45).

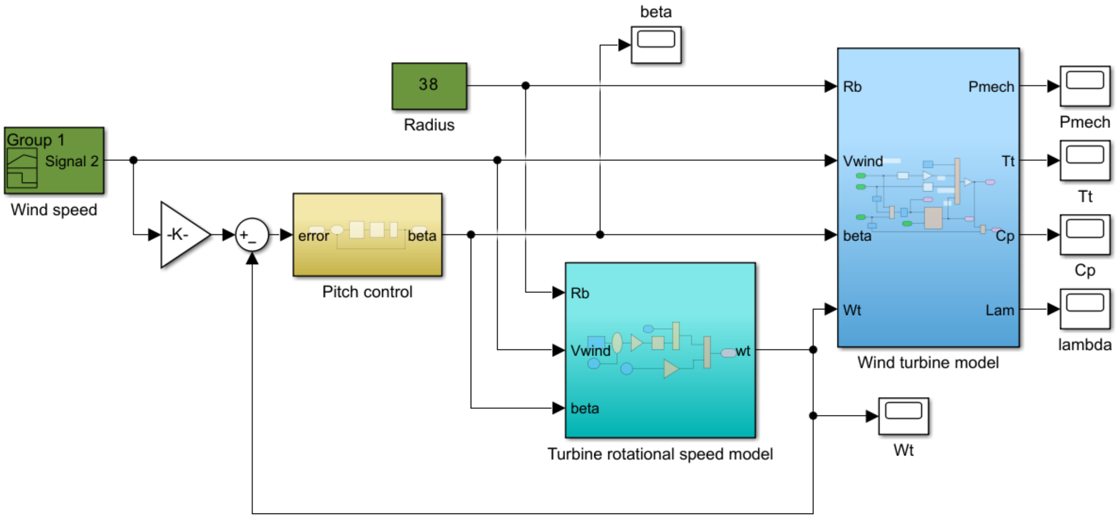

Figure 4.4: Pitch and turbine speed control Simulink model

The characteristics of the model of the wind turbine designed with the pitch controller are shown in Figure 4.5.

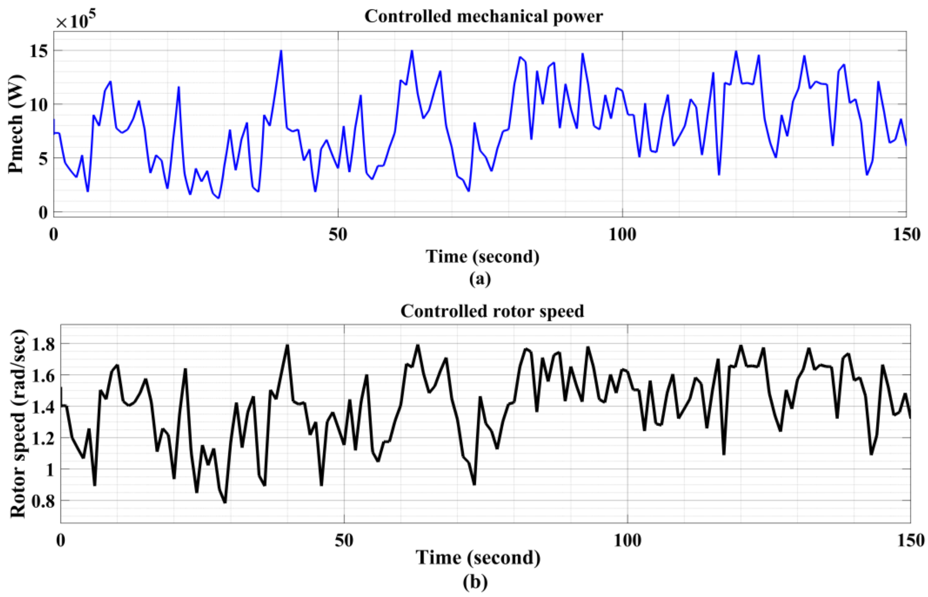

Figure 4.5: Responses of a) mechanical wind turbine and b) rotor speed

To prevent physical harm to the wind turbine, the controller adjusts the pitch angle when the wind speed increases to prevent the power and rotor speed don't exceed from their rated value of 1.5 MW and 1.8 rad/sec as shown in Figure 4.5 (a) and (b), respectively.

4.3 Simulation Results of the RSC and GSC

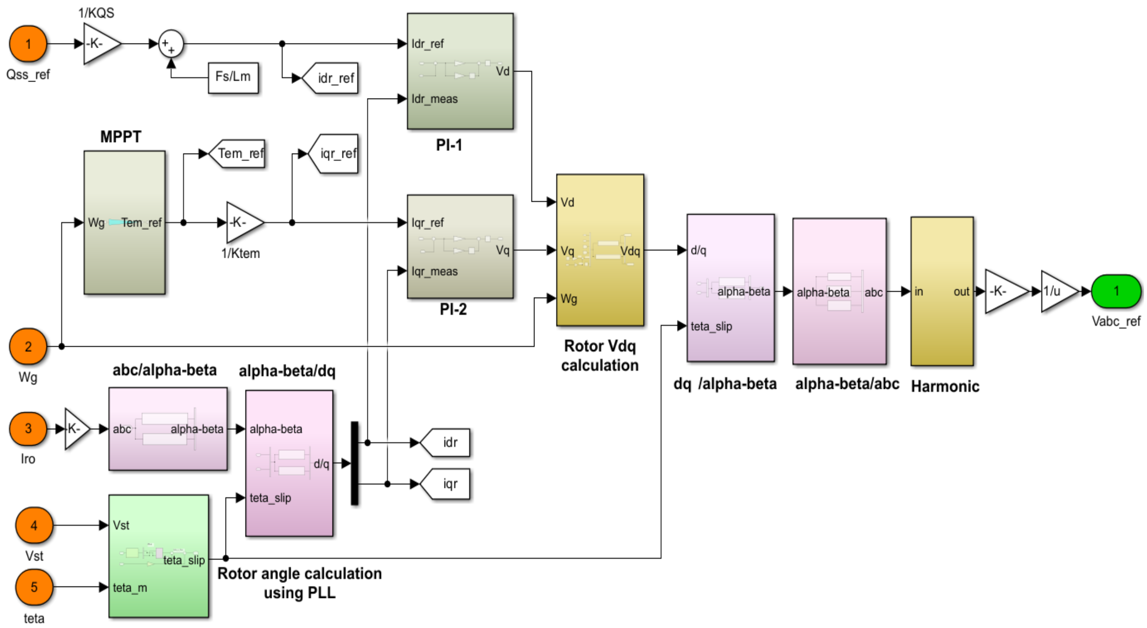

Figure 4.6: RSC Simulink diagram

RSC acts as a bridge between the variable wind speed and constant grid frequency. Its MATLAB/Simulink is designed in Figure 4.6 using equations from (3.55) to (3.58) and from (3.76) to (3.81). On the Simulink the orange colors depicted by numbers 1, 2, 3, 4, and 5 are reference stator reactive power, generator rotor speed, rotor current, stator voltage, and rotor angle of the generator, respectively are the inputs, and the green color is three phase rotor voltage, which is the output of RSC. The two PI controllers PI-1 and PI-2 were designed for rotor direct and quadrature current control, respectively. The four transformations are shown in magenta color.

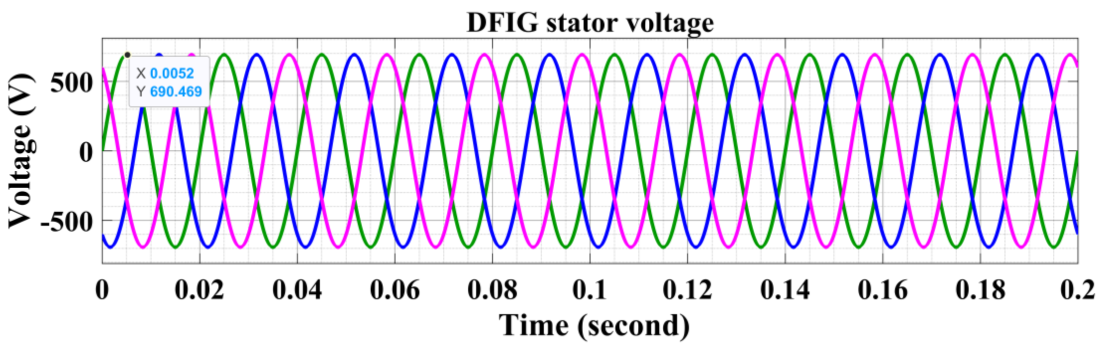

(a)

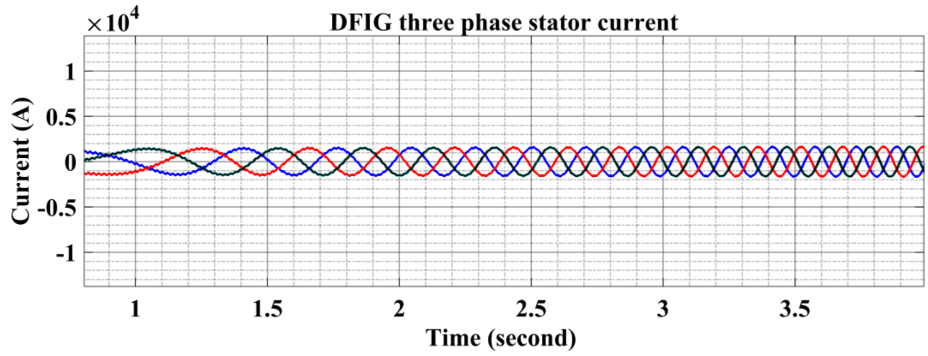

(b)

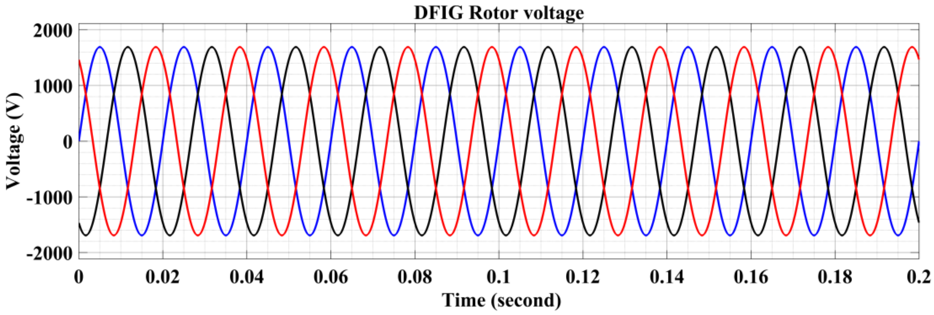

(c)

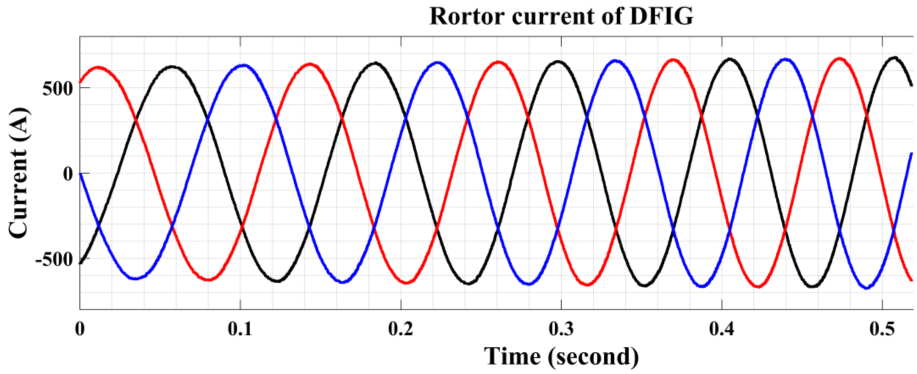

(d)

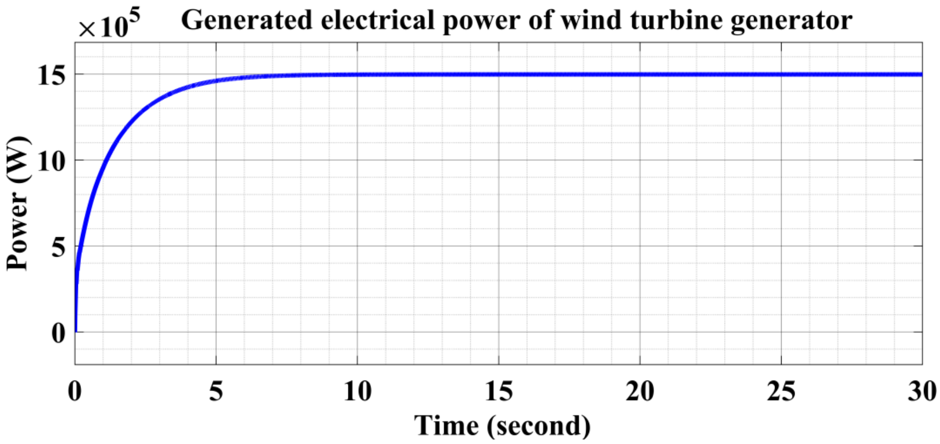

(e)

Figure 4.7: Input and output of RSC, (a) stator voltage, (b) stator voltage, (c) rotor voltage, (d) rotor current, and (e) generated electrical power of WTG at 11m/s.

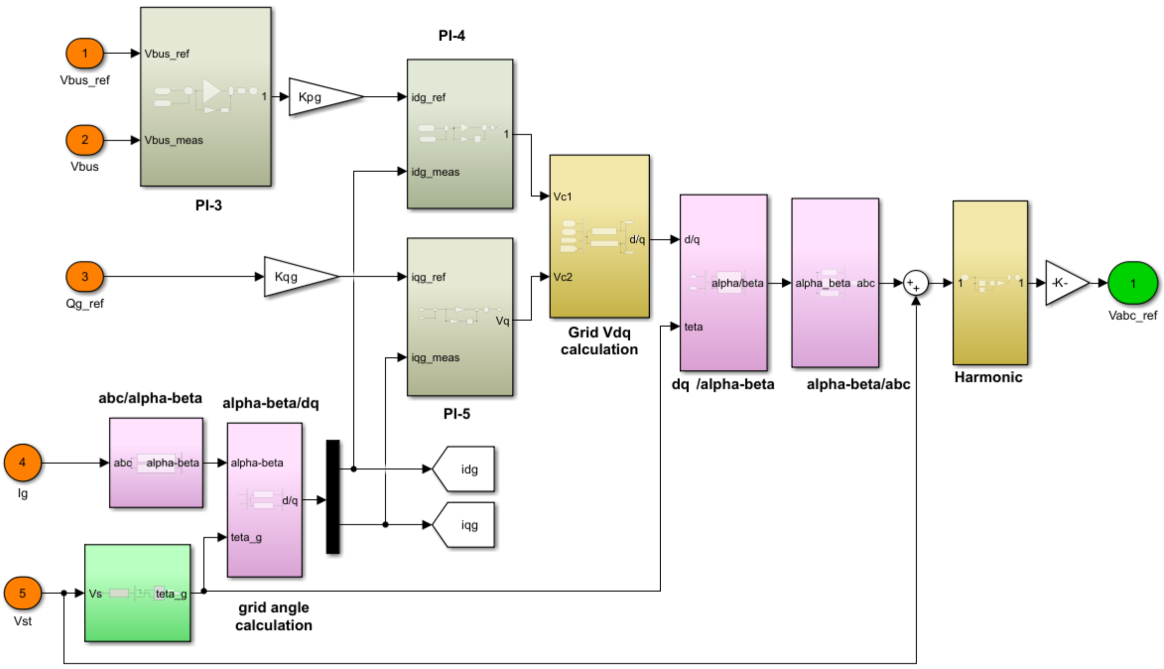

Figure 4.8: GSC Simulink diagram

The GSC is simulated in above Figure 4.8. Similar to RSC, the orange colors are inputs. Inputs 1 & 2 are a reference and measured bus voltage, 3 is the reference reactive power of the grid, 4 is grid current and 5 is stator voltage. The output is of the three-phase grid voltage indicated by green color.

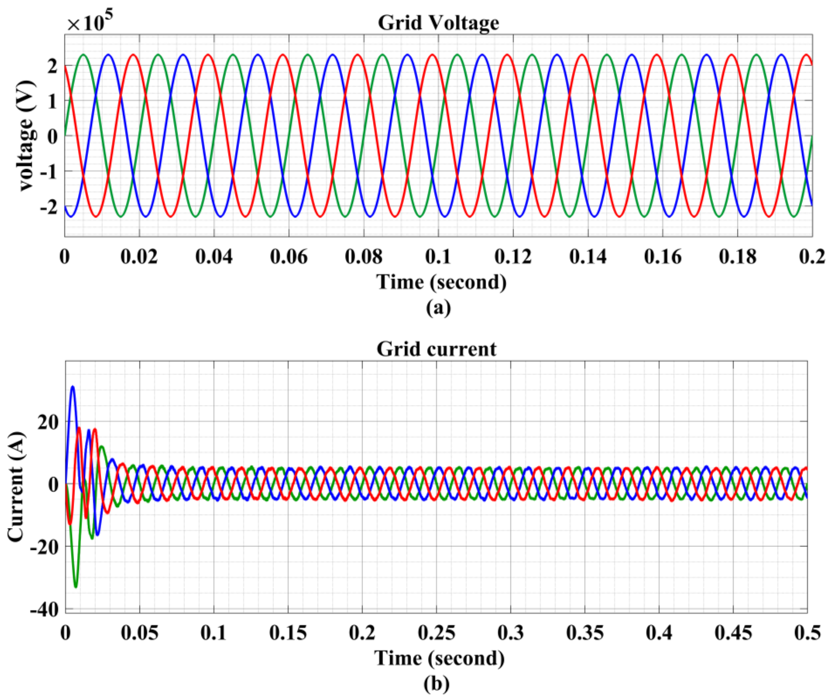

Figure 4.9: Output of GSC after adding of step-up transformer (a) grid voltage, (b) grid current

The results in both Figure 4.7 and 4.9 are displayed from the connection of the WT with DFIG at the normal operating condition. Initially, a 690V source is given to DFIG, then using a step-up transformer the stator voltage is increased to 33KV. Again, increase the voltage from 33KV to 230KV using another step-up transformer. So, the grid voltage is 230KV shown in Figure 4.9(a).

Three cases are investigated for this thesis work simulation.

4.3.1 Case one: System Operation in the Nominal State

The system performances of the FPOA-PID controller, PSO-PID controller, PI-controller $(k_p = 9.104, k_i = 0.854)$ and system without controller when the change in load ($\Delta P_L =$ $0.05\,p.u$) and rated wind speed (11m/s) are presented in Figure 4.10. It shows the simulation results of the frequency deviation, $\Delta f\,(p.u.)$, the frequency response, $f\,(HZ)$ and the power deviation, $\Delta P(p.u.)$.

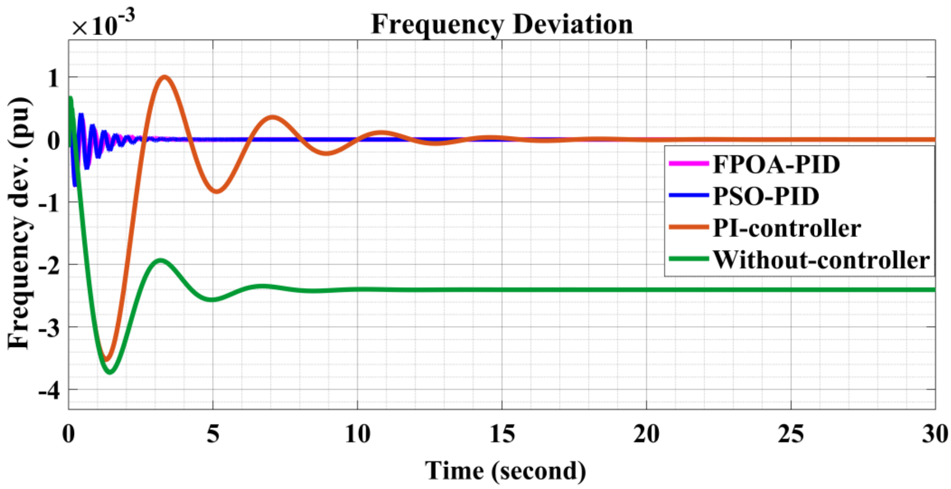

(a)

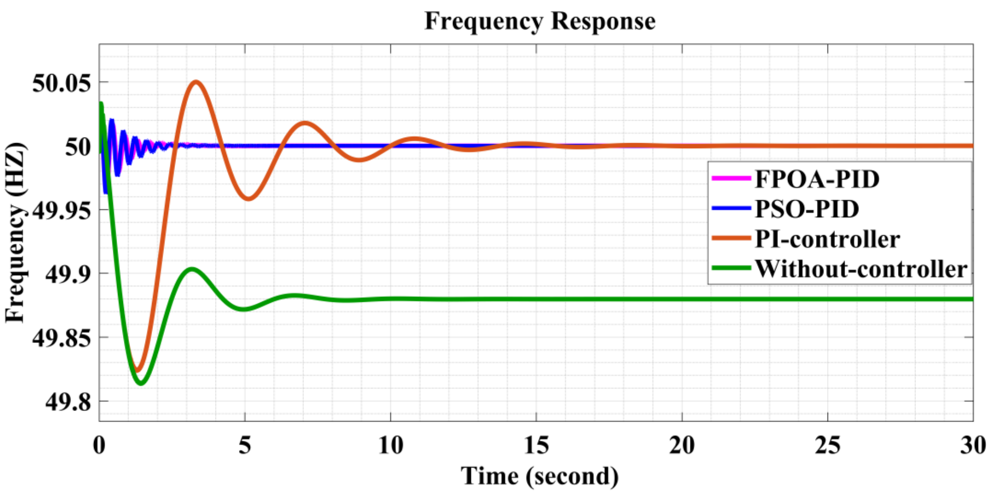

(b)

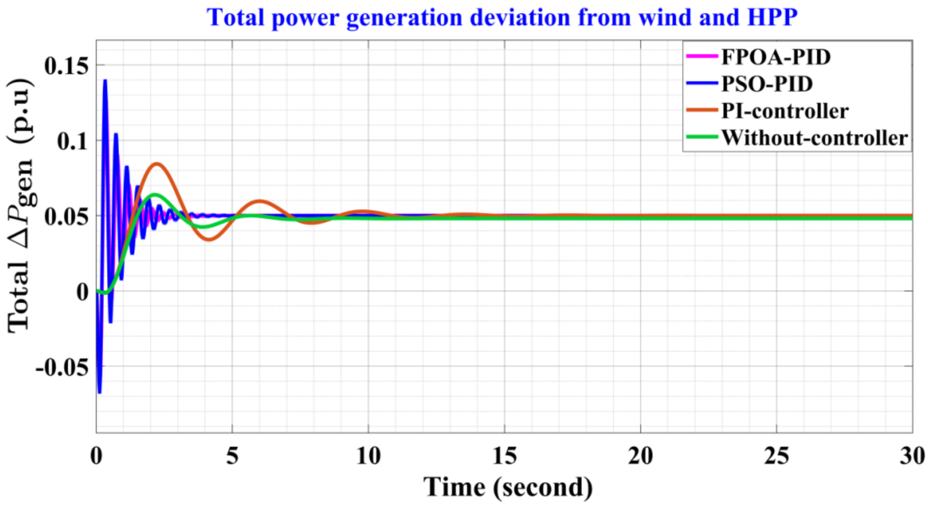

(c)

Figure 4.10: Responses of the system: (a) frequency deviation, (b) frequency response, and (c) total generated power deviation

It can be seen that even at a small change in load and rated wind speed, the system without a controller doesn't bring the responses back to the reference value. But, for the FPOA-PID, PSO-PID, and PI-controller performances are at normal operating or wanted values. The conventional PI-controller gradually brings the response back to its reference point; however, it took a longer time. With the proposed FPOA-PID controller, the response is more stable and faster as compared to the response with PSO-PID or conventional PI controller. That is under the proposed controllers use, the steady state values are $\Delta f = 0, f = 50Hz, \Delta P_L = \Delta P_{gen} = 0.05\, p.u.$

Table 4.1: Performance of frequency controller 11m/s wind speed and 0.05pu load change.

Controller	Step-information			
	Overshoot (Hz)	Undershoot (Hz)	Settling time (sec)	Steady-state error (Hz)
FPOA-PID	0.02280	0.0289	1.0106	0.0000
PSO-PID	0.02943	0.0375	1.9406	0.0000
PI	0.0496	0.1759	15.1128	0.0000
Without controller	0.0308	0.1859	7.4758	0.1202

The above table shows the step information of frequency response for FPOA-PID, PSO-PID, PI and system without controller at rated wind speed and 0.05pu load change. And the proposed method has lower overshoot, undershoot and small settling time.

Figure 4.11 shows even at high change in load and low wind speed, the system response with FPOA-PID, PSO-PID controller brings response back to its reference point; but with the proposed FPOA-PID controller, the response is more stable and faster as compared to the response with PSO-PID or conventional PI controller. The system without a controller doesn't bring the responses back to the wanted value. Its nadir frequency and steady state value is 46.25 HZ and 47.6 HZ, respectively. That is under the proposed controllers use, the steady state values are $\Delta f = 0,\ f = 50Hz$.

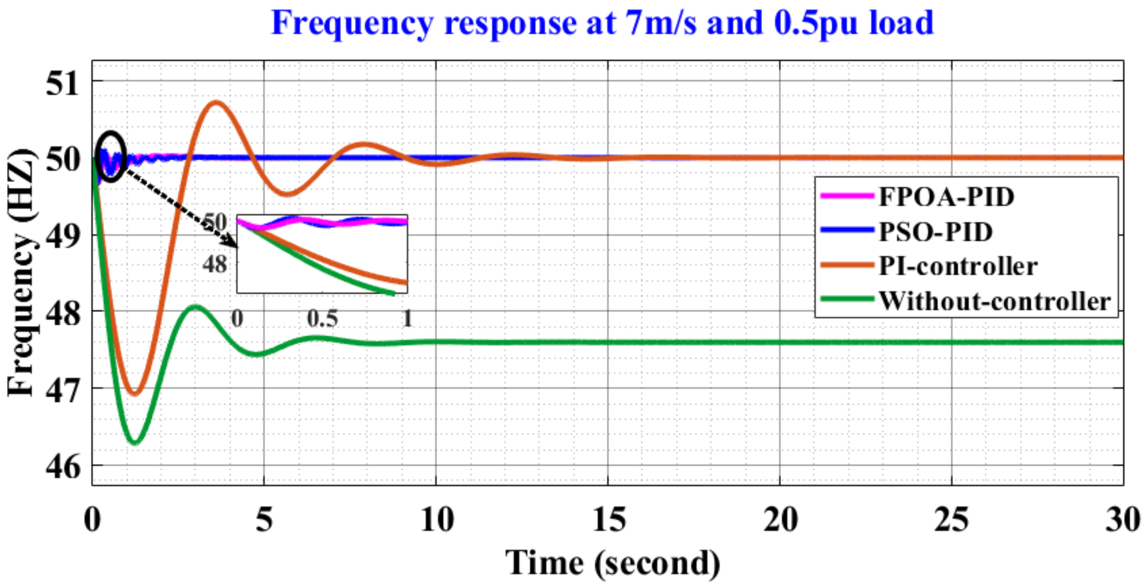

Figure 4.11: Frequency response compared with three controllers and without controller.

Table 4.2: Performance of frequency controller 7m/s wind speed and 0.5pu load change.

Controller	Step-information			
	Overshoot (Hz)	Undershoot (Hz)	Settling time (sec)	Steady-state error (Hz)
FPOA-PID	0.0467	0.3370	2.4593	0.0000
PSO-PID	0.1134	0.3528	2.7698	0.0000
PI	0.4772	3.1257	15.2403	0.0000
Without controller	0.0000	3.7758	9.3469	2.7294

Following the color of the result in the figure 4.11, the transient response characteristics for proposed method, PSO-PID, PI and system without controller at 7m/s wind speed and 0.5pu load depicted in Table 4.2.

4.3.2 Case two: Robustness Evaluation

(a) Under various changes in load

Under various load and rated wind speed (11 m/s), responses of the system for the FPOA-PID controller are depicted in Figure 4.12. For the proposed controller, the responses are stable and fast. That is for any changes in the load, the steady-state values are $\Delta f = 0$, $f = 50Hz$, and $P_L = P_{gen}$.

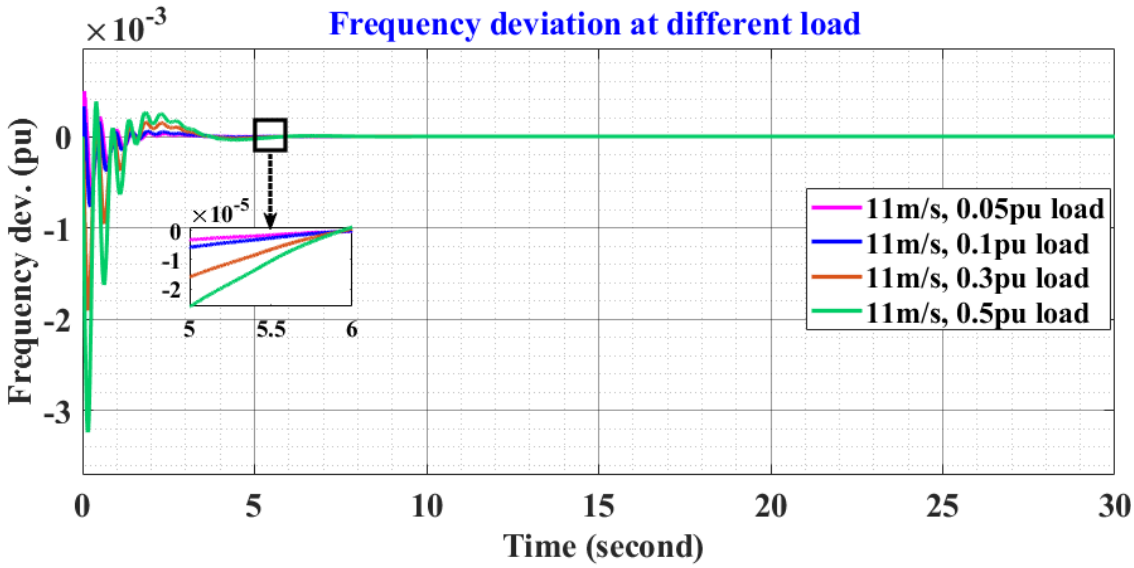

(a)

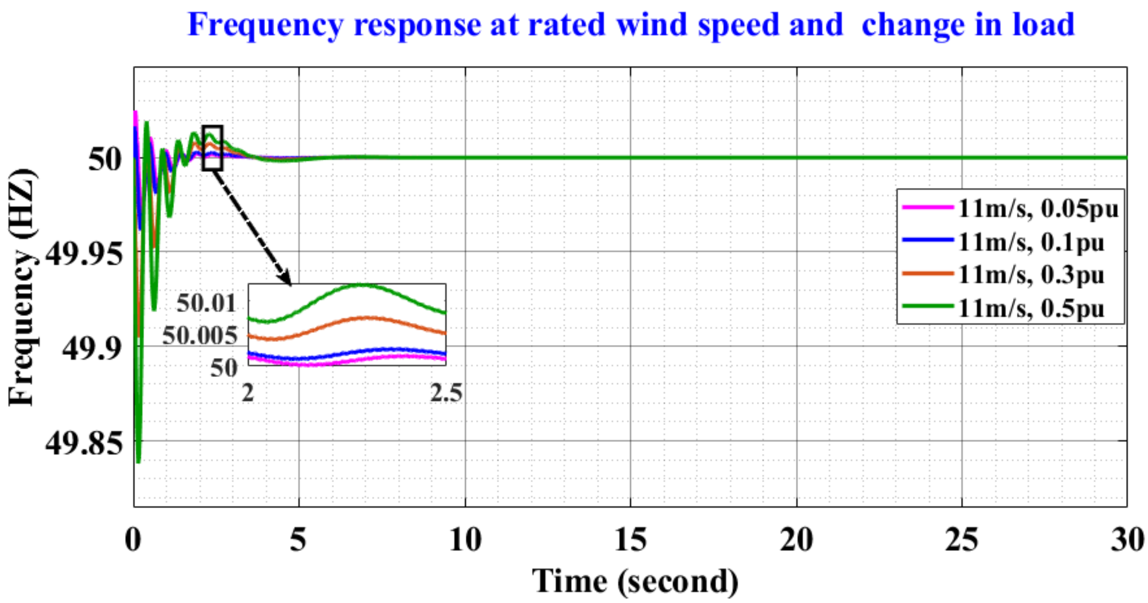

(b)

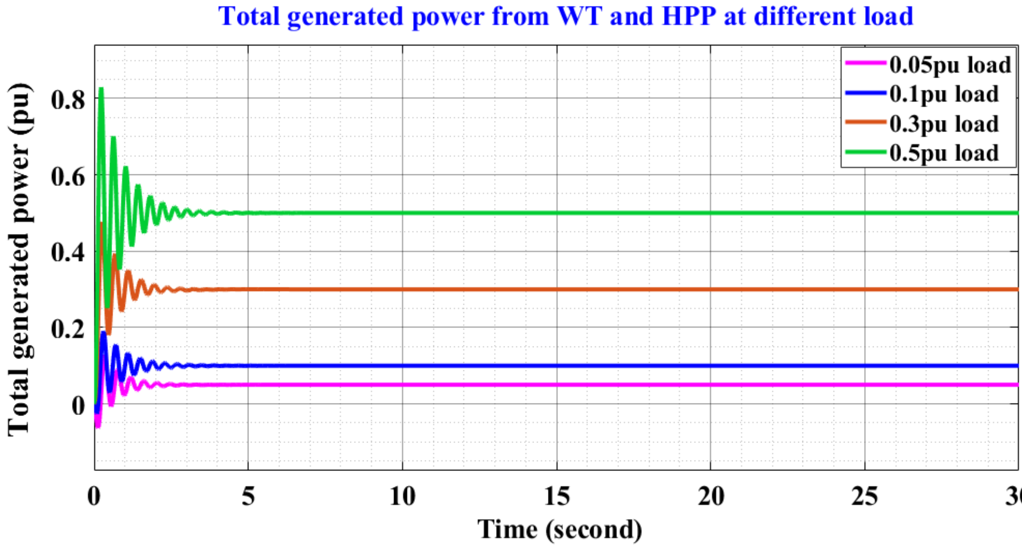

(c)

Figure 4.12: Responses of the system under different load changes: (a) frequency deviation, (b) frequency response, and (c) total generated power deviation

The performance of FPOA-PID controller and load sharing between WT and hydropower plant for different loads and rated wind speed (maximum power generated) are shown in Table 4.3 and Table 4.4, respectively. The colors of the tables correspond to the results.

Table 4.3: Performance of frequency controller with change in load and rated wind speed.

Load (*p.u.*)	Step-information			
	Overshoot (Hz)	Undershoot (Hz)	Settling time (sec)	Steady-state error (Hz)
0.05	0.0228	0.0289	1.0106	0.0000
0.1	0.0201	0.0400	1.4257	0.0000
0.3	0.0103	0.0946	2.8782	0.0000
0.5	0.0102	0.1612	3.0094	0.0000

Table 4.4: Load sharing between WT and HPP for different load and rated wind speed.

Load (P_L)		Load Change (ΔP_L)		Power (MW) from wind turbine at 11m/s	Power (MW) from HPP
(*p.u.*)	(MW)	(*p.u.*)	(MW)		
0.05	0.05*80 = 4	0	0	1.5	4 − 1.5 = 2.5
0.1	0.1*80 = 8	0.05	4	1.5	8 − 1.5 = 6.5
0.3	0.3*80 = 24	0.2	16	1.5	24 − 1.5 = 22.5
0.5	0.5*80 = 40	0.2	16	1.5	40 − 1.5 = 38.5

(b) Under the changes in wind speed

Figure 4.13 shows the frequency responses of the system at 0.05 *p.u.* load and various wind speeds when the FPOA-PID controller is implemented. Figure 4.13 (a) is the frequency deviation, which indicates the maximum changes in the frequency response is 0.0006 *p.u.*, while Figure 4.13 (b) is the frequency response in Hz, which depicts a small oscillation in the transient part between 49.97 and 50.02 Hz, and the steady state response is almost 50 Hz.

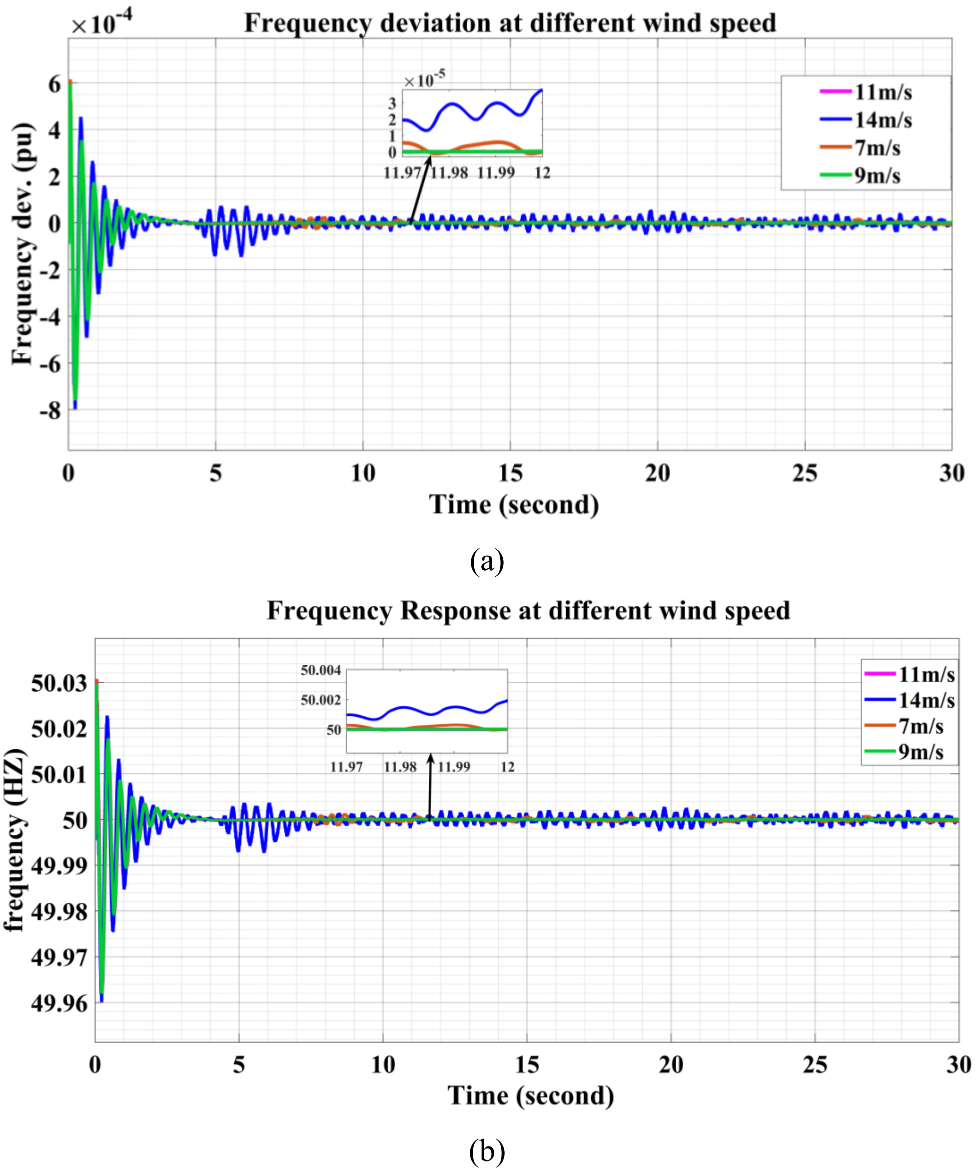

Figure 4.13: frequency response of the system for FPOA-PID controller at four different wind speeds: (a) frequency deviation and (b) frequency response

The performance of the FPOA-PID controller at different wind speeds and 0.05 *p.u.* loads is depicted in Table 4.5 below, and the response at rated wind speeds is the best among others.

Table 4.5: Performance of controller with change in wind speed and 0.05pu load change.

Wind speed (m/s)	Step-information			
	Overshoot (Hz)	Undershoot (Hz)	Settling time (sec)	Steady-state error (Hz)
14	0.0246	0.0304	2.9825	0.0000
11	0.0228	0.0289	1.0106	0.0000
9	0.0239	0.0306	2.9571	0.0000
7	0.0235	0.0322	2.9817	0.0000

Table 4.6: Load sharing between WT and HPP for different wind speed and 0.05 *p.u.* load

Wind speed (m/s)	Load (MW)	Power (MW) from wind turbine	Power (MW) from HPP
14	$0.05*80=4$	1.501	$4-1.501=2.499$
11	$0.05*80=4$	1.500	$4-1.500=2.500$
9	$0.05*80=4$	0.8213	$4-0.8213=3.1787$
7	$0.05*80=4$	0.3864	$4-0.3864=3.6136$

Table 4.6 shows when the wind speed decrease from 14 to 7 m/s the generated power from wind decreases from 1.501 to 0.3864MW; at this time in order to meet the demand, the generated power from HPP increases from 2.499 to 3.6136MW for constant load of 4MW.

4.3.3 Case three: System Performance under Varying Load and Wind Speed

Figure 4.14 shows the frequency responses of the system under various load and varying wind speed when the FPOA-PID controller is implemented. Figure 4.14(a) is the frequency deviation in *p.u.*, which indicates a small oscillation in the transient part that is between -0.0032 and 0.0005*p.u.*, while Figure 4.14(b) is the frequency response in Hz, which depicts a small oscillation in the transient part that is between 49.85 and 50.01 Hz, and the steady state response is 50 Hz. Figure 4.14(c) is the total generated power from WT and HPP when both the wind speed and load vary. This figure indicates that the variation in the generated power and varying load are equal. This shows power balance as depicted in Figure 4.14(d).

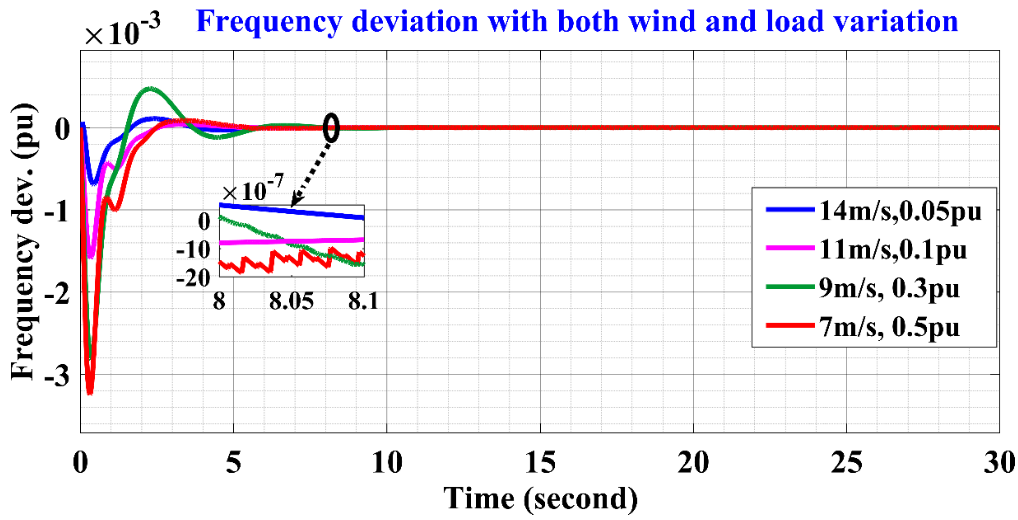

Frequency deviation with both wind and load variation
×10^-3
Frequency dev. (pu)
0
-1
-2
-3
×10^-7
0
-10
-20
8
8.05
8.1
14m/s,0.05pu
11m/s,0.1pu
9m/s, 0.3pu
7m/s, 0.5pu
0
5
10
15
20
25
30
Time (second)

(a)

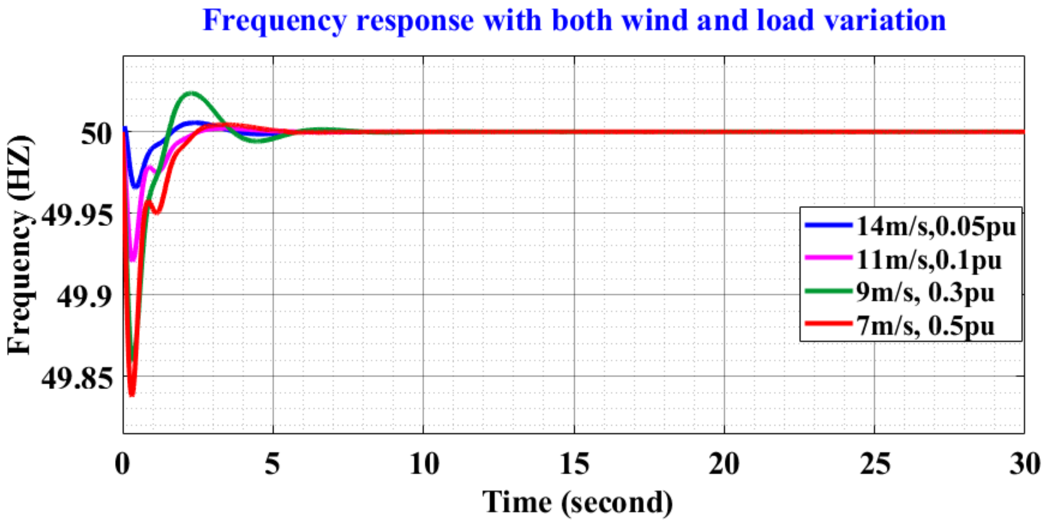

Frequency response with both wind and load variation
Frequency (HZ)
50
49.95
49.9
49.85
14m/s,0.05pu
11m/s,0.1pu
9m/s, 0.3pu
7m/s, 0.5pu
0
5
10
15
20
25
30
Time (second)

(b)

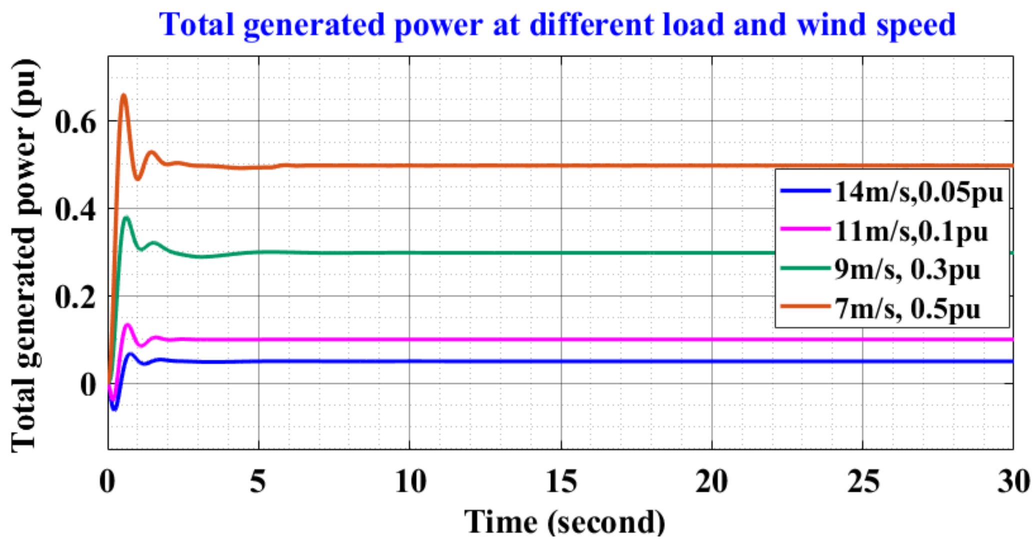

Total generated power at different load and wind speed
Total generated power (pu)
0.6
0.4
0.2
0
14m/s,0.05pu
11m/s,0.1pu
9m/s, 0.3pu
7m/s, 0.5pu
0
5
10
15
20
25
30
Time (second)

(c)

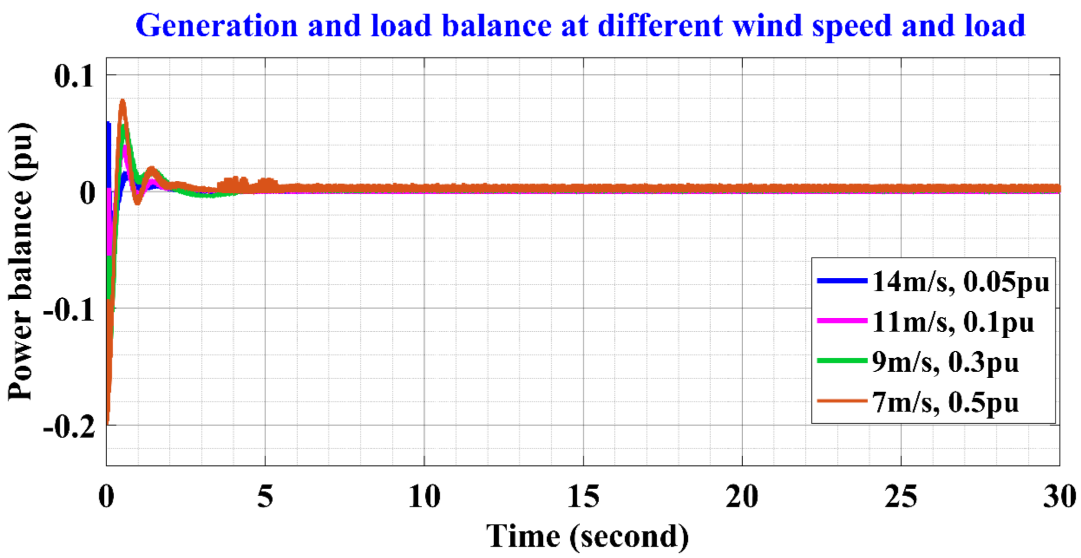

(d)

Figure 4.14: Responses of the system under varying load and wind speed: (a) frequency deviation, (b) frequency response (c) total generated power deviation (d) power balance.

Table 4.7: Performance of controller with simultaneous change in wind speed and load.

Wind speed (m/s), Load change (*p.u.*)	Step-information			
	Overshoot (Hz)	Undershoot (Hz)	Settling time (sec)	Steady-state error (Hz)
14, 0.05	0.0246	0.0304	1.5825	0.0000
11, 0.1	0.0201	0.0400	2.4257	0.0000
9, 0.3	0.0124	0.0964	4.8135	0.0000
7, 0.5	0.0467	0.3371	2.4593	0.0000

Table 4.8: Load sharing between WT and HPP for different wind speed and load

Wind speed (m/s)	Load (P_L)		Load Change (ΔP_L)		Power (MW) from wind turbine	Power (MW) from HPP
	(pu)	(MW)	(pu)	(MW)		
14	0.05	0.05*80=4	0	0	1.501	4-1.501=2.499
11	0.1	0.1*80=8	0.05	4	1.5	8-1.5=6.5
9	0.3	0.3*80=24	0.2	16	0.8213	24-0.8213=23.1787
7	0.5	0.5*80=40	0.2	16	0.3864	40-0.3864=39.6136

Table 4.8 shows when the generated power from wind decreases from 1.501 to 0.3864MW because of wind speed and the load increase from 4 to 40MW, at this time in order to meet the demand, the generated power from HPP increases from 2.499 to 39.6136MW.

Generally, according to the Ethiopian National Transmission system grid code in Table 2.2 and the frequency range of European countries in Table 2.3, the unlimited or normal operating range is between 49.5 and 50.5 and 49 and 51Hz, respectively. But at frequencies below 47Hz and above 52.5Hz, the system may and must be disconnected, respectively. The simulation result in Figure 4.12 shows that the system without a controller has a response of 46.2242Hz, so the system must be disconnected. And we can conclude that at any load change and wind speed fluctuation, the proposed method has a response between 49.85Hz and 50.03Hz. This indicates unlimited operation of the system.

5 CONCLUSION AND RECOMMENDATION

5.1 Conclusions

This research investigates robust frequency regulation for a single-area system in the presence of a WT and Hydropower plant based on the FPOA-PID control technique. A MATLAB simulation has been executed so as to validate the performance of the suggested approach. Tests have been conducted on the suggested controller for nominal case, load disturbance at rated wind speed, different wind speeds at small load and both wind speed and load changes. Simulation results demonstrate that quick response time, robustness against wind speed variation, and load changes could be viewed as some benefits of the proposed FPOA-PID controller. It is demonstrated that the FPOA-PID controller response outperforms both the conventional PI and PSO-PID responses in terms of effectiveness and can handle variations in load as well as wind speed more efficiently.

Generally, the proposed method can effectively reduce the deviation of grid frequency and generated power caused by wind power fluctuations, which can improve the impact of the intermittent nature of the output power of wind turbine on the operation of the power grid. This study provides the simplest, most robust and most economical control technique to limit the impact of wind power fluctuations on the power system response, consequently regulating the grid frequency.

5.2 Recommendations

Nowadays, generating electricity from RES, especially wind, solar, and hydropower plants, have gotten more attention in the world to decrease environmental pollution and balance demand and generation of electricity. This research focuses only on the frequency regulation of grid-connected WT and hydropower generation systems using FPOA based optimal PID controller. I recommended that future research will focus on applying the proposed control strategy to interconnect the above power generation systems with solar systems.

The system interacts with many controllers. Seven controllers with AGC of HPP are proposed for this thesis, but the frequency regulation can be further improved by reducing the number of controllers required. I also recommend using battery energy storage system to balance supply and demand by absorbing and injecting power from and into the grid when needed. However, this will be expensive and require a very sophisticated connection with converters.

Acknowledgements

The research for this paper was financially supported by Adama Science and Technology University under the grant number of **ASTU/SM-R/1008/24**, Adama, Ethiopia.

REFERENCES

Al-Haddad. (2014). *Power Electronics for Renewable Energy Systems, Transportation and Industrial Applications.* Hoboken,USA.

B. Singh and S.N. Singh. (2009). Wind Power Interconnection into the Power System: A Review of Grid Code Requirements. *The Electricity Journal, 22*(5), 54-63.

Chaine S. Tripathy M. and Satoathy S. (2015). NSGA-II based optimal control scheme of wind thermal power system for improvement of frequency regulation characterstics. *Engineering Journal, 6*(3), 851-863.

Chao L. and Qingquan L. (2022). *Multi-Objective Mayfly Optimization-Based Frequency Regulation for Power Grid With Wind Energy Penetration.* China.

D. Lakshmi, and A. Peer Fathima. (2016). A Novel Flower Pollination Algorithm to Solve Load Frequency Control for a Hydro-Thermal Deregulated Power System. page(172).

Endalew. (2021). *Soft computing based control strategies to improve the performance of wind turbines in uncertain conditions.* Adis Ababa.

Ethiopia Electricity Authority (EEA), E. e. (2018). *Ethiopia National Electricity Transmission Grid Code.*

European, P. (2018). Grid code of EU countries frequency ranges and time periods. 42-43.

Global Wind Energy Council. (2021). *GWEC Global Wind Report 2021.* Germany: WindEnergy Hamburg Press Releases.

GWEC. (2009). *The Global Wind Energy Council, Latest News.* US and China in race to the top of global wind industry.

H Bouregba , M Hachemi,M Bey. (2022). Stability analysis of the pitch angle control of large wind turbines using different controller strategies. 5-6.

Hansen, A.D.; Rensen, P.S.; Blaabjerg, F.; Becho, J. . (2002,26,). Dynamic Modelling of Wind Farm Grid Interaction. *Wind. Eng,*, 191-210.

Inigo Martinez de Alegria. (n.d.). Connection requirements for wind farms: A survey on technical requirements and regulation,. *Renewable and Sustainable Energy Reviews, Vol.11*(Issue 8).

Ioannis D. Margaris, Stavros A. (2012). Frequency Control in Autonomous Power Systems With High Wind Power Penetration. *3*(2).

Jayshree P. and Vijayakumar V. (2021). A Review of Maximum Power Point Tracking Algorithms for Wind Energy Conversion Systems. page (2).

Khan, W. (2018, may 11). *Hydroelectric power*. Retrieved from https://electronicslovers.com/2018/05.

Kumari S. and Shankar G. (2020, 3 30). *Application of cascade tilt-integral-derivative controller in load frequency control of deregulated power system.* Retrieved from https://doi.org/10.1002/2050-7038.12257.

L. Zhang and W. Shepherd. (2017). Electricity Generation Using Wind Power. *[Hackensack], World Scientific,New Jersey, NJ,* .

Luta, D. (September 2014). *Modelling of Hybrid Solar Wind Intergrated Generation Systems in an Electrical Distribution Network.* The Cape Peninsula University of Technology, Cape Town, South Africa, .

Michael Z. Bernard. (2019). PI-MPC Frequency Control of Power System in the Presence of DFIG Wind Turbines.

Mohamed E. and Gonzalo A. (2011). *Double fed induction machine modeling and control for wind energy generation.*

P.Kundur. (1994). Power system stability and control.

S. Domingos and F. Oliveira. (2018). in Advances in Renewable Energies and Power Technologies. In *"Chapter 15-doubly fed induction generator in wind energy conversion systems"* (pp. 461-490). Elsevier, Amsterdam, Netherlands.

Saadat, H. (n.d.). *Power System Analysis.*

Sabahi K. and Badamchizadeh M. (2016). *Designing an adaptive type-2 fuzzy logic system load frequency control for a nonlinear time delay power system.* Retrieved from https://doi.org/10.1016/j.asoc.2016.02.012.

Samaneh M. (2021). Control coordination between DFIG-based wind turbines and synchronous generators for optimal primary frequency response. 2.

Srikanth V. and Yadaiah N. (2018). An AHP based optimized tuning of modified active disturbance rejection control. *An application to power system load frequency control problem. ISA Trans., 81*(2).

Standard EN 50160. (2004, july). *Voltage Characteristics in Public Distribution Systems.* Retrieved from http://www.leonardoenergy.org/webfm_send/2703

Stephen O. and Zenghui W. (2022). An enhanced flower pollinated algorithm with a modified fluctuation rate for global optimization and load frequency control system. *Renewable power generation*.

T. Burton and N. Jenkins. (2001). *Wind energy handbook, John Wiley &Sons Ltd chichester.* UK.

Tadesse, A. (2022). *Pitch Angle Control for PMSG-Based Variable Speed Horizontal Axis Wind Turbine Using Supper Twisting Sliding Mode Controller.* Bahir Dar.

Tilahun W., Aderajew A. (2021). Modeling and design of an automatic generation control for hydropower plants . *Energy reports*, 6629-6630.

Vincent N. Sajjad Hussain. (2023). Load Frequency Control Using the Particle Swarm Optimisation Algorithm and PID Controller for Effective Monitoring of Transmission Line. 5-7.

Wiley, J. (2011). *Power conversion and control of wind energy systems.* Canada.

Xu, H. (2023). frequency control of wind turbine in power system. *AIP conference proceedings*.

Y. D. S. A. H. M. M. M.Iqbal A,. (2020). Proposed particle swarm optimization technique for the wind turbine control system,. *Measurement and Control.,, vol. 53*.

Zhiwei Wanga, Xiangyu Lyu. (2023). *Intelligent load frequency control for improving wind power.* Beihai, China: Elsevier Ltd.

APPENDICES

Appendix A: List of Parameters used for this Thesis

Table A.1: Data set of 1.5MW wind turbine

Parameter lists	Amount	Measured in
Radius of blade	38	M
Cut-in speed of wind	3.5	m/s
Rated wind speed	11	m/s
Cut-out wind speed	25	m/s
Speed of turbine rotation range	16 - 19	Rpm
Density of air	1.225	kg/m^3
Maximum coefficient of power conversion C_{p_opt}	0.4055	------
Optimal ratio of tip speed λ_{wt_opt}	6.33	-------

Table A.2: Data set of main generator characteristics

Parameter lists	Amount	Measured in
Rated stator real power	1.5	MW
Stator rated voltage	690	V
Rated torque	9549	Nm
Rated generator speed	1750	Rpm
Generator speed range	1200 – 1750	Rpm
Pole pairs	2	------

Table A.3: Pitch control parameters

Variable pitch system performance	
Nominal rate of change of pitch angle	$5\ {}^{\circ}\!/_{s}$
Turbine pitch angle range	$0 \sim 90^{\circ}$
Maximum rate regulation of pitch angle	$\pm 10\ {}^{\circ}\!/_{s}$
Accuracy of pitch angle adjustment	$0.0128 \sim 0.01333\%$

Table A.4: 1.5 MW DFIM characteristics

Features	Symbol	Value	Unit
Rated power	P_s	1.5	MW
Stator rated voltage (L-L-rms)	V_{st}	690	V
Stator rated current	I_{st}	1068.3	A
Generator rated speed	ω_g	1750	Rpm
Rated torque	τ_g	8185	Nm
Pole pair	p	2	------
Rated rotor voltage (L-L-rms)	V_{ro}	1040	V
Turn ratio	u	1/3	------
Stator resistance	R_{st}	0.0026	Ohm
Rotor resistance	R_{ro}	0.0029	Ohm
Stator and rotor linkage reactance	L_{lst}, L_{lro}	0.000087	H
Stator inductance	L_{st}	0.002587	H
Rotor inductance	L_{ro}	0.002587	H
Nominal frequency	f	50	HZ
Maximum slip	$S_{\max}$	1/3	----
Bus capacitor	C_{bus}	0.05	F
Filter resistance and inductance	R_{gf}, L_{gf}	20e-6, 400e-6	Ohm, H

Table A.5: Parameters of Hydropower plant

Parameters	Value	Unit
P_H, Rated power	43	MW
ω_H, Rated speed	1000	Rpm
τ_w, Start time of water in hydropower plant	1	Sec
τ_1, reset time of governor	5	Sec
τ_2, time constant of transient drop	41.6	Sec
τ_3, time constant of servomotor	0.513	Sec
H_{sy}, inertia constant of system	3	Sec
D_{sy}, system damping factor	1	Nm/rad.s
K_g, gain of governor	1	-----

Appendix B: Simulink Block Diagram

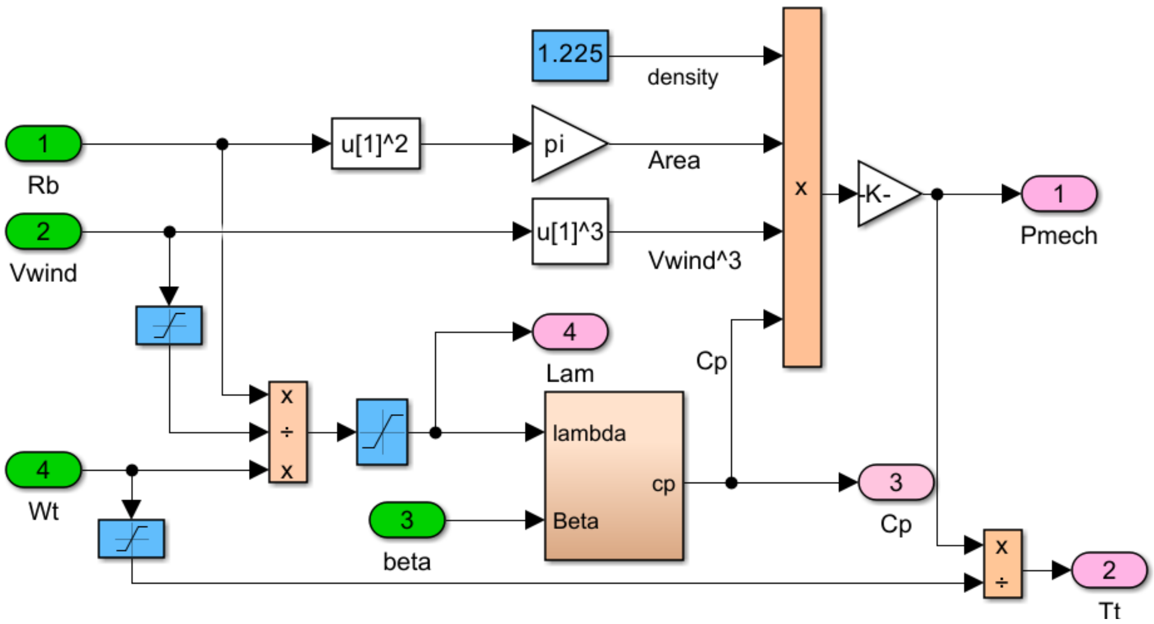

Figure B.1: Wind turbine Simulink model

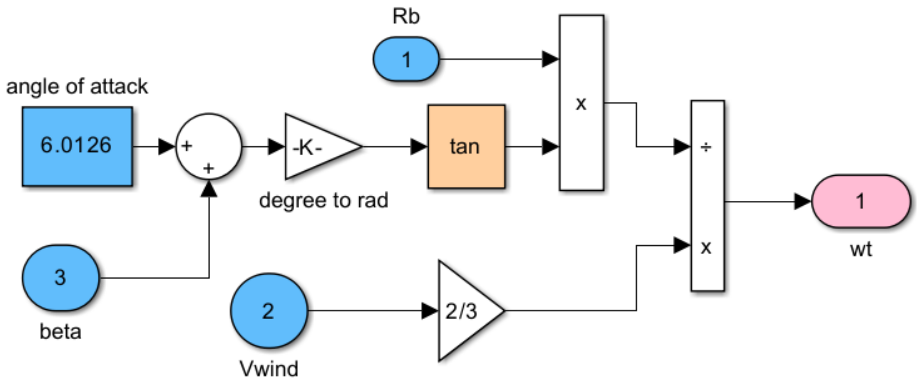

Figure B.2: Wind turbine rotor speed Simulink model

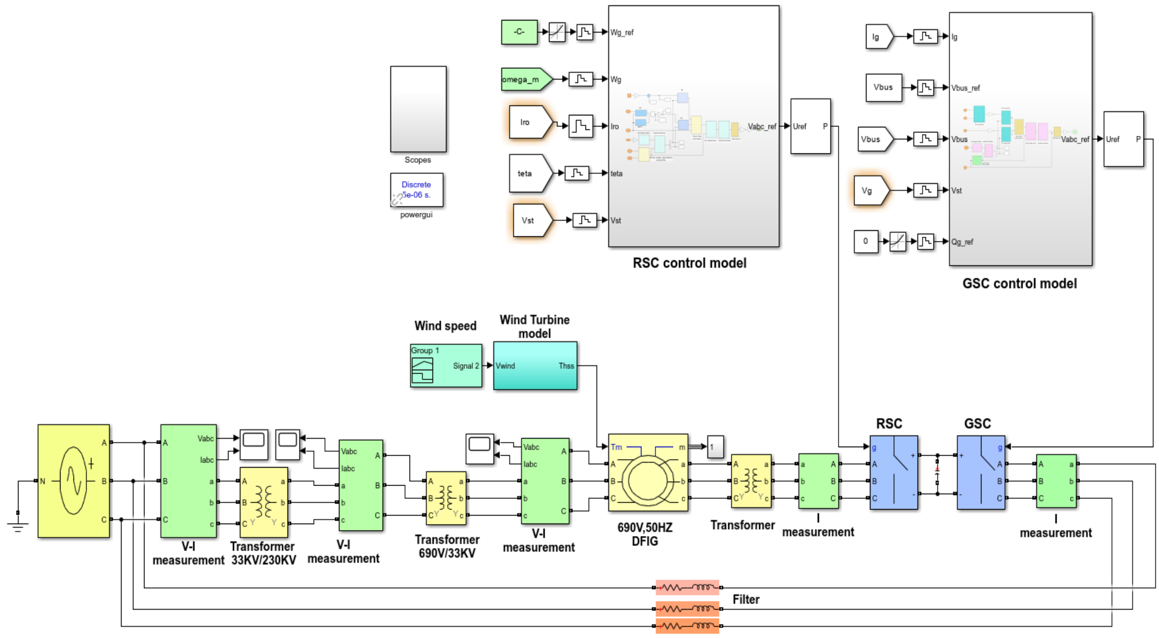

Figure B.3: DFIG Simulink diagram with WT, RSC, and GSC.

Appendix C: Some Optimization Algorithm (FPOA codes)

```
tic
clear all
close all
% FPA parameter
N=30; % no of pollen/population
T=100; % no of iteration
c=0.5; %step size
p=0.65; %switching probability
var=3;
% Search space
lb=[-21 0 0];
ub=[600 600 53.0098];
% optimization step
c_cf=0; %counter
% initilization
for i=1:N
```

```
    for w=1:var
        x(i,w)=lb(w)+rand()*(ub(w)-lb(w));
    end
        %calculate the objective function
    ffb(i)=tunning(x(i,:));
end
%Gbest
[obj_Gbest,Gbest_location]=min(ffb);
xg=x(Gbest_location,:);%initial global best
y=x;

%Main Loop
for tt=1:T
    for i=1:N
        r=rand;
        if r<p
            for w=1:var
                y(i,w)=xg(1,w)+(rand*c*(y(i,w)-xg(1,w)));
                %check boundary
               if y(i,w)<lb(w);y(i,w)=lb(w);end
               if y(i,w)>ub(w);y(i,w)=ub(w);end
            end
        else
            j=1+round(rand*(N-1));
            k=1+round(rand*(N-1));
            for w=1:var
                y(i,w)=xg(1,w)+rand*c*(y(j,w)-y(k,w));
                if y(i,w)<lb(w);y(i,w)=lb(w);end
                if y(i,w)>ub(w);y(i,w)=ub(w);end
            end
        end
        % evaluate the new objective function
        fnew(i)=tunning(y(i,:));
     % compare
     if fnew(i)<obj_Gbest
         obj_Gbest=fnew(i);
         xg=y(i,:);
     end
    end
    outmsg=['iteration#',num2str(tt),'obj_Gbest=',num2str(obj_Gbest)];
    disp(outmsg);
    aaa(tt)=obj_Gbest;
end
% cost function
IAE=obj_Gbest
% % PID parameter
best_value=xg
semilogy(aaa);
xlabel('Iteration')
ylabel('Objective function')
```

```
function cost= tunning(k)
assignin('base','k',k);
sim('FPOA_tunning_PID.slx');
cost=IAE(length(IAE));
end
%############################################################
% tunning determine objective function from MATLAB/Simulink model to tune PID
% cost=tunning(k) displays the fitness function value cost determined using
% the gain of controller, k=[k(1) k(2) k(3)].
```